Thermal Evolution and Sediment Provenance of the Cooper-Eromanga Basin: Insights from Detrital Apatite

Thesis submitted in accordance with the requirements of the University of Adelaide for an Honours Degree in Geology

Angus Leslie Nixon

October 2017

THE UNIVERSITY of ADELAIDE

THERMAL EVOLUTION AND SEDIMENT PROVENANCE OF THE COOPER-EROMANGA BASIN: INSIGHTS FROM DETRITAL APATITE

RUNNING TITLE: Thermal History and Provenance of the Cooper-Eromanga Basin

ABSTRACT

Despite the prolific hydrocarbon and geothermal potential within the Cooper-Eromanga Basin, the thermal history of the region has largely remained elusive. This study presents new fission track, U-Pb and rare earth geochemical data for apatite samples from five wells within the Cooper-Eromanga Basin. Based on these data, thermal history models were constructed and an apatite provenance study was carried out. The apatite samples taken from the upper Eromanga Basin sediments (*Winton, Mackunda* and *Cadna Owie Formations*) yielded a dominant population of early Cretaceous and minor population of late Permian – Triassic apatite ages that are (within error) equivalent to corresponding fission track age populations. Furthermore, the obtained Cretaceous apatite ages correlate well with the stratigraphic ages for each analysed formation, suggesting (1) little time lag between apatite exposure in the source region and sediment deposition; and (2) that no significant (>~100^{o}C) reheating occurred after deposition. The apatites were likely distally sourced from an eastern Australian volcanic arc, (e.g. the Whitsunday Igneous Association), mixed with sediment sources from the New England and/or Mossman Orogens. Deeper samples (>2000m) from within the Cooper Basin (*Toolachee Formation*) yielded (partial) reset fission track ages, indicating heating to temperatures exceeding ~80-100^{o}C after deposition. The associated thermal history models are broadly consistent with previous studies, and suggests that maximum temperatures were reached at ~95-70 Ma as a result of progressive heating by sedimentary burial and/or radiogenic basement heat loss. The interpretation of subsequent late Cretaceous – Palaeogene cooling remains more enigmatic, and may be related with enhanced thermal conductivity as a response to aquifer flow and/or cementation. Four of the five wells recorded a Neogene heating event, however, more data would be required to assess the significance of this more recent thermal perturbation.

KEYWORDS

Thermal History, Provenance, Detrital Apatite, Cooper-Eromanga Basin, Whitsunday Volcanic Association, Burial

TABLE OF CONTENTS

LIST OF FIGURES AND TABLES

[1] INTRODUCTION

The Cooper-Eromanga Basin in central Australia is a largely non-marine sedimentary basin which has remained one of Australia's most significant economic petroleum reservoirs for many decades (e.g. Gravestock, Hibburt, & Drexel, 1998). Consequently, the basin has been the subject of extensive research with relation to structural history, lithology, evolution of stress fields, and geothermal gradient. However, relatively little work has been done to constrain the thermal history of the basin. Understanding the evolution of the thermal regime in the basin has the potential to provide temporal constraints on the burial history in the basin, which has important implications for petroleum and geothermal exploration (Armstrong, 2005; Beardsmore, 2004; Deighton & Hill, 1998; Mavromatidis, 2007). Previous studies have predicted a complex thermal history within the basin, suggesting elevated temperatures during the early to mid-Cretaceous, reaching a peak at ~90 Ma, followed by a period of cooling before temperatures increased to reach present day conditions since ~5-2 Ma. (Duddy, Moore, Marshallsea, & Green, 2002). Progressive burial of sediments above high heat producing granites in the Big Lake Suite below the Eromanga Basin explains heating in the late Cretaceous. Cooling and subsequent Neogene reheating, however, are more enigmatic, but may be explained by hydrological processes within the basin (Deighton & Hill, 1998).

Sedimentary provenance for the Cooper-Eromanga Basin has not been studied extensively. Previous studies based on whole-rock Sm-Nd and zircon U-Pb ages of sediment from the Eromanga Basin have suggested contemporaneous volcanism at the eastern Australian margin as the primary source (Boult, Theologou, & Foden, 1997; Tucker et al., 2016; Whitford, Hamilton, & Scott, 1994). The similarity between

radiometric and depositional ages in the Eromanga Basin could be explained by prolonged volcanism in the Whitsunday Igneous Association between ~125-90 Ma coincident with the duration of sedimentation in the upper Eromanga Basin (Tucker et al., 2016), however , a direct link between the Eromanga sediments in central Australia has not been extensively explored.

This study aims to enhance our understanding of the thermal history and provenance of the basin, through the application of combined apatite U-Pb (AUPb) and fission track analysis and low temperature thermal history modelling. The AUPb ages constrain the timing at which the apatite crystals cooled below temperatures of ~350-550^{o}C (Chew & Spikings, 2015). Within unmetamorphosed rocks, AUPb ages hold complementary provenance information to the more traditional zircon U-Pb ages. However, since apatites can grow in both mafic and felsic sources (unlike zircons) the AUPb system is able to trace mafic provenances (Pochon et al., 2016). Apatite fission track (AFT) ages reflect the time since apatites last resided at ~60-120^{o}C (Wagner & Van den haute, 1992) which can be applied to both thermal history and provenance studies. When apatite samples show partial reset in response to elevated (~60-120^{o}C) temperatures, low temperature thermal history modelling can be performed to elucidate the post-depositional thermal history of the samples. When the samples were not heated to temperatures of ~60-120^{o}C after deposition, the apatite fission track ages retain a provenance age that complementary to the AUPb system (Reiners & Ehlers, 2005).

In this thesis, new apatite U-Pb and fission track data and associated thermal history models are presented and discussed for five wells in the Cooper-Eromanga Basin.

[2] GEOLOGIC SETTING

[2.1] Cooper Basin

The Cooper-Eromanga Basin is a major onshore petroleum reserve and intriguing geothermal prospect (e.g. Hall et al., 2015) located in central Australia. In South Australia the Cooper Basin uncomformably overlies the eastern Warburton Basin (Figure 1). Latter sedimentary basin is intruded by highly radiogenic granitic intrusions of the Big Lake Suite, that were emplaced ~330-295 Ma (Gatehouse, Fanning, & Flint, 1995; Middleton, 1979). The Cooper Basin sediments were deposited in northeast-southwest trending troughs that developed during the Devonian – Carboniferous Alice Springs Orogeny (Alexander & Hibburt, 1996; Gravestock et al., 1998; Munson, 2014). Deposition in the Cooper Basin spanned from the late Carboniferous – mid-Triassic, initially in a glacial to periglacial environment before transitioning to fluvial and lacustrine

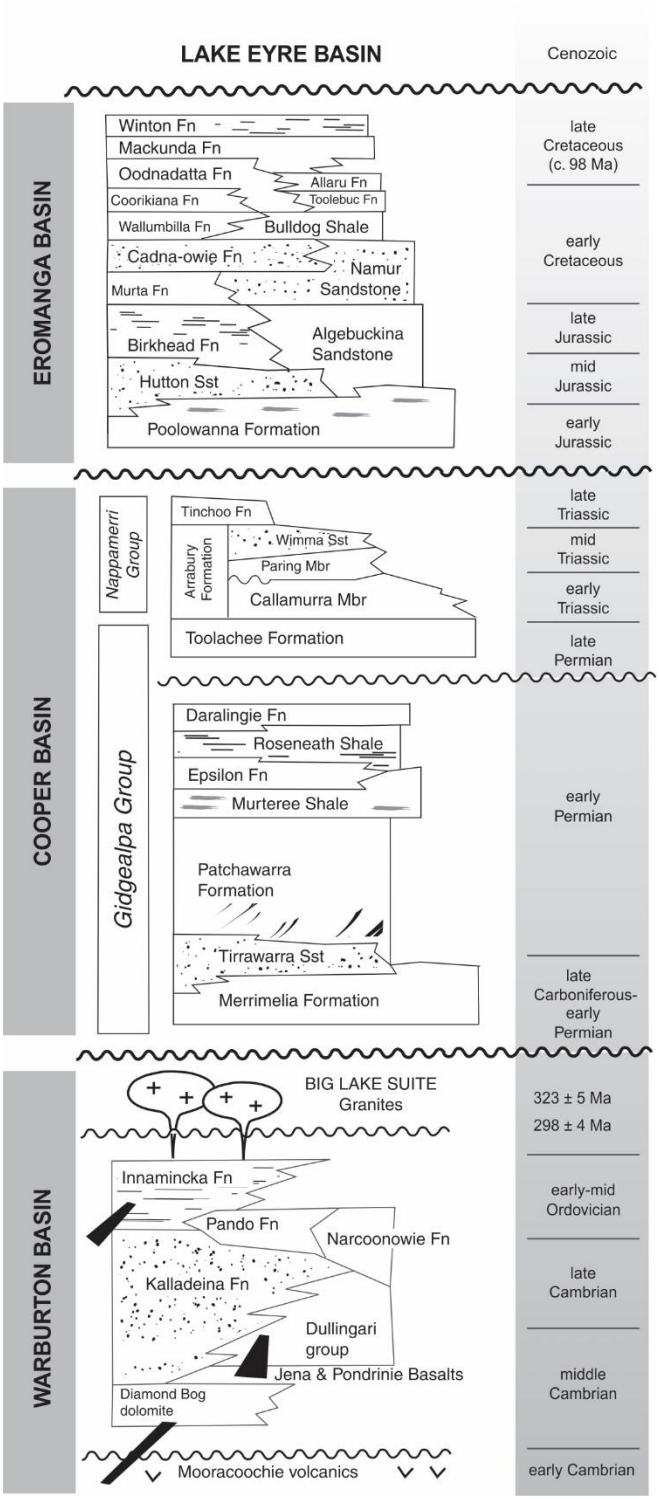

Figure 1: Generalised stratigraphic column for the Cooper-Eromanga Basin in South Australia. Modified from McLaren & Dunlap (2006).

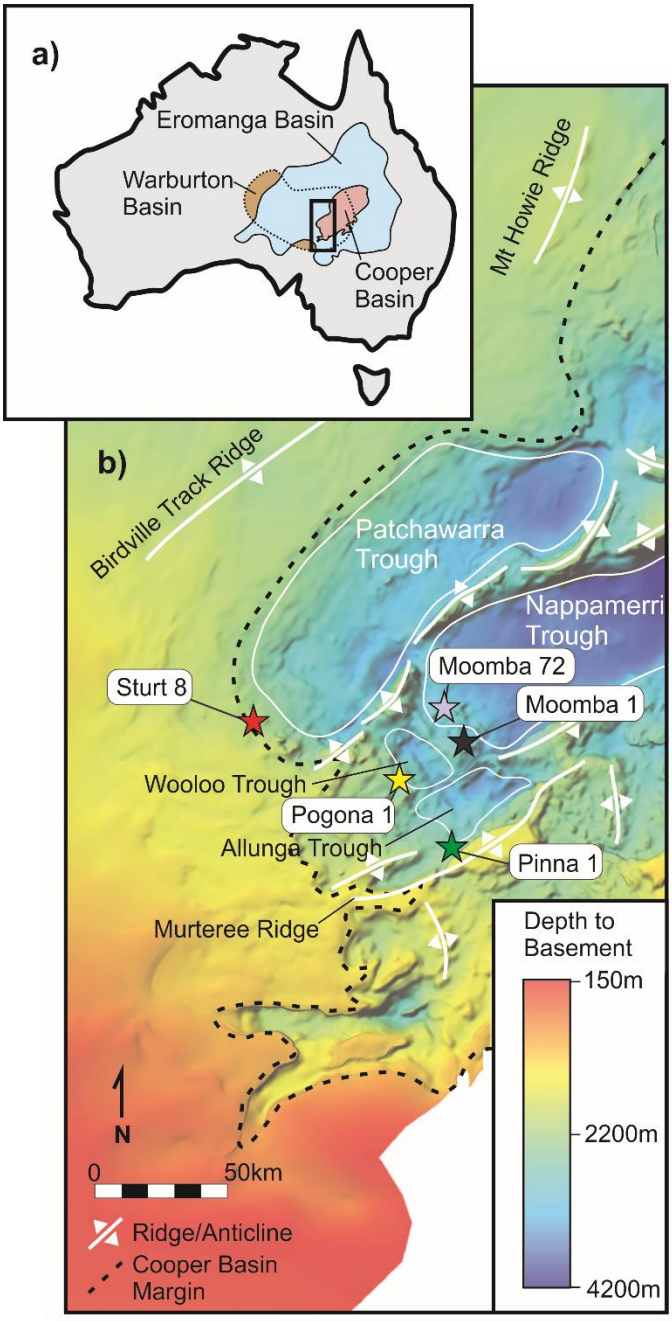

Figure 2: (a) Locations of the Warburton, Cooper and Eromanga Basin in Australia. Location of study area is shown by the black rectangle. Reproduced from figures presented by Gravestock et al. (1998) and McLaren & Dunlap (2006); (b) Depth to pre-Permian basement below the Cooper-Eromanga Basin in South Australia. Locations of sample wells and major structural features have been marked, and the extent of Cooper Basin is shown by the dashed line. Depth to basement map sourced from Government of South Australia, Department of State Development (2014), and major structural features adapted from Hall et al. (2015).

environments (Alexander & Hibburt, 1996; Drexel & Preiss, 1995; Jadoon et al., 2017). Due to the complex depositional environments, the sedimentary thickness varies considerably across the basin and many units are not laterally continuous across the basin (e.g. Gravestock et al., 1998).

[2.2] Eromanga Basin

The intracratonic Eromanga Basin is laterally more extensive in size than the Cooper Basin, covering much of central and eastern Australia (Figure 2a). Deposition in the Eromanga Basin began in the early Jurassic and continued to the late Cretaceous as the basin experienced progressive subsidence (Veevers, 2000), in a combination of fluvial, lacustrine and marine environments (Alexander & Hibburt, 1996). In north-eastern South Australia the Eromanga Basin blankets the undelying Cooper Basin, reaching maximum thicknesses of up to 3km in the Patchawarra Trough (Alexander &

Hibburt, 1996; Drexel & Preiss, 1995). Sediments in the Eromanga Basin are separated from upper Cooper Basin units by a major erosional unconformity that is attributed to basin uplift in the waning stages of the Hunter-Bowen Orogeny (~265-235 Ma) (Gravestock et al., 1998; Hall et al., 2015; Li, Rosenbaum, & Rubatto, 2012). Eromanga Basin sediments are unconformably overlain by the Eocene – Quaternary non-marine Lake Eyre Basin (Alexander & Hibburt, 1996; Mavromatidis, 2006, 2007). Erosion in the Eromanga Basin began in the late Cretaceous (~90 Ma) as the basin regime transitioned from subsidence to uplift (Idnurm & Senoir, 1978; O'Sullivan, Kohn, Foster, & Gleadow, 1995).

[2.3] Thermal History

Thermal history modelling of the Cooper-Eromanga Basin conducted by Duddy et al. (1999, 2002), using a combination of apatite fission track, zircon fission track and vitrinite reflectance data, suggests that basin temperatures were dominantly controlled by sedimentary burial, while periods of uplift and erosion had little effect. These authors proposed that temperature in the basin increased slowly with burial from the Permian to mid-Cretaceous, before increasing sharply to reach maximum paleotemperatures at ~97-75 Ma.

The cause of this rapid temperature increase is poorly defined, but may have been a response to rapid deposition of marine sediments with low thermal conductivity in the upper Eromanga Basin at ~120-95 Ma (Deighton & Hill, 1998). Thermal history modelling has suggested the basin cooled rapidly after the late Cretaceous thermal maximum (Duddy et al., 2002), which has been attributed to cooling of basement granites and/or hydrological processes (Deighton & Hill, 1998). Recent heating (~5-2 Ma) has been recognised by Duddy et al. (1999, 2002) from detrital apatite fission track

analysis, and McLaren & Dunlap (2006) through $^{40}Ar/^{39}Ar$ study of thermochronlogy in Big Lake Suite granites, although no robust explanation has yet been identified.

[2.4] Sedimentary Provenance

Provenance of the Cooper-Eromanga Basin to date has been poorly studied, with only minor radiometric dating of sediment conducted within the basin. Analysis of detrital zircons from the *Winton Formation* in the Eromanga Basin (stratigraphic age of 105-90 Ma, Alexander & Hibburt, 1996) from north-east Queensland by Tucker et al. (2016) yielded strong zircon U-Pb age peaks between 134-94 Ma, as well as minor age peaks from the Triassic to Mesoproterozoic. Grains from the Cretaceous age peak lie with the depositional age of the formation, and coincide with major pulses of volcanism in the Whitsunday Igneous Association (Ewart, Schon, & Chappell, 1992). Minor sediment input was sourced from the New England Orogeny, Thomson Orogeny, Musgrave Province, or recycled sediment from Tasmanide orogens (Tucker et al., 2016). Detrital zircon U-Pb ages from the *Mackunda Formation* (stratigraphic age of 105-90 Ma, Alexander & Hibburt, 1996) have shown no evidence of syn-depositional provenance, with the youngest age peak occurring at 133Ma (Tucker et al., 2016), however, do provide evidence of older populations, similar to those observed in the stratigraphically higher *Winton Formation*.

Detrital zircons from the *Namur Sandstone* (stratigraphic age of 150-138 Ma, Alexander & Hibburt, 1996) have yielded significantly older U-Pb age populations, with major age peaks in the Cambrian and Mesoproterozoic (Stephens, Reid, Hore,

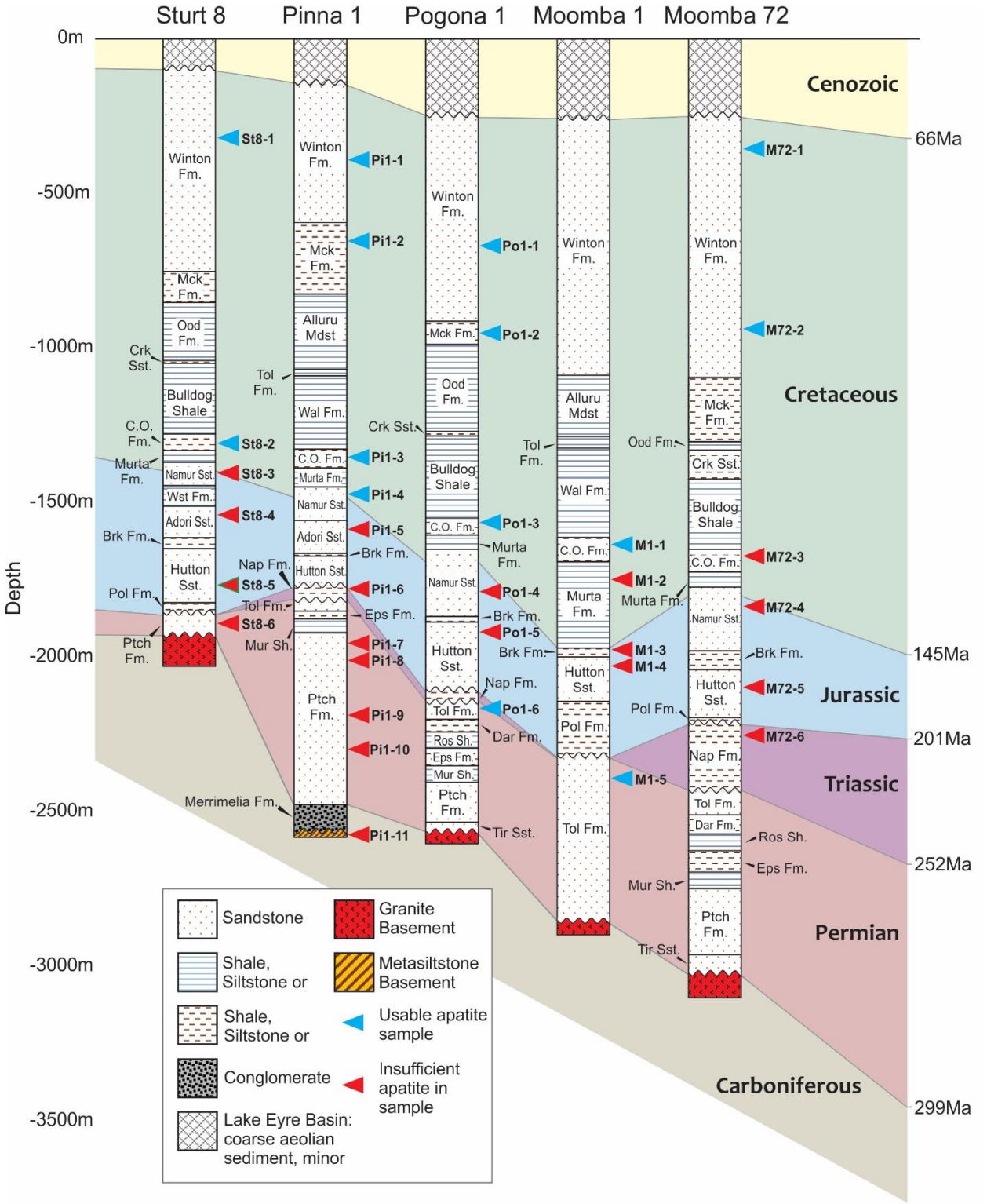

Figure 3: Summarised stratigraphy of sampled wells, correlated with the age of deposition. Markers denote the top of the area from which samples were taken. Samples were always constrained within a single stratigraphic unit. Blue sample markers represent those samples that yielded a sufficient quantity of apatites for analysis, red markers show samples with no apatite present or too little for analysis. Abbreviated lithologies are as follows: Mck Fm = Mackunda Formation; Ood Fm. = Oodnadatta Formation; Crk Sst. = Coorikiana Sandstone; Tol Fm. = Toolebuc Formation; Wal Fm. = Wallumbilla Formation; C.O. Fm. = Cadna Owie Formation; Wst Fm. = Westbourne Formation; Brk Fm. = Birkhead Formation; Pol Fm. = Poolawanna Formation; Nap Fm. = Nappamerri Formation; Tol Fm. = Toolachee Formation; Dar Fm. = Daralingie Formation; Ros Sh. = Roseneath Shale; Eps Fm. = Epsilon Formation; Mur Sh. = Murteree Shale; Ptch Fm. = Patchawarra Formation; Tir Sst. = Tirrawarra Sandstone. The stratigraphy was sourced from well completion reports (Delhi Petroleum Ltd, 1966, 1980; Santos Ltd, 1990, 1991, 1993).

Gilmore, & Hill, 2017), attributed to Tasmanide orogens and proximal basement outcrops. The stratigraphically lower *Birkhead Formation* (stratigraphic age of 150-138 Ma, Alexander & Hibburt, 1996) has shown evidence of volcanogenic provenance from ~800-1000 Ma (Boult et al., 1997).

Clast properties observed in the lowest Cooper Basin formation, the *Merrimelia Formation*, suggest that ~87% of sediment in this formation was sourced from intra-basinal material, derived from the underlying Warburton Basin (Chaney, Cubitt, & Williams, 1997). Minor distal sediment was likely derived from the nearby Neoproterozoic to Carboniferous Alice Springs or Petermann Orogenies.

[2.5] Sample Locations

Samples were taken from cuttings from five wells located on structural highs in the Cooper-Eromanga Basin (Figure 2b), to obtain samples presently below apatite partial annealing zone temperatures of ~60-120^{o}C. Two sampled wells, Moomba 1 and Moomba 72, were located on the western margin of the Nappamerri Trough, an area dominated by Carboniferous granites from the Big Lake Suite (Beardsmore, 2004; Gatehouse et al., 1995). The Pogona 1 and Sturt 8 wells were situated on the south-western margin of the Wooloo Trough and Patchawarra Trough, respectively. In these wells, the lowest Cooper Basin sediments directly overlie basement granites (Figure 3) from the Big Lake Suite (Gatehouse et al., 1995; Santos Ltd, 1990, 1991). The Pinna 1 well was located on the southern margin of the Allunga Trough, and differs from other sampled wells in that the Cooper Basin sediments were underlain by a meta-siltstone unit from the Warburton Basin (Delhi Petroleum Ltd, 1980). Present day thermal

gradients of sampled wells were constrained between ~42-50^{o}C (Dehli Petroleum Ltd, 1966, 1980; Santos Ltd, 1990, 1991, 1993).

[3] METHODS

[3.1] Laboratory Processing

Apatite samples were prepared using conventional methods for fission track and U-Pb laser-ablation analysis (e.g. Glorie et al., 2017). Mineral separation was performed using a combination of magnetic and heavy liquid processing, and apatite grains mounted in EpoxyCure resin (see Appendix B for full process outline). Samples were etched in a solution of 5M nitric acid (HNO_3) at 20±0.5^{o}C for 20±0.5 seconds to reveal fission tracks for counting.

[3.2] Fission Track Counting

Individual grains from apatite bearing samples were imaged on a Zeiss AXIO Imager M2m Autoscan System, and surface track densities and confined track lengths measured using FastTracks software. These fission track densities are known to be correlated with the fission track age and ^{238}U concentration (Wagner & Van den haute, 1992). The fission track age reflects the timing of passage through the so-called apatite partial annealing zone (APAZ) at temperatures of ~60-120^{o}C (Wagner & Van den haute, 1992).

[3.3] LA-ICP-MS Analysis

Analysis for U, Pb, Cl and rare earth elements was conducted using laser ablation inductively coupled plasma mass spectrometry (LA-ICP-MS) on a solid state New Wave-213 laser connected to an Agilent 7900x mass spectrometer (analytical

Table 1: Analytical details for LA-ICP-MS analysis used in AUPb and AFT dating. Standards used with reference to Chew et al. (2014)

Laser	
Type	Solid State Nd:YAG
Brand and Model	ESI NWR213
Wavelength	213nm
Pulse Duration	~4ns
Spot Size	30µm
Repetition Rate	5Hz
Energy Attenuation	50%
Laser Fluency	~4 J/cm^2
ICP-MS	
Brand and Model	Agilent 7900x
Forward Power	1350W
Torch Depth	4.5mm
Gas Flows	
Plasma (Ar) Auxiliary (Ar)	15L/min 1L/min
Carrier (He)	0.7L/min
Sample (Ar)	0.88L/min
Data Acquisition Parameters	
Data Acquisition Protocol	Time-resolved Analysis
Scanned Isotopes	Si-29, Cl-35, Ca-43, Ca-44, V-51, Mn-55, Sr-88, Y-89, Zr-90, La-139, Ce-140, Pr-141, Nd-146, Sm-147, Eu-153, Gd-157, Tb-159, Dy-163, Ho-165, Er-166, Tm-169, Yb-172, Lu-175, Hg-202, Pb-204, Pb206, Pb-207, Pb-208, Th-232, U-238
Detector Mode	Peak Hopping, Pulse & Analog Counting
Background Collection	30s
Ablation for Age Calculation	30s
Washout	20s
Standards	
Primary Standards	NIST 610, Madagascar apatite
Secondary Standards	Durango apatite, McClure apatite

details provided in Table 1). A single 30µm spot was ablated for each grain, excluding grains that exhibited clear zonation patterns in fission track densities. Data collection was performed over three analytical sessions, with standard blocks interspaced within each session. Data reduction was performed with Iolite software (Paton, Hellstrom, Paul, Woodhead, & Hergt, 2011) using Madagascar apatite as the primary standard for U-Pb analysis, and NIST 610 as the primary standard for AFT and REE analysis. Durango and McClure apatite were used as secondary standards to test the accuracy of results.

[3.4] ^{252}Cf Irradiation

After laser ablation, samples were repolished to remove all previously etched tracks and laser damage, to be irradiated with a ^{252}Cf source at the University of Melbourne. This treatment was performed to increase the likelihood of revealing confined tracks (e.g. Donelick & Miller, 1991) for use in thermal modelling. The irradiated samples were subsequently etched and

analysed for confined track lengths using the same protocols as with un-irradiated samples.

[3.5] Apatite U-Pb Age Analysis

Unlike minerals such as zircon, apatite contains significant quantities of common-Pb and cannot produce robust single grain AUPb ages. Therefore, a population of grains is needed to calculate an AUPb age, using a linear regression in a Tera-Wasserburg Concordia plot. The lower intercept of this regression through apatite grains of a single population exhibits the AUPb age for the analysed sample. This age reflects the timing of cessation of Pb diffusion at typical temperatures of ~350-550ºC (Chew, Petrus, & Kamber, 2014). The common-Pb line can also be used to correct for common-Pb in individual grains using a ^{207}Pb correction (Chew et al. 2014), to produce a ^{207}Pb corrected ^{238}U/^{206}Pb weighted mean AUPb age from all grains in a single age population.

[3.6] Rare Earth Elemental Analysis

Rare earth elemental (REE) signatures in apatite can give insight into the conditions in which grains crystallised, which can be used to help constrain provenance. REE concentrations were measured by LA-ICP-MS and normalised to chondrite data from Sun & McDonough (1989) for comparison with other studies. Mafic-sourced apatites show depletion in heavy rare earth elements compared to signatures typically observed in felsic-sourced apatite (Belousova, Griffin, O'Reilly, & Fisher, 2002), while metamorphic apatites show depletion in light rare earth elements (Harlov, 2015; Henrichs, Chew, & Babechuk, In Press).

[3.7] Apatite Fission Track Thermochronology

Fission track ages were calculated by comparing direct measurements of ^{238}U obtained from LA-ICP-MS for each grain against the number of spontaneous tracks using in-house Excel spreadsheets, following the methodology outlined in Gillespie et al. (2017), Gleadow, Harrison, Kohn, Lugo-Zazueta, & Phillips (2015) and Glorie et al. (2017). To correct for analyst counting bias, a Durango apatite standard was counted and analysed in the same laser sessions as unknown samples to produce a zeta calibration factor (Vermeesch, 2017). Fission track age populations present in apatite samples were identified using radial plots, generated using the Java plugin RadialPlotter (Vermeesch, 2009, 2017).

Thermal history modelling was performed using QTQt software (Gallagher, 2012) with modelling inputs of single grain ATF ages and associated uncertainty, confined track lengths, and single grain Cl concentration. Samples were modelled as a depth profile, constrained to present day depth, to produce internally consistent models. In addition, vitrinite reflectance (VR) data obtained from samples at comparable depths to the analysed samples was used in the modelling protocols to constrain the maximum heating temperatures (VR data provided in Appendix A). Each individual sample was constrained to present day temperature, and to 22.5±2.5^{o}C at stratigraphic age to represent surface temperatures at the time of deposition.

[4] RESULTS

[4.1] Apatite U-Pb

[4.1.1] DATA ACCURACY

Secondary standards of Durango apatite and McClure apatite were analysed interspaced with the unknown apatite samples to act as accuracy checks on the U-Pb data. Durango apatite returned a ^{207}Pb corrected ^{238}U/^{206}Pb weighted mean age of 32.3±1.5 Ma, while McClure apatite standards returned a weighted mean age of 516±13 Ma (Figure 4). These ages fall within error of published ^{40}Ar/^{39}Ar ages for Durango apatite of 31.44±0.18 Ma (McDowell, McIntosh, & Farley, 2005) and published AUPb ages for McClure apatite of 524.6±3.2 Ma (Chew et al., 2014). Therefore, the AUPb ages for the unknown samples presented in this study can be used with confidence. However, it must be noted that several samples in this study exhibit high common-Pb and, therefore, cluster near the upper intercept in Tera-Wasserburg plots. This adds uncertainty to the calculated common-Pb regression lines, and hence any ^{207}Pb–corrected ages derived from this regression.

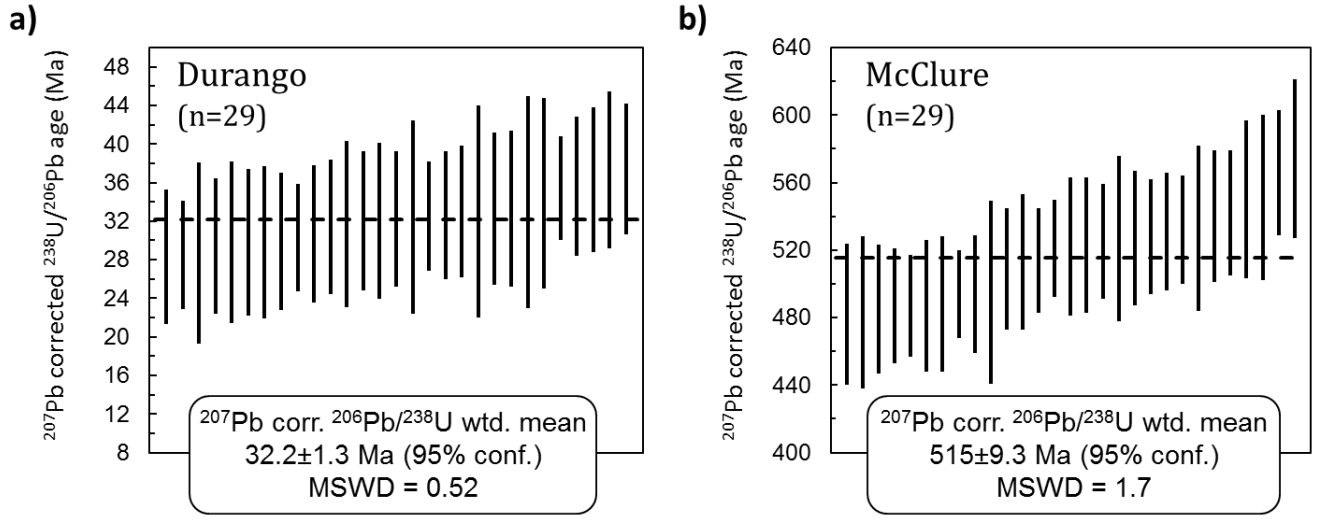

Figure 4: Weighted mean U-Pb ^{207}Pb corrected ^{206}Pb/^{238}U ages for the analysed secondary standards: (a) Durango apatite and (b) McClure apatite.

WINTON FORMATION

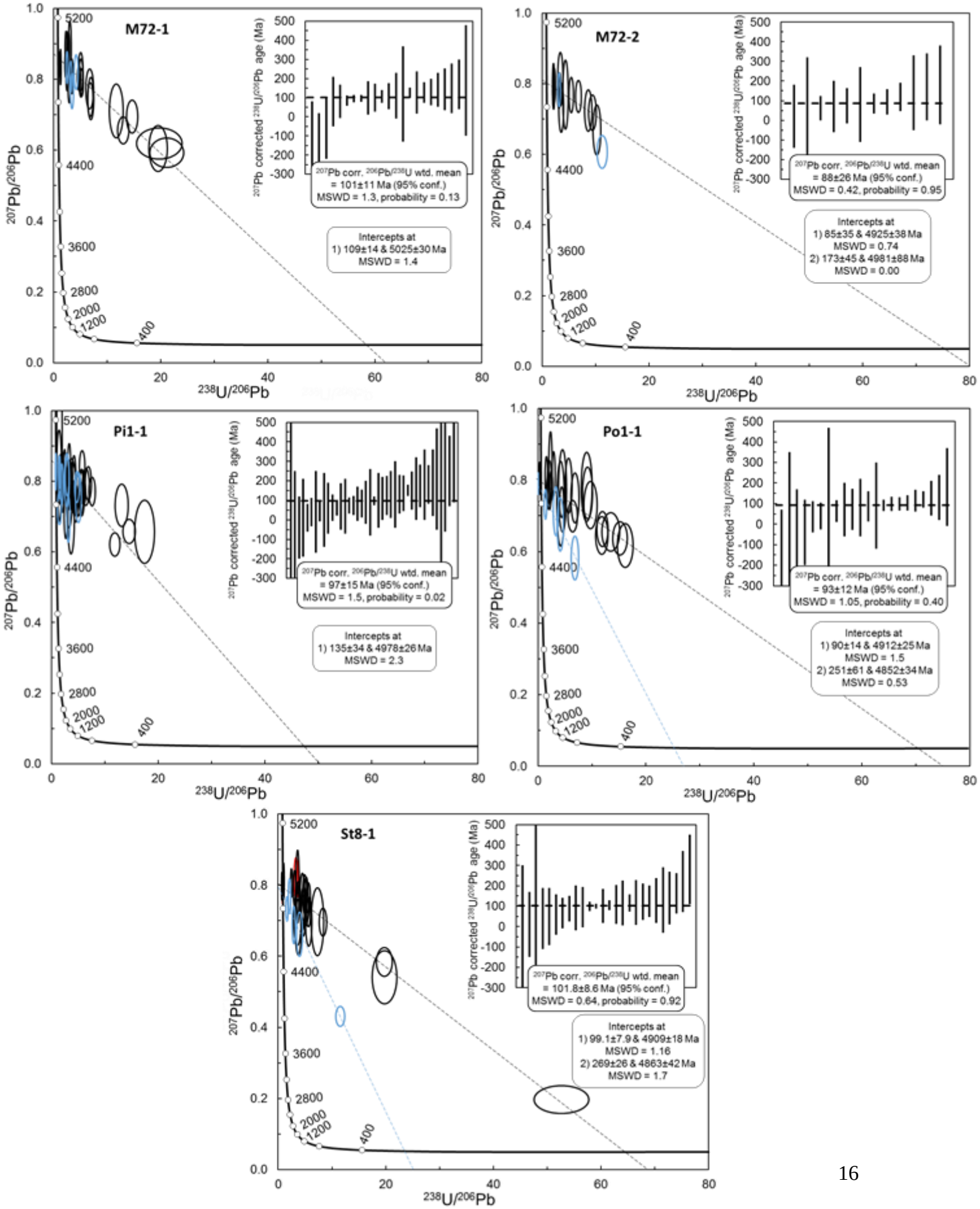

MACKUNDA FORMATION

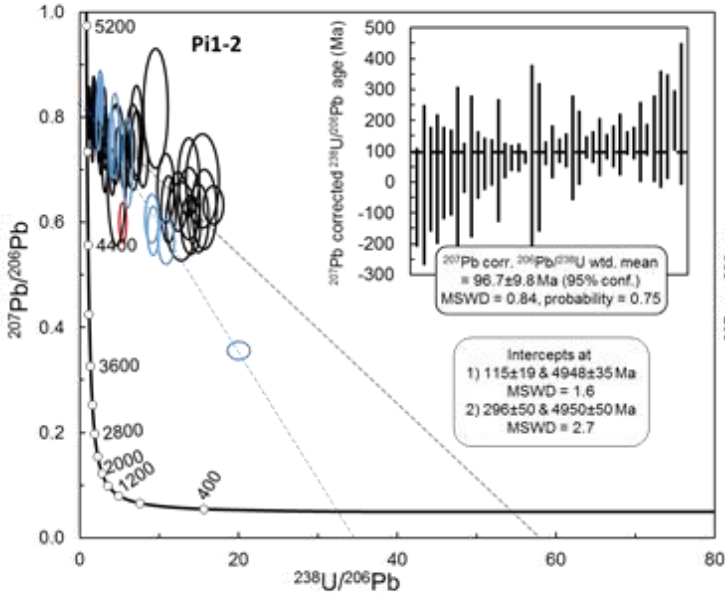

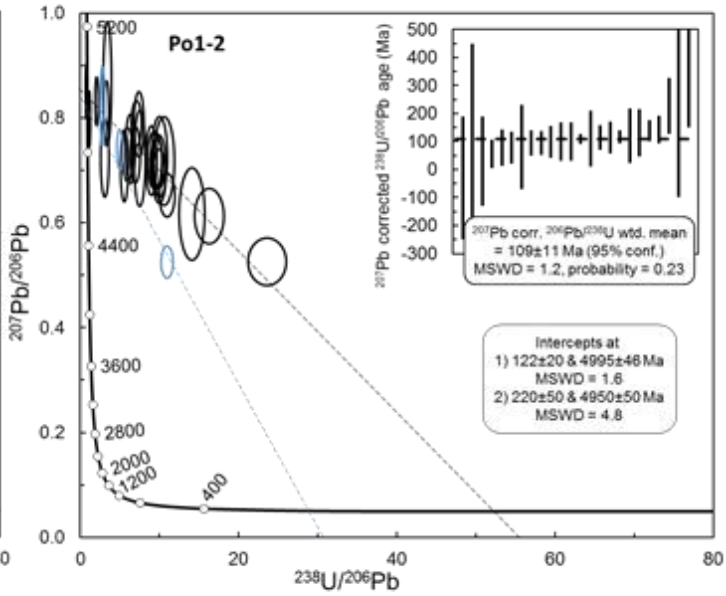

CADNA OWIE FORMATION

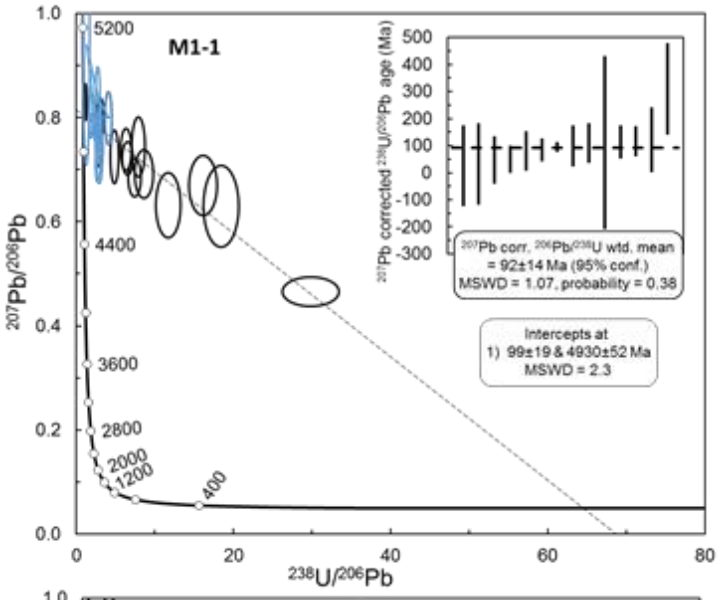

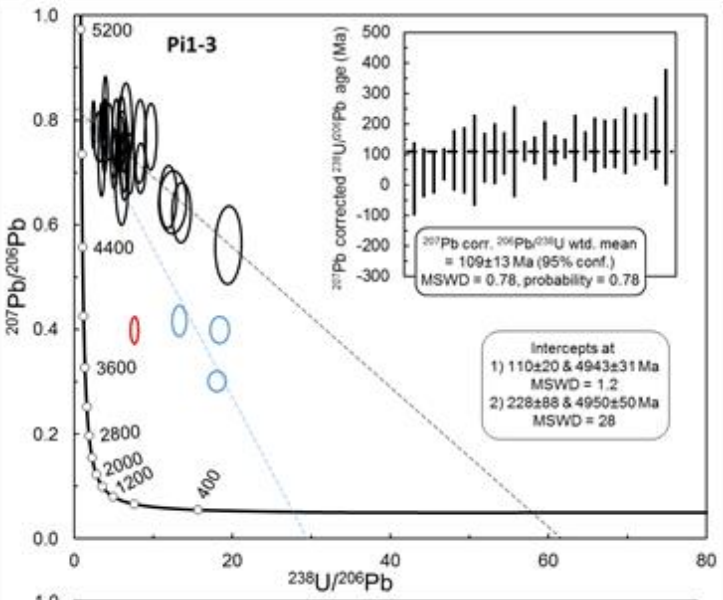

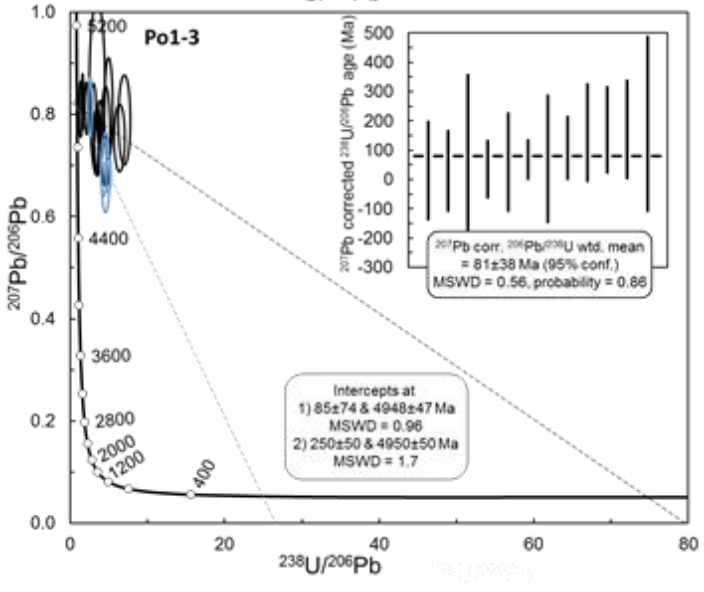

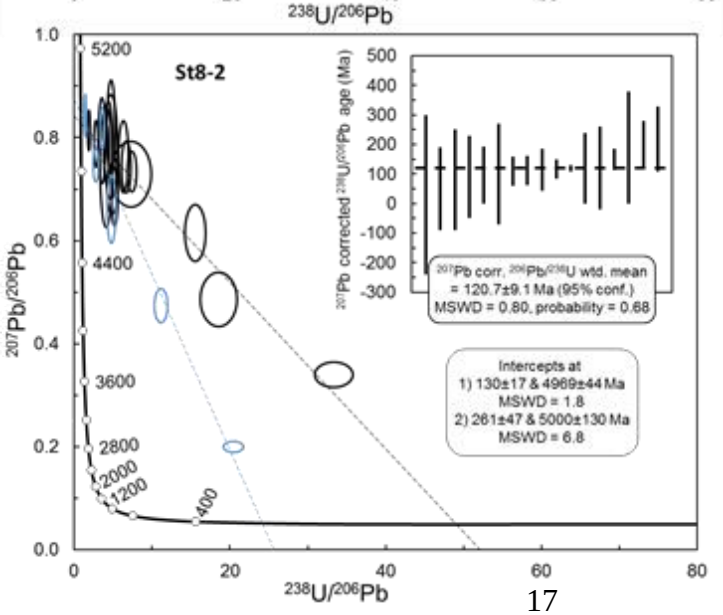

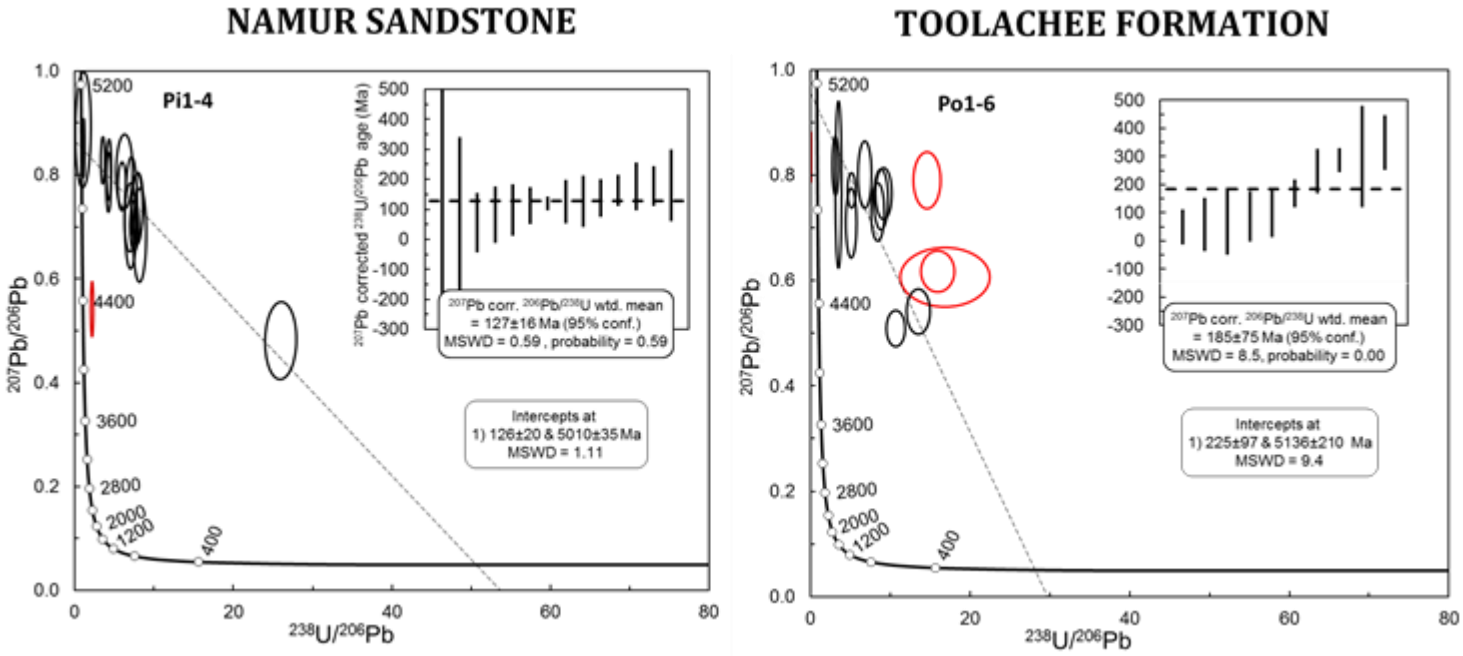

Figure 5: Tera-Wasserburg Concordia plots for all Cooper-Eromanga Basin samples. Each ellipse represents 2σ error range for ^{207}Pb/^{206}Pb and ^{238}U/^{206}Pb of an individual apatite grain. Black ellipses denote samples used to produce the primary common-Pb line. The lower intercept of common-Pb lines represents the time grains cooled below the Pb diffusion temperature of ~350-550ºC (Chew et al., 2014; Chew & Spikings, 2015). In many cases samples contained a secondary age population, for which the data ellipses are colour coded in blue. Samples Pi1-2, Pi1-3 Po1-2 and Po1-3 showed poor spread of ^{207}Pb/^{206}Pb and ^{238}U/^{206}Pb ratios in secondary age populations, which produced high uncertainty for both upper and lower age intercepts. However, blue ellipses for these samples confidently define an older secondary age population, as respective AFT ages for these grains yield ages that match with an older (~300-200 Ma) age population (as further discussed below in section 4.3.2). For these samples, the upper intercept of the common-Pb regression to was anchored values consistent with those of better defined secondary age populations from the same formation, and yielded lower intercept ages comparable to these samples. Similarly, samples M1-1, M72-1, M72-2 and Pi1-1 yielded grains that defined an older, secondary age population, as shown by AFT ages of corresponding grains, but did not display adequate variations in common-Pb abundance to perform reliable regression (for full treatment rational see Appendix B). Red ellipses denote outliers that were excluded in further discussion. Inserts show weighted mean ^{207}Pb corrected ^{206}Pb/^{238}U ages for each grain used in primary common-Pb lines, where error bars represent 2σ. Weighted mean plots for all samples produced MSWD values ≤1.5, and illustrate that grains included in primary age populations can likely be considered as a single population (with the exception of sample Po1-6), however, since uncertainty of the common-Pb regression was not considered for these plots, only Tera-Wasserburg intercept ages have been used in further discussion.

[4.1.2] EROMANGA BASIN

Twelve apatite samples were analysed from the Eromanga Basin. Tera-Wasserburg Concordia plots for these samples show that most samples contained grains that cannot be satisfied by a single common-Pb regression line (Figure 5). The presence of these outliers suggests some grains experienced open system behaviour (e.g. resetting by a thermal event), or that multiple age populations were present. Given that the

outliers often define a secondary common-Pb regression line, outliers in each sample were treated as a separate (secondary) population.

Primary Age Populations

The majority of grains from each sample plot along a single regression line and, therefore, define a (primary) age population (Table 2, Figure 5). The primary ages for all samples fall within error of the depositional age of their host sedimentary formation. For the *Winton Formation* (stratigraphic age of 105-90 Ma, Alexander & Hibburt, 1996), the weighted mean AUPb age from the five samples was 100±12 Ma (Figure 6). For the *Mackunda Formation* (stratigraphic age of 105-90 Ma, Alexander & Hibburt, 1996), the obtained weighted mean AUPb age from the two samples was 118±13Ma. For the *Cadna Owie Formation* (stratigraphic age of 125-120 Ma, Alexander & Hibburt, 1996), the weighted mean AUPb age from four samples was 114±25 Ma. For the *Namur Sandstone* (stratigraphic age of 150-138 Ma, Alexander & Hibburt, 1996), only one sample was analysed, yielding an AUPb age of 126±20 Ma.

Samples Po1-3 (85±74 Ma) and M72-2 (85±35 Ma) showed exceptionally large errors associated with lower intercept ages, which can be attributed the relatively high abundance of common-Pb in all analysed grains from these samples. Consequently the, common-Pb regression is poorly defined for these samples, and quoted ages should be treated with caution.

Secondary Age Population

Samples Po1-1, Po1-2, Po1-3, Pi1-2, Pi1-3, St8-1 and St8-2 contain grains fitting an older (secondary) common-Pb regression on Tera-Wasserberg Concordia plots (Figure 5). Secondary age populations were largely consistent across all Eromanga

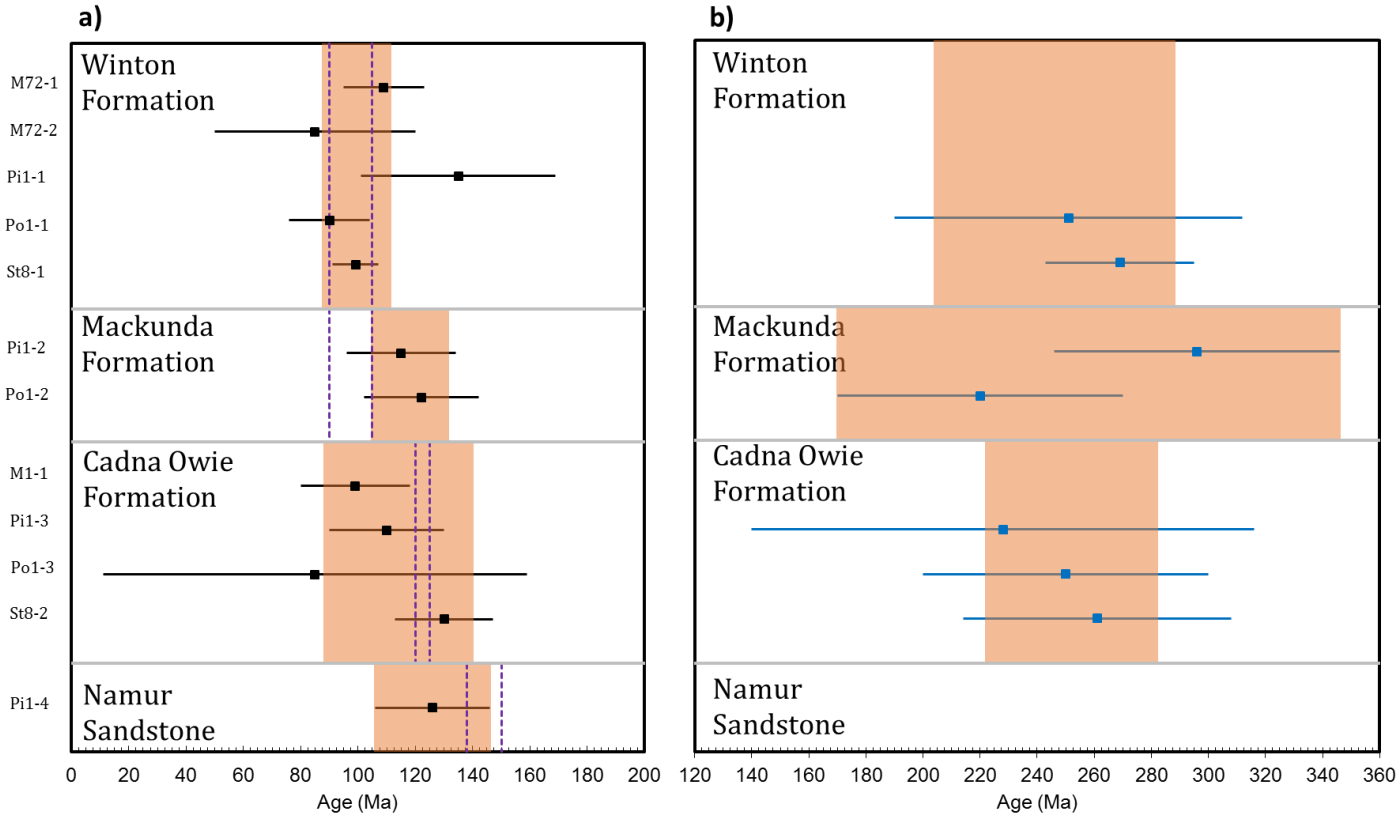

Figure 6: Apatite U-Pb ages from all samples from the Eromanga Basin. Tera-Wasserburg lower intercept ages and associated uncertainties have been shown for each sample individually, with primary age populations in panel (a), and secondary age populations in panel (b) (where applicable). Orange envelopes show mean apatite U-Pb age for all samples from a single formation, and dashed lines constrain allowable depositional ages for formation (Alexander & Hibburt, 1996; Gravestock et al., 1998). For the *Namur Sandstone*, only one sample yielded a primary AUPb age, which has been used instead of a mean age for this formation.

formations analysed (excluding the *Namur Sandstone*, which yielded no secondary age peak), with AUPb ages ranging between 296±50 Ma and 228±88 Ma (Table 2).

The *Winton Formation* (stratigraphic age of 105-90 Ma, Alexander & Hibburt, 1996) yielded a mean secondary AUPb age of 266±23 Ma (Figure 6). The *Mackunda Formation* (stratigraphic age of 105-90 Ma, Alexander & Hibburt, 1996), yielded a mean secondary AUPb age of 258±88Ma. For the *Cadna Owie Formation* (stratigraphic age of 125-120Ma, Alexander & Hibburt, 1996), the weighted mean AUPb age was 252±31Ma. The *Namur Sandstone* did not produce a secondary age population.

In addition to the secondary age populations discussed above, older grains attributed to secondary populations were identified for samples M1-1, M72-1, M72-2

and Pi1-1 (Figure 5), based on apatite fission track data. These grains yield AFT ages significantly older than the stratigraphic age of the rock and thus reflect provenance information (as discussed below in section 4.3.2). Given the high common-Pb ratios for grains in these samples, populations could not be distinguished with the use of U-Pb data alone (see Appendix B for extended selection method). Furthermore, the lack of variation in common-Pb hindered reliable isochron regression, hence, no AUPb age could be calculated for grains in these samples.

Table 2: Summary of apatite U-Pb ages from Cooper-Eromanga Basin samples, as determined by Tera-Wasserburg Concordia lower intercepts. Primary and secondary age populations correspond to those identified in Tera-Wasserburg plots given in Figure 5. Unassigned grains denote all grains not included in either primary or secondary age populations. Stratigraphic ages for units are based on palynostratigraphy presented by Alexander & Hibbert (1996) and Gravestock et al. (1998).

Sample	Primary Age Population (Ma)	Grains	Secondary Age Population(Ma)	Grains	Unassigned Grains
Winton Formation 105-90Ma					
M72-1	109±14	23	-	4	0
M72-2	85±35	12	-	2	0
Pi1-1	135±34	40	-	12	0
Po1-1	90±14	22	251±61	5	0
St8-1	99.1±7.9	26	269±26	5	3
Mackunda Formation 105-90Ma					
Pi1-2	115±19	40	296±50	10	1
Po1-2	122±20	24	220±50	3	0
Cadna Owie Formation 125-120Ma					
M1-1	99±19	13	-	8	0
Pi1-3	110±20	26	228±88	3	1
Po1-3	85±74	12	250±50	4	0
St8-2	130±17	17	261±47	5	0
Namur Sandstone 150-138Ma					
Pi1-4	126±20	14	-	-	1
Toolachee Formation 257-248Ma					
Po1-6	225+97	10	-	-	3

[4.1.3] COOPER BASIN

Only two samples from the Cooper Basin were analysed for AUPb age in this study. As sample M1-5 only yielded three apatite grains it was not considered in further discussion. Sample Po1-6 from the *Toolachee Formation* (stratigraphic age of 257-248 Ma, Gravestock et al., 1998), however, did yield sufficient apatite for U-Pb analysis. Unlike the Eromanga Basin samples, this sample exhibited a large scatter of $^{207}Pb/^{206}Pb$ and $^{238}U/^{206}Pb$ ratios, hindering robust age calculations. Excluding the three anomalously young grains in the Tera-Wasserburg plot (for which no confident AUPb age could be derived), a single common-Pb regression yielded an AUPb age of 225±97 Ma, which lies within uncertainty of the stratigraphic age of this sample. The large uncertainty and large associated MSWD (9.4), however, suggest that a single regression is not appropriate, and that multiple age populations exist in the sample. Due to the low number of grains in this sample, however, individual populations could not be distinguished.

[4.2] Rare Earth Elements

[4.2.1] EROMANGA BASIN

Chondrite normalised rare earth elemental patterns showed strong similarities between Eromanga Basin formations (Figure 7), exhibiting a decreasing trend from light rare earth elements (LREEs) to heavy rare earth elements (HREEs). Some grains showed a negative Eu anomaly, while others exhibited little to no deviation from the general trend. The negative Eu anomaly, however, was not diagnostic of neither primary nor secondary populations.

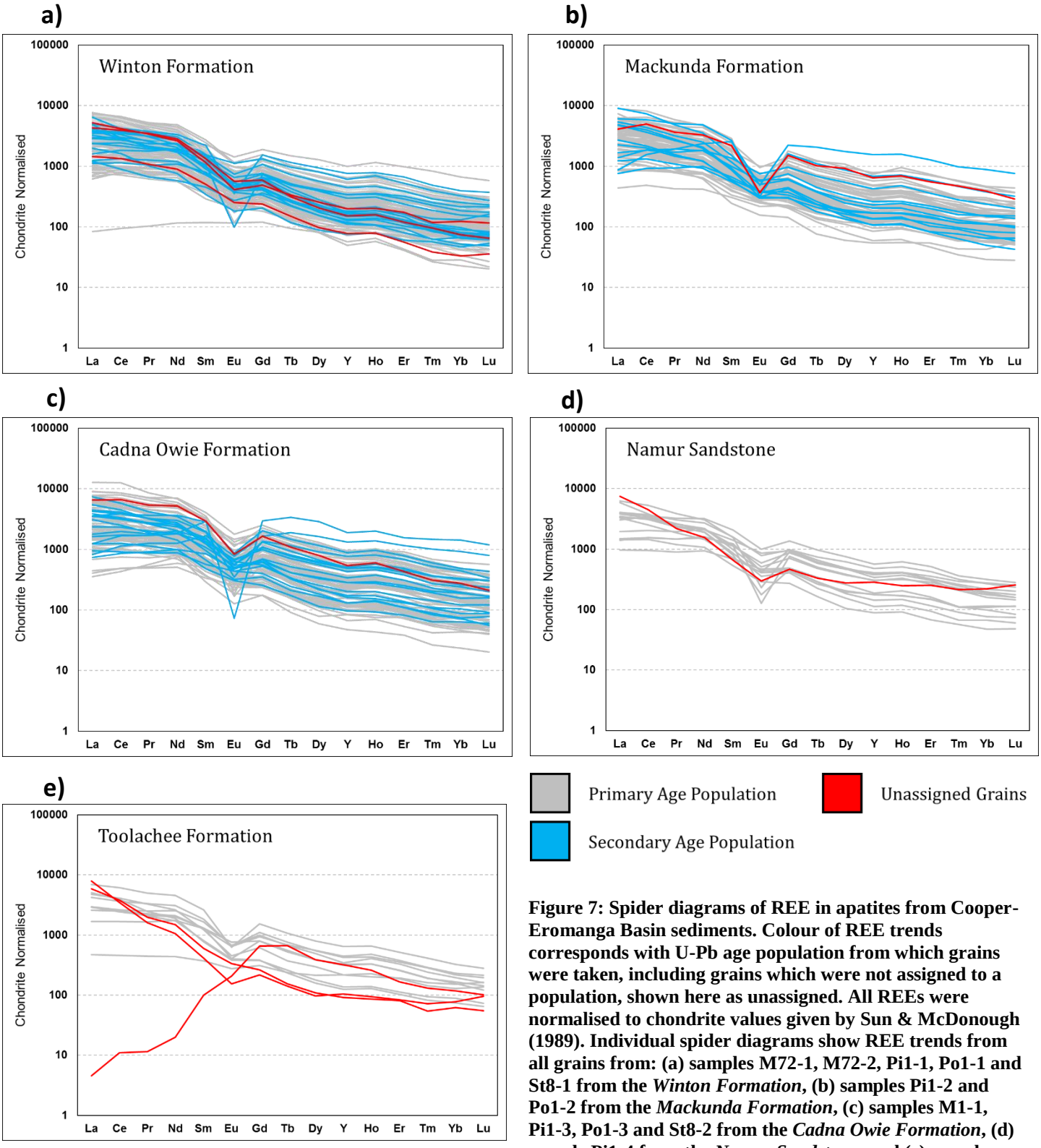

Figure 7: Spider diagrams of REE in apatites from Cooper-Eromanga Basin sediments. Colour of REE trends corresponds with U-Pb age population from which grains were taken, including grains which were not assigned to a population, shown here as unassigned. All REEs were normalised to chondrite values given by Sun & McDonough (1989). Individual spider diagrams show REE trends from all grains from: (a) samples M72-1, M72-2, Pi1-1, Po1-1 and St8-1 from the *Winton Formation*, (b) samples Pi1-2 and Po1-2 from the *Mackunda Formation*, (c) samples M1-1, Pi1-3, Po1-3 and St8-2 from the *Cadna Owie Formation*, (d) sample Pi1-4 from the *Namur Sandstone*, and (e) sample Po1-6 from the *Toolachee Formation*.

[4.2.2] COOPER BASIN

Sample Po1-6 from the *Toolachee Formation* was the only sample in this study from the Cooper Basin analysed for REEs. The majority of grains yielded trends comparable to those observed in Eromanga Basin samples (Figure 7), however, one grain displayed LREE abundances reduced by ~3 orders of magnitude.

[4.3] Apatite Fission Track

[4.3.1] DATA ACCURACY

Single grain AFT ages for unknown samples were corrected with a zeta calibration derived using Durango apatite standards of known age (Vermeesch, 2017). The mean AFT age of 30.6±1.3 Ma (Figure 8) was within error of the published $^{40}Ar/^{39}Ar$ age of 31.44±0.18 Ma (McDowell et al., 2005), suggesting fission track counting and LA-ICP-MS analysis were reliable.

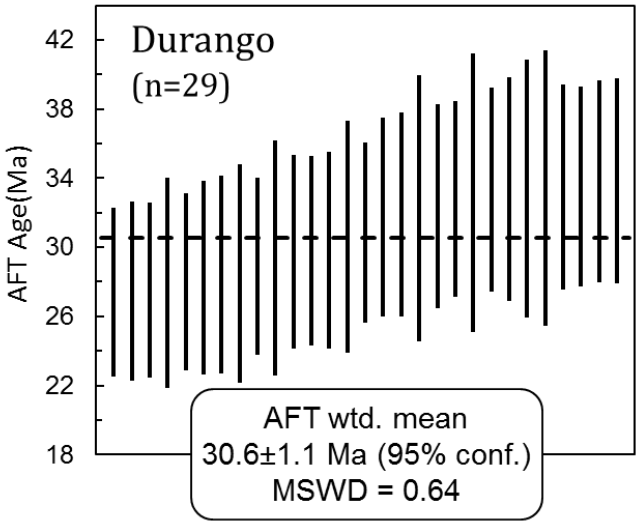

Figure 8: Weighted mean AFT age for Durango apatite standard.

[4.3.2] RADIAL PLOTS

The following section describes AFT results as obtained from the radial plots in Figure 9. Individual grains in radial plots were colour coded in accordance with the AUPb age peak to which they were assigned (black for grains in the younger, primary AUPb populations, and white for grains in the older, secondary AUPb populations or

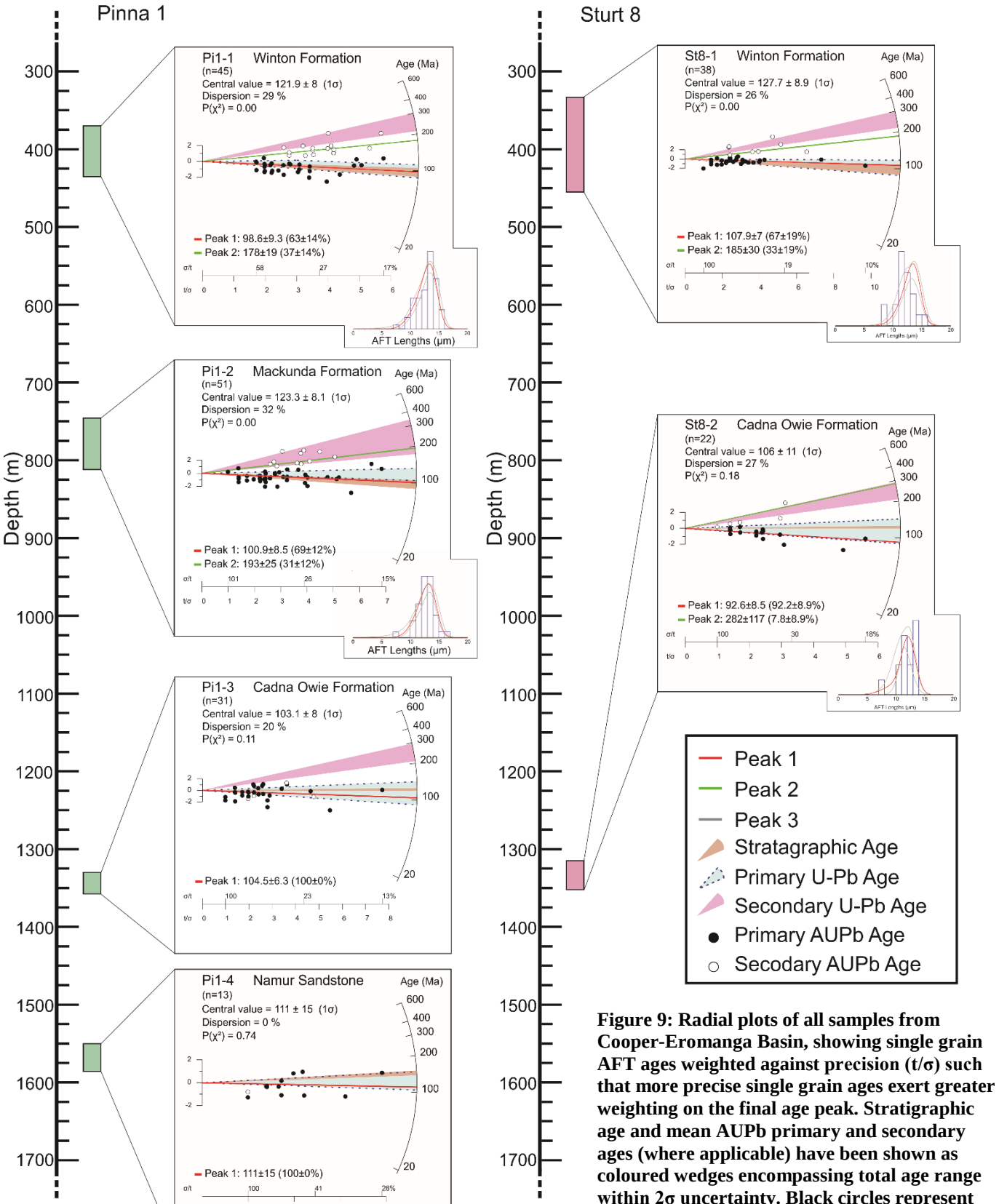

Figure 9: Radial plots of all samples from Cooper-Eromanga Basin, showing single grain AFT ages weighted against precision (t/σ) such that more precise single grain ages exert greater weighting on the final age peak. Stratigraphic age and mean AUPb primary and secondary ages (where applicable) have been shown as coloured wedges encompassing total age range within 2σ uncertainty. Black circles represent attributed to primary AUPb age populations, white circles encompass grains from secondary AUPb ages and grains not assigned to an age population. Insets show distributions of confined track lengths.

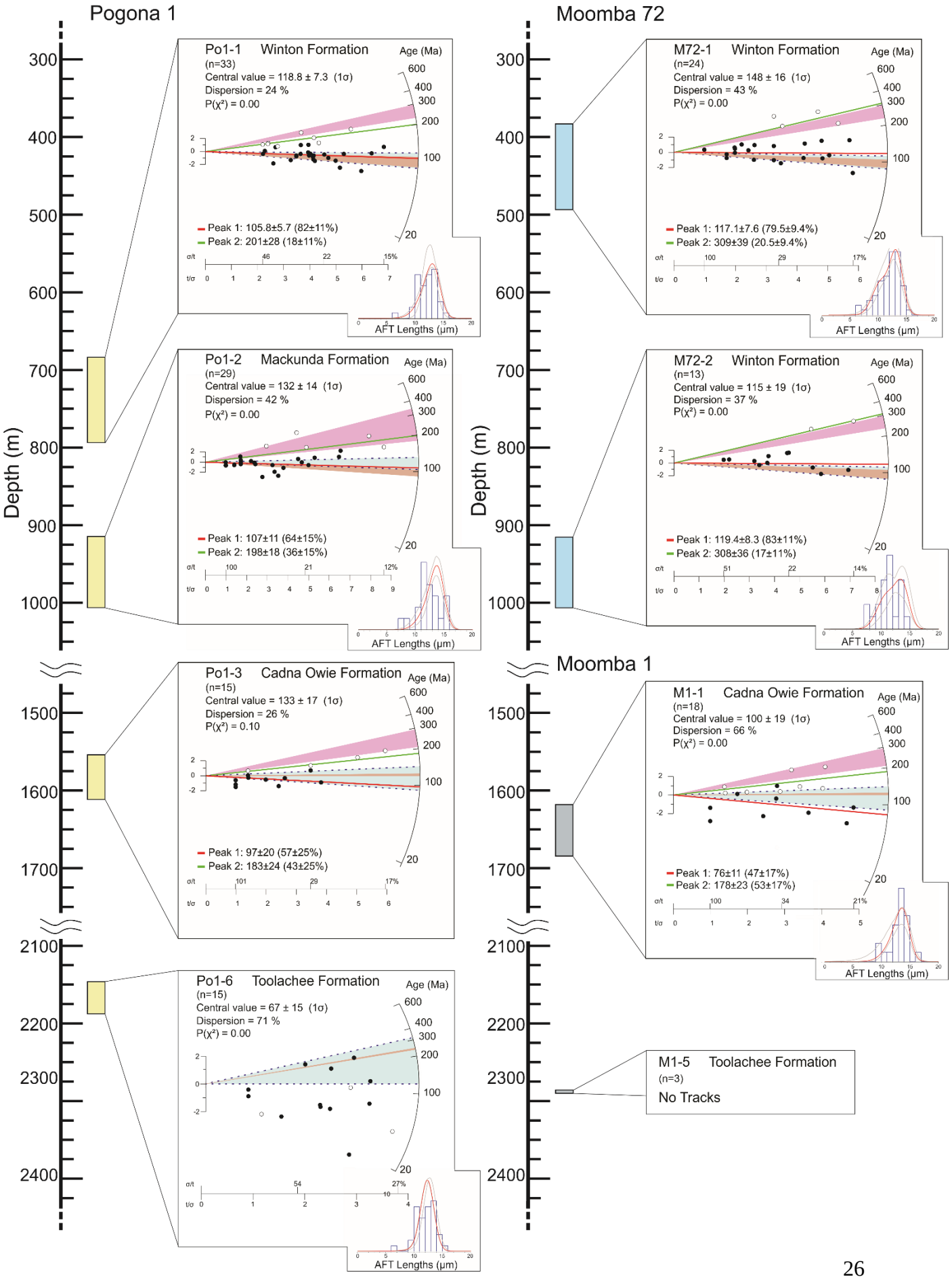
Pogona 1
Moomba 72
Moomba 1
Depth (m)
Po1-1 Winton Formation
(n=33)
Central value = 118.8 ± 7.3 (1σ)
Dispersion = 24 %
P(χ²) = 0.00
Peak 1: 105.8±5.7 (82±11%)
Peak 2: 201±28 (18±11%)
Po1-2 Mackunda Formation
(n=29)
Central value = 132 ± 14 (1σ)
Dispersion = 42 %
P(χ²) = 0.00
Peak 1: 107±11 (64±15%)
Peak 2: 198±18 (36±15%)
Po1-3 Cadna Owie Formation
(n=15)
Central value = 133 ± 17 (1σ)
Dispersion = 26 %
P(χ²) = 0.10
Peak 1: 97±20 (57±25%)
Peak 2: 183±24 (43±25%)
Po1-6 Toolachee Formation
(n=15)
Central value = 67 ± 15 (1σ)
Dispersion = 71 %
P(χ²) = 0.00
M72-1 Winton Formation
(n=24)
Central value = 148 ± 16 (1σ)
Dispersion = 43 %
P(χ²) = 0.00
Peak 1: 117.1±7.6 (79.5±9.4%)
Peak 2: 309±39 (20.5±9.4%)
M72-2 Winton Formation
(n=13)
Central value = 115 ± 19 (1σ)
Dispersion = 37 %
P(χ²) = 0.00
Peak 1: 119.4±8.3 (83±11%)
Peak 2: 308±36 (17±11%)
M1-1 Cadna Owie Formation
(n=18)
Central value = 100 ± 19 (1σ)
Dispersion = 66 %
P(χ²) = 0.00
Peak 1: 76±11 (47±17%)
Peak 2: 178±23 (53±17%)
M1-5 Toolachee Formation
(n=3)
No Tracks
Age (Ma)
AFT Lengths (µm)

Table 3: Summary of AFT results grouped by sample well. ρ_s represents the average surface density of spontaneous fission tracks. Ns represents the total number of spontaneous fission tracks counted in all grains analysed in the sample. n is the number of grains analysed in the sample. ^{238}U represents average concentration of ^{238}U in all grains analysed, with uncertainty given as 1σ. P.Age is the pooled AFT age (Donelick, O'Sullivan, & Ketcham, 2005), calculated by in-house Excel spreadsheets (e.g. Glorie et al., 2017). C. Age is the central AFT age as calculated with RadialPlotter (Vermeesch, 2009), and is the preferred age in further discussions for samples with a single AFT age population. Disp. represents the percentage of dispersion of single grain AFT ages calculated with Radial Plotter. P(χ^2) is the chi-squared probability that all grains in a sample belong to a single age population. When P(χ^2) is >0.05 and dispersion is <25% the sample passes this test. nl is the number of confined tracks measured from all grains in a sample. MTL is the mean track length of confined tracks per sample, with uncertainty quoted as 1σ. Using RadialPlotter, samples were tested for multiple age populations, where P1 and P2 represent different identified populations.

Sample ID	ρ_s (x10^5/cm^2)	Ns	n	^{238}U±1σ (ug/g)	P. Age ±1σ (Ma)	C. Age ±1σ (Ma)	Disp (%)	P(χ^2)	nl	MTL ±SD (µm)	P1±1σ (Ma)	P2±1σ (Ma)
Moomba 1												
M1-1	4.146	176	17	6.05±0.44	85.5±27.3	116±17	44	0.00	22	13.1±1.7	76±11	178±23
M1-5	0	0	3	69.63±4.97	0	0	-	-	-	-	-	-
Moomba 72												
M72-1	4.287	356	23	5.78±0.39	142.1±36.7	148±16	43	0.00	59	11.8±2.1	117.1±7.6	309±39
M72-2	7.899	390	13	4.63±0.31	168.7±45.6	115±19	37	0.00	21	11.2±2.0	119.4±8.3	308±36
Pinna 1												
Pi1-1	5.230	563	45	4.43±0.29	111.5±32.3	121.9±8	29	0.00	28	12.7±1.7	98.6±9.3	178±19
Pi1-2	3.393	754	51	6.94±0.42	129.0±34.5	123.3±8.1	32	0.00	38	12.8±1.5	100.9±8.5	193±25
Pi1-3	2.726	331	31	8.36±0.53	97.1±30.3	108±10	20	0.11	-	-	-	-
Pi1-4	2.017	58	13	4.89±0.37	95.1±45.6	111±15	0	0.74	-	-	-	-
Pogona 1												
Po1-1	5.777	677	33	6.54±0.41	114.5±26.3	188.8±7.3	24	0.00	38	12.1±1.8	105.8±5.7	201±28
Po1-2	4.835	655	29	6.33±0.43	155.0±34.3	132±14	42	0.00	21	12.2±2.2	107±11	198±18
Po1-3	4.080	173	15	3.00±0.18	166.7±50.1	133±17	26	0.10	-	-	97±20	183±24
Po1-6	2.810	105	15	7.79±0.52	68.3±26.2	67±15	71	0.00	16	11.9±2.4	-	-
Sturt 8												
St8-1	3.389	652	38	6.629±0.42	157.0±39.2	127.7±8.9	26	0.00	22	12.1±1.8	107.9±7.0	185±30
St8-2	1.956	188	22	16.27±1.26	55.7±19.5	106±11	27	0.18	14	11.9±1.5	92.6±8.5	282±117

grains unassigned to an age population). This strategy allowed validation of the AFT populations and cross calibration of AFT and AUPb populations for provenance analysis (discussed further below).

For well Moomba 72, only two samples at shallow depth (*Winton Formation*) yielded sufficient apatites. Conversely, the Moomba 1 well only produced apatites from deeper

Table 4: Comparison of AFT and AUPb age populations. The AUPb ages are presented as mean ages for each population for formations (where applicable). AFT populations are as presented in Table 3, calculated from radial plots in Figure 9. Stratigraphic ages were taken from Alexander & Hibburt (1996) and Gravestock et al. (1998).

Sample ID	Youngest AUPB Population (Ma)	Youngest AFT Population (Ma)	Oldest AUPb Population (Ma)	Oldest AFT Population (Ma)
Winton Formation 105-90Ma				
M72-1	100±12	117.1±7.6	266±23	309±39
M72-2	100±12	119.4±8.3	266±23	308±36
Pi1-1	100±12	98.6±9.3	266±23	178±19
Po1-1	100±12	105.8±5.7	266±23	201±28
St8-1	100±12	107.9±7.0	266±23	185±30
Mackunda Formation 105-90Ma				
Pi1-2	118±13	100.9±8.5	258±88	193±25
Po1-2	118±13	107±11	258±88	198±18
Cadna Owie Formation 125-120Ma				
M1-1	114±25	76±11	252±31	178±23
Pi1-3	114±25	104.5±6.3	252±31	-
Po1-3	114±25	97±20	252±31	183±24
St8-2	114±25	92.6±8.5	252±31	282±117
Namur Sandstone 150-138Ma				
Pi1-4	126±20	111±15	-	-
Toolachee Formation 252-247Ma				
M1-5	225±97	0	-	-
Po1-6	225±97	-	-	-

stratigraphy (*Cadna Owie* and *Toolachee Formations*). Given the rather low apatite yields and the close proximity of the wells (Figure 2b), the Moomba 1 and Moomba 72 wells have been combined for further discussion and modelling.

Pinna 1

Sample Pi1-1 yielded two AFT age populations at 98.6±9.3 Ma and 178±19 Ma (Figure 9). The younger age population overlapped with both the mean AUPb age (100±12 Ma) and stratigraphic age (105-90 Ma) for the *Winton Formation* (Table 4). Similarly, sample Pi1-2 showed two AFT age populations, where the youngest population (100.9±8.5 Ma) overlapped with both the mean AUPb (118±13 Ma) and stratigraphic age (105-90 Ma) for the *Mackunda Formation*. The equivalence between

AFT, AUPb and stratigraphic ages suggests that the AFT age has not been thermally reset after deposition and thus records provenance information. The older AFT age populations from samples Pi1-1 (178±19 Ma) and Pi1-2 (193±25 Ma) were significantly older than stratigraphic ages, but comparable to the obtained secondary AUPb ages, where the oldest AFT peak in sample Pi1-1 was slightly below the secondary AUPb age (266± 23 Ma), and that of Pi1-2 was within error of the secondary AUPb age (258±88 Ma). Therefore, these older AFT peaks also record provenance information and no (partial) reset after deposition.

Sample Pi1-3 only produced one AFT age peak (central age) at 103.1±8 Ma, within error of the mean primary AUPb age (114±25 Ma) and slightly below error of the stratigraphic age (125-120 Ma) of the *Cadna Owie Formation*. Sample Pi1-4 yielded a single AFT peak (central age) at 111±15 Ma, within error of the primary of AUPb age (126±20 Ma) but below the stratigraphic age (150-138 Ma) of the *Namur Sandstone*. Only samples Pi1-1 and Pi1-2 yielded sufficient confined tracks for use in modelling, with both length distributions showing single peaks with very similar mean track lengths of 12.7±1.7µm and 12.8±1.5µm, respectively.

Sturt 8

Both samples from the Sturt 8 well displayed significant scatter in single grain AFT ages (Figure 9) and were, therefore, decomposed into two AFT age populations. For sample St8-1, the youngest age population at 107.9±7 Ma contained ~80% of grains analysed, and overlapped with both the mean AUPb (100±12 Ma) and stratigraphic ages (105-90Ma) for the *Winton Formation*. The oldest age peak at 185±30 Ma was significantly older than stratigraphic age, and slightly younger than the mean secondary AUPb age for the *Winton Formation* (266±23 Ma). Therefore, similarly as for *Winton*

Formation samples in the Pinna 1 well, both AFT age populations likely reflect un-reset provenance ages.

The second sample, St8-2 from the *Cadna Owie Formation*, yielded similar AFT peaks as defined for sample St8-1. The oldest age population at 282±117 Ma was based on two grains, and is associated with an extremely large error due to the very low number of data within this peak. This age was equivalent, within error, to the mean secondary AUPb age (252±31 Ma) for the *Cadna Owie Formation*. The younger age population at 92.6±8.5 Ma was within error of primary AUPb age (114±25 Ma), but below the stratigraphic age (125-120 Ma), and could, therefore, be indicative of very minor post-depositional reset of the AFT system. Track length distributions were similar for both samples at 12.1±1.8µm in St8-1 and 11.9±1.5µm in St8-2.

Pogona 1

The Pogona 1 well produced three samples from the Eromanga Basin (Po1-1, Po1-2 and Po1-3) and one from the Cooper Basin (Po1-6). Sample Po1-1 from the *Winton Formation* yielded two AFT age populations, a larger population at 105.8±5.7 Ma and smaller population at 201±28 Ma. The younger population overlapped with both the mean primary AUPb (100±12 Ma) and stratigraphic ages (105-90 Ma) of the *Winton Formation*, while the oldest population was slightly younger than the mean secondary AUPb age for this formation (266±23 Ma). The AFT ages, therefore, reflect provenance with no evidence for subsequent thermal reset after deposition. Similarly, sample Po1-2 from the *Mackunda Formation* can be decomposed into a larger, younger AFT population (107±11 Ma) and more minor older population (198±18 Ma). The younger population was within error of both the primary AUPb age (118±13 Ma) and stratigraphic age (105-90 Ma), while the older population was comparable to that

observed in Po1-1, and falls within error of the secondary AUPb age for the *Mackunda Formation* (258±88 Ma). The mean confined track length is similar between samples, with average lengths of 12.1±1.8µm (Po1-1) and 12.2±2.2µm (Po1-2). As for sample Po1-1, it appears that AFT ages in Po1-2 were not reset after deposition.

As with shallower samples, two age populations were observed for sample Po1-3. The oldest population was defined at 183±24 Ma, slightly below error of the mean secondary AUPb age for the *Cadna Owie Formation* (252±31 Ma). The younger age population at 92±20 Ma was within error of the primary AUPb age (114±25 Ma) but marginally below the stratigraphic age (125-120 Ma). The deepest sample from the Pogona 1 well, Po1-6, was taken from the *Toolachee Formation* in the Cooper Basin, however, this sample displayed exceptionally high dispersion (71%), and no meaningful age peaks were recovered. The three oldest AFT ages from this sample were consistent with both AUPb age (225±97 Ma) and stratigraphic age (252-247 Ma) of the *Toolachee Formation*, while all other single grain AFT ages were significantly younger. The AFT data thus shows evidence for partial reset, suggesting that the sample has resided extensively within the APAZ of ~60-120^{o}C (Wagner & Van den haute, 1992) after deposition. The confined track length distribution in this sample was also slightly shorter and broader than previous samples, with a mean track length of 11.9±2.4µm, confirming a longer residence in the APAZ.

Moomba 72 and Moomba 1

Samples M72-1 and M72-2 from the *Winton Formation* yielded two consistent AFT age populations, a larger population at 117.1±7.6 Ma (M72-1) and 119.4±8.3 Ma (M72-2), and a smaller population at 309±39 Ma (M72-1) and 308±36 Ma (M72-2). The larger populations were within error of the mean primary AUPb age of this sample

(100±12 Ma), and slightly above the stratigraphic age (105-90 Ma) of the *Winton Formation*. The smaller populations were significantly older than the stratigraphic age, but within error of the mean secondary AUPb age for the *Winton Formation* (266±23 Ma). Sample M72-2 showed a slightly lower mean confined track length than M72-1 (11.2±2.0µm as compared to 11.8±2.1µm), as would be expected if the lower sample had resided in the APAZ longer than M72-1, however, neither sample shows any indication of resetting of AFT ages after deposition.

For well Moomba 1, only one sample (M1-1) displayed spontaneous fission tracks (Table 3), yielding two age populations, at 76±11 Ma and 178±23 Ma. The youngest age population was below error of both the mean primary AUPb age (114±25 Ma) and stratigraphic age (125-120 Ma) for the *Cadna Owie Formation*. The oldest age population was significantly older than both the stratigraphic and primary AUPb age, but younger than the secondary AUPb population (252±31 Ma). The presence of AFT ages consistently younger than respective AUPb populations, and a Cretaceous peak that was younger than the stratigraphic age, indicates this sample resided within the APAZ (~60-120^{o}C) after deposition and shows evidence of partial resetting after deposition. The deepest sample from this study, M1-5, yielded no spontaneous fission tracks, which was unremarkable as present day temperatures at this sampling zone are comfortably above APAZ temperatures at ~132^{o}C.

[4.3.3] THERMAL HISTORY MODELLING

The thermal history of the sampled wells was modelled separately for each well, and produced a broadly similar thermal history. The models give evidence for a period of post-burial heating in the late Cretaceous, and second heating event during the Cenozoic to reach modern day temperatures. As models did not show significant

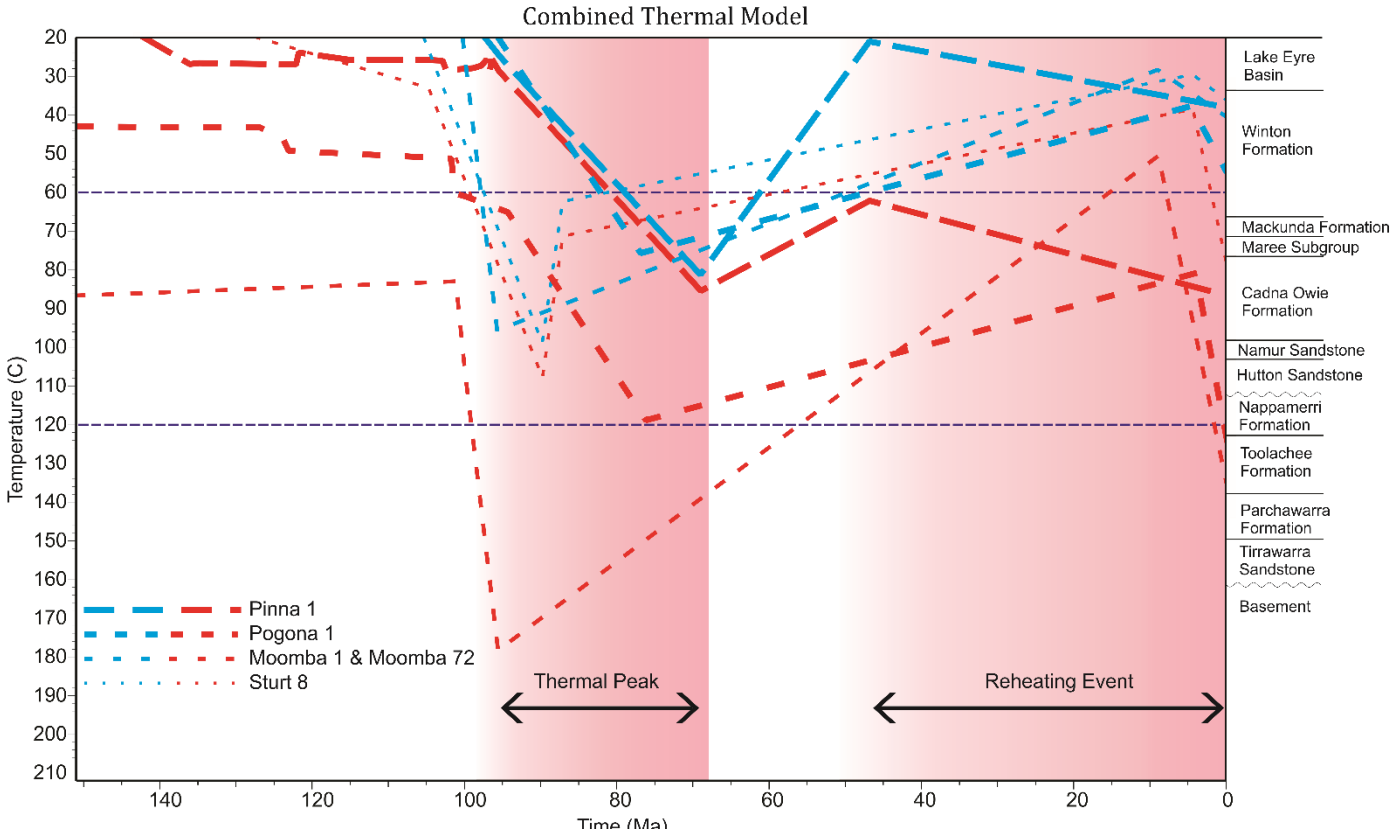

Figure 10: Combined thermal history model for the Cooper-Eromanga Basin, constructed from individual time-temperature paths from shallowest and deepest apatite samples from component models from wells Pogona 1, Pinna 1, Sturt 8, and combined modelling of Moomba 1 & Moomba 72 samples. The models for individual wells were weighted by reliability, as determined by the number of samples and grains used in modelling. Thicker time-temperature lines denote more reliable models, with Pinna 1 (4 samples, 140 grains) judged as the most reliable, followed by Pogona 1 (4 samples, 92 grains), Moomba 1 & Moomba 72 combined (4 samples, 58 grains), and Sturt 8 (2 samples, 60 grains). Timing of thermal events was constrained in pink, where darker shading reflects more likely timing of event. A thermal peak was observed at ~95-70 Ma, and reheating event from ~45 Ma to present day. The most reliable model (Pinna 1) constrains the initiation of the second heating event at ~45 Ma, however, all other models (Pogona 1, Sturt 8 and Moomba 1 & 72 combined) suggested reheating began much later at ~10-5 Ma. Stratigraphy has been provided on the right axis, correlated to present day temperature. The Maree Subgroup unit comprises of the *Allaru Mudstone*, *Toolebuc Formation*, *Wallumbilla Formation*, *Oodnadatta Formation*, *Coorikiana Sandstone* and *Bulldog Shale* members, which represent marine formations that are not continuous across the Eromanga Basin, and thus are not all represented in each well.

differences based on location in the Cooper-Eromanga Basin, all four models were combined into a single time-temperature history model (Figure 10) to illustrate major trends (individual models contained within Appendix C). The timing of the post-depositional thermal peak was constrained at ~95-70 Ma (~85-70 Ma for the best constrained models). The Cenozoic reheating event showed much less agreement between samples in both rate and timing. Three of the four thermal history models suggested reheating began at ~10-5 Ma, while modelling from the Pinna 1 well

suggested reheating began as early as ~45 Ma. Despite using multiple apatite samples from a depth profile, only one apatite sample (M1-5) exceeded the APAZ after deposition, while other samples passed into the APAZ but did not exceed ~120ºC.

[5] DISCUSSION

[5.1] Provenance

[5.1.1] UPPER EROMANGA BASIN (*WINTON, MACKUNDA* AND *CADNA OWIE FORMATIONS*)

Primary (Cretaceous) Age Populations

Deposition in the upper Eromanga Basin in the *Cadna Owie* to *Winton Formations* occurred between ~125-90 Ma, in an evolving marine and fluvial environment (Alexander & Hibburt, 1996). The *Cadna Owie Formation* (~125-120 Ma) was deposited at the interface between the Eromanga Sea and terrestrial environments. As marine transgression progressed, the entirety of the Eromanga Basin became submerged by ~118 Ma (Figure 11), facilitating deposition of the *Mackunda Formation* (105-90 Ma) during the latter stages of inundation (Veevers, Powell & Roots, 1991). During the late Cretaceous, the Eromanga Sea disappeared and the depositional regime transitioned to a large west-flowing fluvial system, in which the *Winton Formation* (105-90 Ma) was deposited. Despite variations in depositional environments, the primary (Cretaceous) AUPb and AFT ages for all upper Eromanga formations obtained in this study were comparable to the stratigraphic age for each respective formation.

In comparison with published zircon U-Pb data, the AUPb ages for the primary population (114±25 Ma to 100±12 Ma) are comparable with the largest and youngest detrital zircon U-Pb age peak in equivalent strata (Figure 12) from the Eromanga Basin

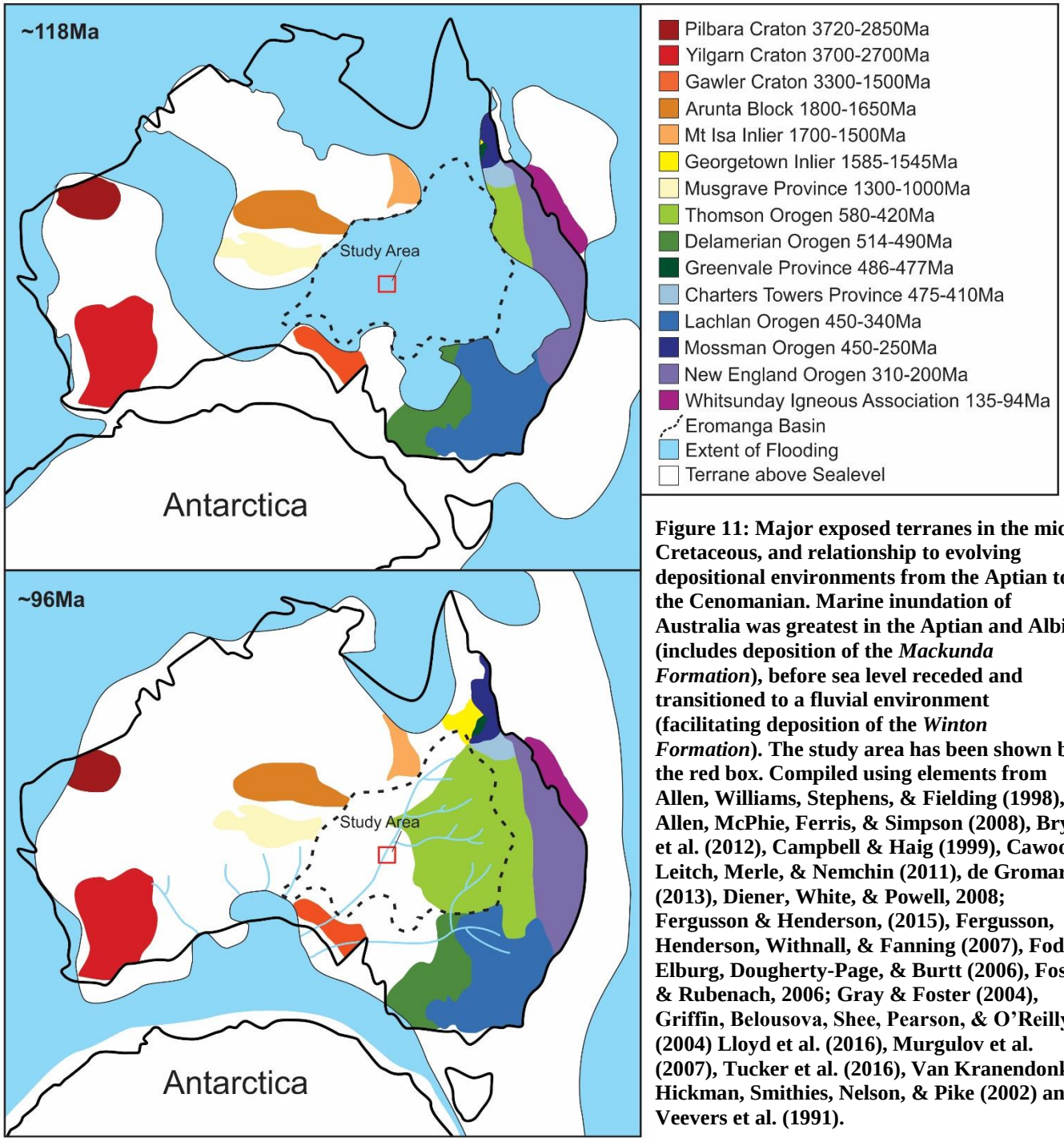

Figure 11: Major exposed terranes in the mid-Cretaceous, and relationship to evolving depositional environments from the Aptian to the Cenomanian. Marine inundation of Australia was greatest in the Aptian and Albian (includes deposition of the *Mackunda Formation*), before sea level receded and transitioned to a fluvial environment (facilitating deposition of the *Winton Formation*). The study area has been shown by the red box. Compiled using elements from Allen, Williams, Stephens, & Fielding (1998), Allen, McPhie, Ferris, & Simpson (2008), Bryan et al. (2012), Campbell & Haig (1999), Cawood, Leitch, Merle, & Nemchin (2011), de Gromard (2013), Diener, White, & Powell, 2008; Fergusson & Henderson, (2015), Fergusson, Henderson, Withnall, & Fanning (2007), Foden, Elburg, Dougherty-Page, & Burtt (2006), Foster & Rubenach, 2006; Gray & Foster (2004), Griffin, Belousova, Shee, Pearson, & O'Reilly (2004) Lloyd et al. (2016), Murgulov et al. (2007), Tucker et al. (2016), Van Kranendonk, Hickman, Smithies, Nelson, & Pike (2002) and Veevers et al. (1991).

in north-east Queensland (Tucker et al., 2016). The REE signatures of grains from Cretaceous AUPb populations were consistent between all formations (Figure 7), and comparable to felsic-sourced apatite (Belousova et al., 2002; Bruand, Storey, & Fowler, 2014). The observed similarities between primary AUPb ages, youngest zircon U-Pb

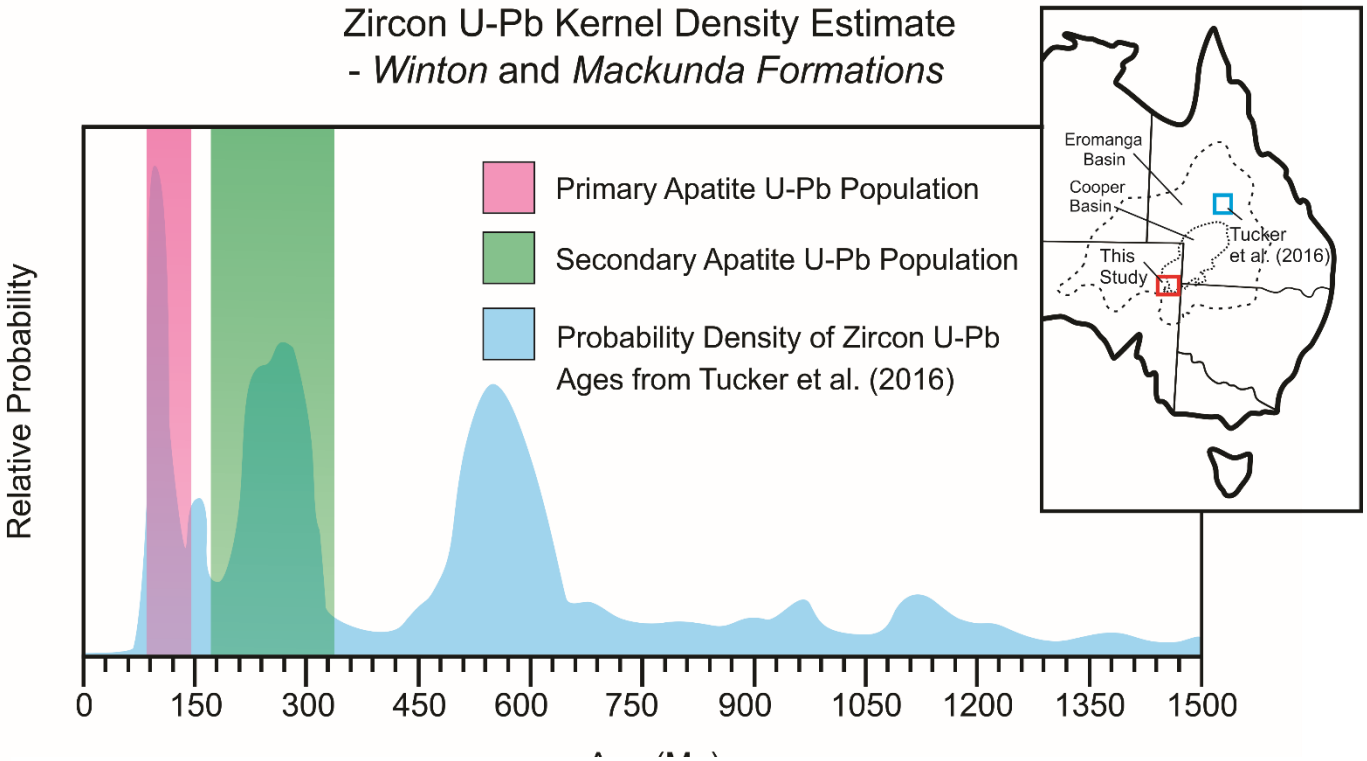

Figure 12: Comparison of primary and secondary apatite U-Pb age populations with detrital zircon U-Pb ages from the *Winton* and *Mackunda Formations* in the Eromanga Basin in north-eastern Queensland presented by Tucker et al. (2016). Zircon U-Pb ages have been presented as Kernel Density Estimate (KDE), while apatite U-Pb ages are shown as range of mean AUPb ages from the *Winton* and *Mackunda Formations*. Data from the *Cadna Owie Formation* from this study has not been included in this figure for consistency with zircon U-Pb data, as the study by Tucker et al. (2016) did not analyse zircons from this formation. Cretaceous and Permian-Triassic apatite U-Pb peaks correspond well to previously identified zircon U-Pb ages from comparable strata in Queensland, closer to the Whitsunday Igneous Association. Inset shows location of comparison study within the Eromanga Basin.

ages and stratigraphic ages, and the felsic nature of REE signatures, suggests that the Cretaceous upper Eromanga apatites formed syn-depositional, from a single, felsic source. The primary AUPb age population was most likely sourced from ~135-90 Ma volcanism in the felsic Whitsunday Igneous Association (Bryan, Ewart, Stephens, Parianos, & Downes, 2000; Ewart et al., 1992) in north-eastern Australia, as proposed by Tucker et al. (2016). Sediment from this distal source was likely transported in marine, and later fluvial environments (Bryan et al., 2000), or as fallout from explosive eruptions carried by easterly polar winds (Barham et al., 2016).

It has been proposed that the Whitsunday Igneous Association was also a major sediment source for the Otway and Gippsland Basins (Bryan et al., 1997), and

potentially provided sediment as far south-west as the Ceduna Delta (MacDonald et al., 2013). It is, therefore, questionable whether the currently recognised extent of the volcanic terrane (Figure 11) would have been able to provide the volume of material required. A potential solution to the problem of volume is that the Whitsunday Igneous Association was once more extensive than observed today, and much of the original terrane now lies submerged off the east coast of Australia (Bryan et al., 1997).

Alternatively to the Whitsunday Igneous Association, MacDonald et al. (2013) suggest that mid-Cretaceous volcanogenic sediments within the Ceduna Delta were sourced from easily eroded inland local volcanic centres which have not been preserved. If sediment was sourced from both the Whitsunday Igneous Association and local volcanic centres it would alleviate the need for such large volumes of detritus to be produced by a single terrane. However, given that there is presently little evidence for inland Cretaceous volcanism, this theory remains highly speculative.

Secondary (Permian – early Jurassic) Age Populations

Analysed apatite crystals from the older (secondary) AUPb age populations represented ~20% of grains in upper Eromanga Basin samples. The mean secondary AUPb ages for the *Winton Formation* (266±23 Ma), *Mackunda Formation* (258±88 Ma) and *Cadna Owie Formation* (252±31 Ma) were very consistent between formations, and comparable to a previously identified Permian age peak in detrital zircon U-Pb ages in the upper Eromanga Basin (Figure 12; Tucker et al., 2016). The oldest AFT age populations showed more variation than observed for the AUPb populations. Samples Pi1-1, Po1-1, M1-1 and St8-1 from the *Winton Formation* yielded AFT ages slightly younger than their respective AUPb mean ages (Table 4), while all other samples fell within error of the AUPb ages. In the case of sample M1-1 from the *Cadna Owie*

Formation, the younger AFT ages were attributed to partial thermal reset after deposition.

The older data suggests that a second, late Permian – Jurassic source terrane supplied apatites into the upper Eromanga Basin. As REE patterns of grains in this age population were consistent with felsic-sourced apatite (Belousova et al., 2002; Bruand et al., 2014), the most likely source was felsic volcanism and S- and I- type granites from the ~300-230 Ma New England Orogen (Cawood et al., 2011; Tucker et al., 2016). Alternatively, the ~450-250 Ma Mossman Orogen (de Gromard, 2013) was also a potential source of Permian sediment, although if this were the source, it is unclear why sediment exclusively from the youngest phase of orogeny would be deposited into the Eromanga Basin.

Disparity between secondary AFT ages may indicate that location within the basin may also have impacted the source of sediment, particularly in the fluvial environment of the *Winton Formation*. Varying location within the basin explains how grains from the Pinna 1, Pogona 1 and Sturt 8 wells could have been sourced from a granite body that was not immediately exhumed (and cooled slowly after crystallisation), while related grains from the Moomba 72 well were sourced from terrane that cooled faster.

Other Sources

Grains unassigned to an AUPb age population made up <2% of total grains analysed from the upper Eromanga Basin. For those grains, no robust AUPb ages could be determined and, therefore, identifying their source terranes is challenging. Potential source terranes for unassigned sediment (Figure 11) include granites or recycled sediments associated with the ~580-230 Ma Tasmanide orogens (Cawood et al., 2011;

Fergusson & Henderson, 2015), or terranes in central Australia such as the ~1300-1000 Ma Musgrave Province (MacDonald et al., 2013), or the ~1800-1650 Ma Arunta Block (Diener et al., 2008).

[5.1.2] LOWER EROMANGA BASIN *(NAMUR SANDSTONE)*

Primary (early Cretaceous) Age Population

The *Namur Sandstone* was deposited in a fluvial environment in a north-flowing river system at 150-138 Ma (Alexander & Hibburt, 1996). The single apatite sample from this formation (Pi1-4) yielded an AUPb age of 126±20 Ma, which falls within error of the allowable stratigraphic age. The AFT population for this sample at 111±15 Ma was younger than the stratigraphic age, and was likely partially thermally reset, similar as described above. The AUPb age suggests a syn-depositional sediment source, however, the onset of volcanism in the Whitsunday Igneous Association at ~135 Ma (Bryan et al., 2012) is later than the suggested minimum depositional age. Volcanism was, however, active on the eastern Australian margin as early as ~175 Ma in the so-called 'Tasman Arcs'. Related sediments are observed in the Otway and Surat Basins (Sircombe, 1999), and such a volcanic system would appear to be the only likely syn depositional provenance source in the Cretaceous prior to the onset of volcanism in the Whitsunday Igneous Association.

Cretaceous AUPb ages obtained from this study, however, contrast strongly with zircon U-Pb ages presented by Stephens et al. (2017), who proposed dominant Cambrian to Mesoproterozoic U-Pb ages in detrital zircons from the *Namur Sandstone* in the Tibooburra area in north-western New South Wales (Figure 13). The observed discrepancy may reflect localised variations in sediment provenance, as sediment from the Tibooburra area were more proximally sourced from basement outcrop (Stephens et al., 2017). An alternative interpretation may be that the apatites were from a more mafic source and, therefore, no zircons of Cretaceous age were deposited in the *Namur Sandstone* strata. However, REE data suggests the apatites were felsic-sourced, similar to other apatites in this study, which is inconsistent with such an interpretation.

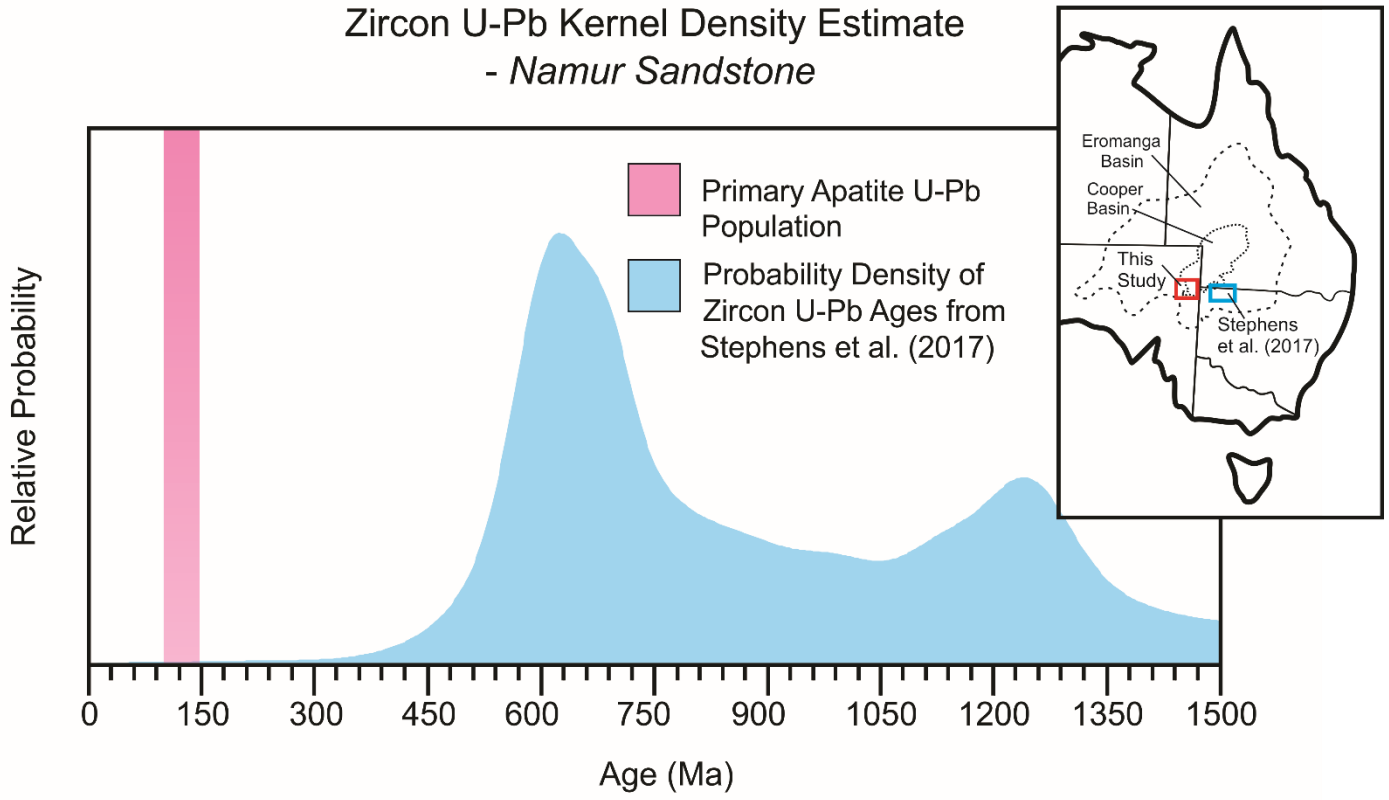

Figure 13: Comparison of apatite U-Pb age population from the *Namur Sandstone* sampled in this study with Kernel Density Estimate (KDE) of detrital zircon U-Pb ages from the *Namur Sandstone* in south-east of the Eromanga Basin, using data from from Stephens et al. (2017). Cretaceous apatite U-Pb ages yielded by this study do not correlate with the dominantly Cambrian-Mesoproterozoic zircon U-Pb ages. Inset shows location of comparison study within the Eromanga Basin.

[5.1.3] UPPER COOPER BASIN (*TOOLACHEE FORMATION*)

Primary (Carboniferous - Permian) Age Population

Deposition of the *Toolachee Formation* in the Cooper Basin occurred in fluvial to lacustrine environments at 252-247 Ma (Drexel & Preiss, 1995; Gravestock et al., 1998). The single AUPb age peak identified in sample Po1-6 at 225±97 Ma was within error of stratigraphic age, but likely comprised multiple age populations that were unable to be distinguished due to the low number of available grains. AFT ages were partially reset after deposition, thus did not return provenance information. REE signatures for all grains from the primary AUPb age population were consistent with felsic-sourced apatite (Belousova et al., 2002; Bruand et al., 2014). The observed AUPb and REE results suggest the proximal Alice Springs Orogeny (~450-300 Ma) in central Australia (Buick, Storkey, & Williams, 2008), which has previously been interpreted to be a source for the stratigraphically lower *Merrimelia Formation* (stratigraphic age of 315-300 Ma, Chaney et al., 1997), may have remained a source of sediment to the upper Cooper Basin strata (*Toolachee Formation*).

The AUPb age and REE signatures were are also consistent with distal provenance from the Mossman (~450-250 Ma) and New England Orogens (~310-200 Ma) as proposed for the younger Eromanga Basin (C. M. Allen et al., 1998; de Gromard, 2013), which may suggest a continued source of apatites from eastern Australia to the Cooper-Eromanga Basin from the late Permian to the Cretaceous. Unfortunately, this theory remains speculative as this study was unable to differentiate between proximal or distal source terranes.

Metamorphic Apatite

A single (unassigned) grain from sample Po1-6 showed significant depletion in LREEs (Figure 7), consistent with metamorphic sourced apatite (Henrichs, et al., In Press). Given that no other grains displayed significant LREE depletion it is unlikely that apatite of this sample experienced significant metamorphism after deposition. This grain was likely derived from metamorphic terranes in the nearby Harts Range Metamorphic Complex, Entia Gneiss Complex or Alice Springs Orogeny (Buick et al., 2008).

[5.2] Thermal History

[5.2.1] CRETACEOUS HEATING PULSE

The thermal history models from all wells suggest steady heating of sediments since ~100-80 Ma, reaching a thermal peak at ~95-70 Ma (Figure 10). The timing of the heating pulse is consistent with results presented by Duddy et al. (2002), who predicted a thermal maximum at ~97-75 Ma. The absolute timing of the thermal maximum for individual samples showed no correlation with the location of wells within the basin, thus variations in the timing do not appear related to basin scale processes. Instead, observed differences in timing of the thermal peaks are attributed to uncertainties in the modelling and differing quality of apatite data between individual wells.

Rapid subsidence has been proposed in central Australia from ~100-90 Ma, which coincides with the timing of deposition of thick sedimentary sequences (Alexander & Hibburt, 1996). The cause for this rapid Cretaceous subsidence has been attributed to a subducted slab stalled in the mantle transition zone below central Australia, which caused a topographic depression below the continental interior

(Gurnis, Müller, & Moresi, 1998). Since the duration of heating coincided with progressive burial in the Eromanga Basin (Alexander & Hibburt, 1996; Duddy et al., 2002), it should be questioned if the Cretaceous thermal maximum was reached by rapid subsidence and associated sedimentary burial alone or if additional heat sources would have been required. The thermal models suggest heating rates of up to ~25^{o}C per Ma, which translates to ~1km burial per Ma (under normal ~25^{o}C/km geothermal gradients) and a total of up to 5km of overburden. Given the maximum thickness of the Eromanga Basin at present day of ~3km (Drexel & Preiss, 1995), and that exhumation in the basin since the late Cretaceous has likely been <1km (Mavromatidis & Hillis, 2005), this simple burial model is highly unlikely. The present geothermal gradient in the basin is high (~40-60^{o}C/km), related to radiogenic heat loss from high heat producing elements in the underlying Big Lake Suite plutons (Beardsmore, 2004; Middleton, 1979). It is therefore likely that a similarly high geothermal gradient affected the basin during the late Cretaceous. The presented data thus suggests that the Cretaceous thermal maximum was driven by radiogenic heating of the Eromanga sediments, enhanced by thermal blanketing during burial.

Thermal blanketing would have been particularly profound when overburden consisted of marine clays with a low thermal conductivity, such as the *Allaru Mudstone* and *Wallumbilla Formation* (Deighton & Hill, 1998). Both low conductivity units lie stratigraphically below the *Winton* and *Mackunda Formations*, therefore, have had a greater thermal insulating effect on lower units, such as the *Cadna Owie Formation*, which experienced notable partial resetting of AFT ages (Figure 9).

Alternatively, Duddy et al. (2002) predicted much higher geothermal gradients in the mid-Cretaceous of ~75-80^{o}C/km, consistent with high heat flow expected in a rift

environment. These authors therefore suggested that the Cretaceous thermal event may have been linked to an aborted rift in central Australia. However, given the lack of evidence for Cretaceous intraplate rifting, this study prefers a simpler interpretation related to radiogenic heating, thermal insulation and burial.

[5.2.2] LATE CRETACEOUS COOLING PHASE

Cooling in the Eromanga Basin occurred after the Cretaceous thermal maximum, and has been previously attributed to a period of exhumation, and hydrological processes (Deighton & Hill, 1998). In the late Cretaceous, sedimentation in the Eromanga Basin ceased as the basin became fully subaerially exposed (Alexander & Hibburt, 1996). Uplift in the Eromanga Basin in the late Cretaceous coincided with uplift on the eastern Australia margin, as westward motion of the Pacific plate increased and the plate rotated clockwise to shift from normal to sinistral subduction below the eastern margin of Australia (Veevers, 2000). Additionally, isostatic rebound in central Australia as the continent moved away from a subducted slab at ~90 Ma may have contributed to the proposed Cretaceous uplift (Gurnis et al., 1998).

Despite experiencing varied magnitudes of exhumation between wells, thermal models appeared spatially consistent. Sediment compaction analysis suggests that the Sturt 8 well would have experienced approximately half as much exhumation as the other modelled wells (Mavromatidis & Hillis, 2005), however, thermal modelling from this well does not differ significantly. Given that there is no significant correlation between magnitude of exhumation and cooling history, exhumation does not appear to be responsible for the entirety of the Cretaceous cooling event. The cooling event cannot be solely linked to progressive cooling of basement granites either, as this process does not explain the rapid rate of cooling (Duddy et al., 2002).

Toupin et al. (1997) proposed that the infiltration of surface water through faults during late Cretaceous uplift depressed the basin isotherms, and was, therefore, responsible for enhanced cooling. Such a model may explain local variations in timing of cooling in the basin observed in thermal modelling, but would likely need to be coupled with lateral heat transfer away from the basin through groundwater movement to achieve the observed magnitude of cooling (Deighton & Hill, 1998; Hall et al., 2015). Additionally, the infiltration of groundwater may have induced cementation of sediments, which enhances thermal conductivity of the sediments and thus induces cooling by reducing thermal insulation.

[5.2.3] CENOZOIC REHEATING

A second phase of heating in the Eromanga Basin has been identified by multiple sources (Duddy et al., 1999, 2002; McLaren & Dunlap, 2006), however the cause of this reheating remains contentious. Thermal models presented in this study are broadly consistent with previous AFT based models proposed by Duddy et al. (2002), but show considerable variation in timing and rate of reheating. The thermal models for the Pogona 1 well, Sturt 8 well and combined Moomba 1 & Moomba 72 wells (Figure 10) predicted abrupt heating beginning in the last ~10-5 Ma, similar to the ~5-2 Ma reheating as proposed by Duddy et al. (2002). Only a single model (Pinna 1) favoured a significantly earlier onset of reheating at ~45 Ma.

As the Cooper-Eromanga region is currently subsiding (e.g. Alexander & Hibburt, 1996; Veevers, 2000), Gallagher (1988) inferred that the cause of reheating was a crustal process rather than a deeper mantle process, as mantle heating would be expected to cause regional uplift. If cooling in the basin was indeed a result of hydrological processes (Deighton & Hill, 1998; Gallagher, 1988; Toupin et al., 1997),

changes in aquifer flow within the Great Artesian Basin during the Cenozoic may have caused a reduction in heat removed from the region, allowing temperatures in the basin to increase. It must be emphasised, however, that at present the cooling and recent heating events observed in the Eromanga Basin are poorly understood, and will require additional research to be confidently explained.

Only one sample (Po1-6) from the Cooper Basin preserved spontaneous fission tracks, and yielded AFT ages that are significantly younger than cessation of deposition in the Cooper Basin at ~237 Ma (Hall et al., 2015). A second sample (M1-5) yielded a zero AFT age and was thus fully reset. Therefore, the apatite fission track system largely fails to model the thermal history of the Cooper Basin, and consequently, the thermal history of the Cooper Basin must be extrapolated from the overlying Eromanga Basin (as presented in this study). Future research into the thermal evolution of the Cooper Basin should use thermochronometers with closure temperatures >120^{o}C, such as zircon fission track (e.g. Tagami, 2005) or $^{40}Ar/^{39}Ar$ dating of feldspars (McLaren & Dunlap, 2006).

[6] CONCLUSIONS

This study has been the first project to successfully conduct combined apatite fission track thermochronology, U-Pb dating and REE analysis in the Cooper-Eromanga Basin, The main conclusions from this study are:

- Despite changes in the depositional environment, major sediment provenance in the upper Eromanga Basin from ~150-90 Ma was dominantly syn-depositional from volcanism on the east coast of Australia. The bulk of analysed apatites in the upper Eromanga Basin were likely sourced from the Whitsunday Igneous

Association, with potential additional input from local volcanic centres. Such a scenario would have required significantly more exposed Whitsunday Igneous Association terrane during the Cretaceous, which is now thought to be largely submerged off the north-eastern coast of Australia.

- A minor ~200-300 Ma apatite fraction was identified in the *Winton*, *Mackunda* and *Cadna Owie Formations*, likely sourced from the New England and/or Mossman Orogens.
- The modelled thermal history of the Eromanga Basin is broadly consistent with previous studies, predicting two post-depositional heating phases. An initial thermal maximum was reached at ~95-70 Ma, likely driven by a combination of sedimentary burial and radiogenic heating by the Big Lake Suite granites.
- Subsequent late Cretaceous – early Cenozoic cooling is likely related with a combination of minor exhumation, increased heat transfer by aquifer systems and/or enhanced thermal conductivity by cementation.
- Three of the four thermal history models suggest that reheating began at ~10-5 Ma, although the cause of this event remains poorly understood.
- Future AFT studies in the Eromanga Basin should sample wells further from basement highs, targeting strata that have exceeded APAZ temperatures post-deposition and contain thermally reset apatite.
- Future work in the Cooper Basin should use thermochronometers with higher closure temperatures than apatite fission track, such as zircon fission track or $^{40}Ar/^{39}Ar$ in feldspars.

[7] ACKNOWLEDGMENTS

I would like to thank my supervisor Stijn Glorie, and associated Ph.D. students Jack Gillespie, Gilby Jepson, Nick Fernie and James Hall from the ATLaS group for all their assistance this project. I would also like to acknowledge the contribution of Betina Bendall and the Geological Survey of South Australia, and the Tonsley Drill Core Library for providing core and cutting samples. Finally, I would like to thank Sarah Gilbert and Adelaide Micoscopy for their assistance during analysis of samples, and Barry Kohn and the University of Melbourne for allowing us to use their ^{252}Cf irradiation source.

[8] REFERENCES

ALEXANDER, E. M., & HIBBURT, J. (1996). *The petroleum geology of South Australia; Volume 2, Eromanga Basin* (Vol. 2): Government of South Australia, Department of State Development.

ALLEN, C. M., WILLIAMS, I. S., STEPHENS, C. J., & FIELDING, C. R. (1998). Granite genesis and basin formation in an extensional setting: the magmatic history of the northernmost New England Orogen. *Australian Journal of Earth Sciences, 45*(6), 875-888.

ALLEN, S. R., MCPHIE, J., FERRIS, G., & SIMPSON, C. (2008). Evolution and architecture of a large felsic Igneous Province in western Laurentia: The 1.6 Ga Gawler Range Volcanics, South Australia. *Journal of Volcanology and Geothermal Research, 172*(1-2), 132-147. doi: 10.1016/j.jvolgeores.2005.09.027

ARMSTRONG, P. A. (2005). Thermochronometers in Sedimentary Basins. *Reviews in Mineralogy and Geochemistry, 58*(1), 499-525. doi: 10.2138/rmg.2005.58.19

BARHAM, M., KIRKLAND, C. L., REYNOLDS, S., O'LEARY, M. J., EVANS, N. J., ALLEN, H., . . . GOODALL, J. (2016). The answers are blowin' in the wind: Ultra-distal ashfall zircons, indicators of Cretaceous super-eruptions in eastern Gondwana. *Geology, 44*(8), 643-646. doi: 10.1130/g38000.1

BEARDSMORE, G. (2004). The influence of basement on surface heat flow in the Cooper Basin. *Exploration Geophysics, 35*(4), 223-235. doi: 10.1071/eg04223

BELOUSOVA, E. A., GRIFFIN, W. L., O'REILLY, S. Y., & FISHER, N. I. (2002). Apatite as an indicator mineral for mineral exploration: trace-element compositions and their relationship to host rock type. *Journal of Geochemical Exploration, 76*(1), 45-69. doi: 10.1016/s0375-6742(02)00204-2

BELOUSOVA, E. A., WALTERS, S., GRIFFIN, W. L., & O'REILLY, S. Y. (2001). Trace-element signatures of apatites in granitoids from the Mt Isa Inlier, northwestern Queensland. *Australian Journal of Earth Sciences, 48*(4), 603-619. doi: 10.1046/j.1440-0952.2001.00879.x

BOULT, P. J., THEOLOGOU, P. M., & FODEN, J. (1997). Capillary seals within the Eromanga Basin, Australia: implications for exploration and production. *AAPG Memoir*(67), 143-167.

BRUAND, E., FOWLER, M., STOREY, C., & DARLING, J. (2017). Apatite trace element and isotope applications to petrogenesis and provenance. *American Mineralogist, 102*(1-2), 75-84. doi: 10.2138/am-2017-5744

BRUAND, E., STOREY, C., & FOWLER, M. (2014). Accessory Mineral Chemistry of High Ba-Sr Granites from Northern Scotland: Constraints on Petrogenesis and Records of Whole-rock Signature. *Journal of Petrology, 55*(8), 1619-1651. doi: 10.1093/petrology/egu037

BRYAN, S. E., CONSTANTINE, A. E., STEPHENS, C. J., EWART, A., SCHON, R. W., & PARIANOS, J. (1997). Early Cretaceous volcano-sedimentary successions along the eastern Australian continental margin: Implications for the break-up of eastern Gondwana. *Earth and Planetary Science Letters, 153*(1-2), 85-102. doi: 10.1016/s0012-821x(97)00124-6

BRYAN, S. E., COOK, A. G., ALLEN, C. M., SIEGEL, C., PURDY, D. J., GREENTREE, J. S., & UYSAL, I. T. (2012). Early-mid Cretaceous tectonic evolution of eastern Gondwana: From silicic LIP magmatism to continental rupture. *Episodes, 35*(1), 142-152.

BRYAN, S. E., EWART, A., STEPHENS, C. J., PARIANOS, J., & DOWNES, P. J. (2000). The Whitsunday Volcanic Province, Central Queensland, Australia: lithological and stratigraphic investigations of

a silicic-dominated large igneous province. *Journal of Volcanology and Geothermal Research, 99*(1-4), 55-78. doi: 10.1016/s0377-0273(00)00157-8

BUICK, I., STORKEY, A., & WILLIAMS, I. (2008). Timing relationships between pegmatite emplacement, metamorphism and deformation during the intra-plate Alice Springs Orogeny, central Australia. *Journal of Metamorphic Geology, 26*(9), 915-936.

CAMPBELL, R. J., & HAIG, D. W. (1999). Bathymetric change during Early Cretaceous intracratonic marine transgression across the northeastern Eromanga Basin, Australia. *Cretaceous Research, 20*(4), 403-446. doi: 10.1006/cres.1999.0161

CAWOOD, P. A., LEITCH, E. C., MERLE, R. E., & NEMCHIN, A. A. (2011). Orogenesis without collision: Stabilizing the Terra Australis accretionary orogen, eastern Australia. *Geological Society of America Bulletin, 123*(11-12), 2240-2255. doi: 10.1130/b30415.1

CHANEY, A., CUBITT, C., & WILLIAMS, B. (1997). Reservoir potential of glacio-fluvial sandstones: Merrimelia Formation, Cooper Basin, South Australia. *The APPEA Journal, 37*(1), 154-177.

CHEW, D. M., PETRUS, J. A., & KAMBER, B. S. (2014). U-Pb LA-ICPMS dating using accessory mineral standards with variable common Pb. *Chemical Geology, 363*, 185-199. doi: 10.1016/j.chemgeo.2013.11.006

CHEW, D. M., & SPIKINGS, R. A. (2015). Geochronology and Thermochronology Using Apatite: Time and Temperature, Lower Crust to Surface. *Elements, 11*(3), 189-194. doi: 10.2113/gselements.11.3.189

DE GROMARD, R. Q. (2013). The significance of E–W structural trends for the Alice Springs Orogeny in the Charters Towers Province, North Queensland. *Tectonophysics, 587*, 168-187.

DEIGHTON, I., & HILL, A. J. (1998). Thermal and burial history. In G. o. S. A. Department of Primary Industries and Resources (Ed.), *The petroleum geology of South Australia* (Vol. 4, pp. 143-155).

DELHI PETROLEUM LTD. (1966). Moomba 1 Well Completion Report. Retrieved from https://map.sarig.sa.gov.au/

DELHI PETROLEUM LTD. (1967). Moomba 3 Well Completion Report. Retrieved from https://map.sarig.sa.gov.au/

DELHI PETROLEUM LTD. (1980). Pinna 1 Well Completion Report. Retrieved from https://map.sarig.sa.gov.au/

DELHI PETROLEUM LTD. (1983). Cowan 1 Well Completion Report. Retrieved from https://map.sarig.sa.gov.au/

DIENER, J., WHITE, R., & POWELL, R. (2008). Granulite facies metamorphism and subsolidus fluid-absent reworking, Strangways Range, Arunta Block, central Australia. *Journal of Metamorphic Geology, 26*(6), 603-622.

DONELICK, R. A., & MILLER, D. S. (1991). Enahnced TINT fission-track densities in low spontaneous track density apatites using Cf-252 derived fission fragment tracks: a model and experimental observations. *Nuclear Tracks and Radiation Measurements, 18*(3), 301-307.

DONELICK, R. A., O'SULLIVAN, P. B., & KETCHAM, R. A. (2005). Apatite fission-track analysis. *Low-Temperature Thermochronology: Techniques, Interpretations, and Applications, 58*, 49-94. doi: 10.2138/rmg.2005.58.3

DREXEL, J. F., & PREISS, W. V. (1995). *The geology of South Australia* (Vol. 2).

DREXEL, J. F., PREISS, W. V., & PARKER, A. J. (1993). *The geology of South Australia* (Vol. 1).

DUDDY, I. R., MOORE, M. E., MARSHALLSEA, S. J., & GREEN, P. F. (2002). *Provenance and thermal history studies in Cooper-Eromanga Basin wells*. (744). Melbourne, Australia: Geotrack International.

EWART, A., SCHON, R. W., & CHAPPELL, B. W. (1992). The Cretaceous volcanic-plutonic province of the central Queensland (Australia) coast - a rift related calc-alkaline province. *Transactions of the Royal Society of Edinburgh-Earth Sciences, 83*, 327-345.

FERGUSSON, C. L., & HENDERSON, R. A. (2015). Early Palaeozoic continental growth in the Tasmanides of northeast Gondwana and its implications for Rodinia assembly and rifting. *Gondwana Research, 28*(3), 933-953. doi: 10.1016/j.gr.2015.04.001

FERGUSSON, C. L., HENDERSON, R. A., WITHNALL, I. W., & FANNING, C. M. (2007). Structural history of the Greenvale Province, north Queensland: Early Palaeozoic extension and convergence on the Pacific margin of Gondwana. *Australian Journal of Earth Sciences, 54*(4), 573-595.

FODEN, J., ELBURG, M. A., DOUGHERTY-PAGE, J., & BURTT, A. (2006). The timing and duration of the Delamerian Orogeny: correlation with the Ross Orogen and implications for Gondwana assembly. *The Journal of Geology, 114*(2), 189-210.

FOSTER, D. R. W., & RUBENACH, M. J. (2006). Isograd pattern and regional low-pressure, high-temperature metamorphism of pelitic, mafic and calc-silicate rocks along an east-west section through the Mt Isa Inlier. *Australian Journal of Earth Sciences, 53*(1), 167-186. doi: 10.1080/08120090500434617

GALLAGHER, K. (1988). *The subsidence history and thermal state of the Eromanga and Cooper Basins.* Australian National University, unpublished thesis.

GALLAGHER, K. (2012). Transdimensional inverse thermal history modeling for quantitative thermochronology. *Journal of Geophysical Research-Solid Earth, 117*, 16. doi: 10.1029/2011jb008825

GATEHOUSE, C. G., FANNING, C. M., & FLINT, R. B. (1995). *Geochronology of the Big Lake Suite, Warburton Basin, northeastern South Australia*. Victoria: Geological Survey of South Australia.

GILLESPIE, J., GLORIE, S., XIAO, W.-J., ZHANG, Z., COLLINS, A. S., EVANS, N. J., . . . DE GRAVE, J. (2017). Mesozoic reactivation of the Beishan, southern Central Asian Orogenic Belt: Insights from low-temperature thermochronology. *Gondwana Research, 43*, 107-122.

GLEADOW, A., HARRISON, M., KOHN, B., LUGO-ZAZUETA, R., & PHILLIPS, D. (2015). The Fish Canyon Tuff: A new look at an old low-temperature thermochronology standard. *Earth and Planetary Science Letters, 424*, 95-108.

GLORIE, S., ALEXANDROV, I., NIXON, A., JEPSON, G., GILLESPIE, J., & JAHN, B.-M. (2017). Thermal and exhumation history of Sakhalin Island (Russia) constrained by apatite U-Pb and fission track thermochronology. *Journal of Asian Earth Sciences, 143*, 326-342.

GOVERNMENT OF SOUTH AUSTRALIA, DEPARTMENT OF STATE DEVELOPMENT. (2014). South Australian Resources Information Gateway [Database]. Retrieved from http://www.minerals.statedevelopment.sa.gov.au/online_tools/free_data_delivery_and_publication_downloads/sarig

GRAVESTOCK, D. I., HIBBURT, J., & DREXEL, J. F. (1998). *The petroleum geology of South Australia; Volume 4, Cooper Basin* (Vol. 4): Government of South Australia, Department of State Development.

GRAY, D., & FOSTER, D. (2004). Tectonic evolution of the Lachlan Orogen, southeast Australia: historical review, data synthesis and modern perspectives. *Australian Journal of Earth Sciences, 51*(6), 773-817.

GRIFFIN, W. L., BELOUSOVA, E. A., SHEE, S. R., PEARSON, N. J., & O'REILLY, S. Y. (2004). Archean crustal evolution in the northern Yilgarn Craton: U–Pb and Hf-isotope evidence from detrital zircons. *Precambrian Research, 131*(3), 231-282.

GURNIS, M., MÜLLER, R. D., & MORESI, L. (1998). Cretaceous vertical motion of Australia and the AustralianAntarctic discordance. *Science, 279*(5356), 1499-1504.

HALL, L. S., HILL, A., TROUP, A., KORSCH, R., RADKE, B., NICOLL, R. S., PALU, T., WANG, L., & STACEY, A. (2015). *Cooper Basin architecture and lithofacies: regional hydrocarbon prospectivity of the Cooper Basin, part 1*. (2015/31). Geoscience Australia Record.

HARLOV, D. E. (2015). Apatite: A Fingerprint for Metasomatic Processes. *Elements, 11*(3), 171-176. doi: 10.2113/gselements.11.3.171

HENRICHS, I. A., CHEW, D. M., & BABECHUK, M. (In Press). Trace-element variation in metamorphic apatite: a tool for provenance studies.

IDNURM, M., & SENOIR, B. (1978). Palaeomagnetic ages of Late Cretaceous and Tertiary weathered profiles in the Eromanga Basin, Queensland. *Palaeogeography, Palaeoclimatology, Palaeoecology, 24*(4), 263-277.

JADOON, Q. K., ROBERTS, E. M., HENDERSON, B., BLENKINSOP, T. G., WUST, R. A. J., & MTELELA, C. (2017). Lithological and facies analysis of the Roseneath and Murteree shales, Cooper Basin, Australia. *Journal of Natural Gas Science and Engineering, 37*, 138-168. doi: 10.1016/j.jngse.2016.10.047

LI, P., ROSENBAUM, G., & RUBATTO, D. (2012). Triassic asymmetric subduction rollback in the southern New England Orogen (eastern Australia): the end of the Hunter-Bowen Orogeny. *Australian Journal of Earth Sciences, 59*(6), 965-981.

LLOYD, J., COLLINS, A. S., PAYNE, J. L., GLORIE, S., HOLFORD, S., & REID, A. J. (2016). Tracking the Cretaceous transcontinental Ceduna River through Australia: The hafnium isotope record of detrital zircons from offshore southern Australia. *Geoscience Frontiers, 7*(2), 237-244. doi: 10.1016/j.gsf.2015.06.001

MACDONALD, J. D., HOLFORD, S. P., GREEN, P. F., DUDDY, I. R., KING, R. C., & BACKE, G. (2013). Detrital zircon data reveal the origin of Australia's largest delta system. *Journal of the Geological Society, 170*(1), 3-6. doi: 10.1144/jgs2012-093

MAVROMATIDIS, A. (2007). Exhumation study in the Cooper-Eromanga Basins, Australia and the implications for hydrocarbon exploration. *Energy Sources Part a-Recovery Utilization and Environmental Effects, 29*(7), 631-648. doi: 10.1080/009083190957775

MAVROMATIDIS, A., & HILLIS, R. (2005). Quantification of exhumation in the Eromanga Basin and its implications for hydrocarbon exploration. *Petroleum Geoscience, 11*(1), 79-92. doi: 10.1144/1354-079304-621

MCDOWELL, F. W., MCINTOSH, W. C., & FARLEY, K. A. (2005). A precise 40 Ar–39 Ar reference age for the Durango apatite (U–Th)/He and fission-track dating standard. *Chemical Geology, 214*(3), 249-263.

MCLAREN, S., & DUNLAP, W. J. (2006). Use of Ar-40/Ar-39 K-feldspar thermochronology in basin thermal history reconstruction: an example from the Big Lake Suite granites, Warburton Basin, South Australia. *Basin Research, 18*(2), 189-203. doi: 10.1111/j.1365-2117.2006.00288.x

MIDDLETON, M. (1979). Heat flow in the Moomba, Big Lake and Toolachee gas fields of the Cooper Basin and implications for hydrocarbon maturation. *Exploration Geophysics, 10*(2), 149-155.

MUNSON, T. J. (2014). *Petroleum geology of the onshore Northern Territory*. (22). Northern Territory Geological Survey.

MURGULOV, V., BEYER, E., GRIFFIN, W. L., O'REILLY, S. Y., WALTERS, S. G., & STEPHENS, D. (2007). Crustal evolution in the Georgetown Inlier, North Queensland, Australia: a detrital zircon grain study. *Chemical Geology, 245*(3), 198-218.

O'SULLIVAN, P., KOHN, B., FOSTER, D., & GLEADOW, A. (1995). Fission track data from the Bathurst Batholith: Evidence for rapid mid-Cretaceous uplift and erosion within the eastern highlands of Australia. *Australian Journal of Earth Sciences, 42*(6), 597-607.

PATON, C., HELLSTROM, J., PAUL, B., WOODHEAD, J., & HERGT, J. (2011). Iolite: Freeware for the visualisation and processing of mass spectrometric data. *Journal of Analytical Atomic Spectrometry, 26*(12), 2508-2518.

POCHON, A., POUJOL, M., GLOAGUEN, E., BRANQUET, Y., CAGNARD, F., GUMIAUX, C., & GAPAIS, D. (2016). U-Pb LA-ICP-MS dating of apatite in mafic rocks: Evidence for a major magmatic event at the Devonian-Carboniferous boundary in the Armorican Massif (France). *American Mineralogist, 101*(11), 2430 - 2442. doi: 10.2138/am-2016-5736

REINERS, P. W., & EHLERS, T. A. (2005). *Low-temperature thermochronology: techniques, interpretations, and applications* (Vol. 58). Washington, America: The Mineralogy Society of America.

SANTOS LTD. (1989). Taloola 1 Well Completion Report. Retrieved from https://map.sarig.sa.gov.au/

SANTOS LTD. (1990). Pinna 1 Well Completion Report. Retrieved from https://map.sarig.sa.gov.au/

SANTOS LTD. (1991). Sturt 8 Well Completion Report. Retrieved from https://map.sarig.sa.gov.au/

SANTOS LTD. (1993). Moomba 72 Well Completion Report. Retrieved from https://map.sarig.sa.gov.au/

SANTOS LTD. (1998). Moomba 89 Well Completion Report. Retrieved from https://map.sarig.sa.gov.au/

SIRCOMBE, K. N. (1999). Tracing provenance through the isotope ages of littoral and sedimentary detrital zircon, eastern Australia. *Sedimentary Geology, 124*(1-4), 47-67. doi: 10.1016/s0037-0738(98)00120-1

STEPHENS, A., REID, A., HORE, S., GILMORE, P., & HILL, S. (2017). Source of Eromanga Basin zircons. *MESA Journal, 84*(3), 10-18.

TAGAMI, T. (2005). Zircon fission-track thermochronology and applications to fault studies. *Reviews in Mineralogy and Geochemistry, 58*(1), 95-122.

TOUPIN, D., EADINGTON, P. J., PERSON, M., MORIN, P., WIECK, J., & WARNER, D. (1997). Petroleum hydrogeology of the Cooper and Eromanga basins, Australia: Some insights from mathematical modeling and fluid inclusion data. *Aapg Bulletin-American Association of Petroleum Geologists, 81*(4), 577-603.

TUCKER, R. T., ROBERTS, E. M., HENDERSON, R. A., & KEMP, A. I. S. (2016). Large igneous province or long-lived magmatic arc along the eastern margin of Australia during the Cretaceous? Insights from the sedimentary record. *Geological Society of America Bulletin, 128*(9-10), 1461-1480. doi: 10.1130/b31337.1

VAN KRANENDONK, M. J., HICKMAN, A. H., SMITHIES, R. H., NELSON, D. R., & PIKE, G. (2002). Geology and tectonic evolution of the archean North Pilbara terrain, Pilbara Craton, Western Australia. *Economic Geology, 97*(4), 695-732.

VEEVERS, J. J. (2000). Change of tectono-stratigraphic regime in the Australian plate during the 99 Ma (mid-Cretaceous) and 43 Ma (mid-Eocene) swerves of the Pacific. *Geology, 28*(1), 47-50.

VEEVERS, J. J., POWELL, C. M., & ROOTS, S. R. (1991). Review of sea-floor spreading around Australia. 1. synthesis of the patterns of spreading. *Australian Journal of Earth Sciences, 38*(4), 373-389. doi: 10.1080/08120099108727979

VERMEESCH, P. (2009). RadialPlotter: A Java application for fission track, luminescence and other radial plots. *Radiation Measurements, 44*(4), 409-410.

VERMEESCH, P. (2017). Statistics for LA-ICP-MS based fission track dating. *Chemical Geology, 456*, 19-27. doi: 10.1016/j.chemgeo.2017.03.002

WAGNER, G. A., & VAN DEN HAUTE, P. (1992). *Fission-track dating*. Amsterdam, Netherlands: Springer.

WHITFORD, D. J., HAMILTON, P. J., & SCOTT, J. (1994). Sedimentary provenance studies in Australian basins using neodymium model ages. *The APPEA Journal, 34*(1), 320-329.

[9] APPENDIX A: WELL DATA

Table 5: Key details of all wells used in this study. Sample Wells denote wells for which apatite samples were obtained and analysed. Additional Wells for VR Data are wells not examined in this study, but from which virtinite reflectance (VR) data has been sourced. Of the wells sampled in this study, VR data was only available for the Pinna 1 well, and for other sample wells VR data had to be sourced from nearby (<6km) wells with comparable stratigraphy, depth and thermal gradient. All VR data (including that from the Pinna 1 well) was obtained from the open source database from the Government of South Australia, Department of State Development (2014). No VR analysis was undertaken in this study. Thermal Gradient was calculated from extrapolation of bottom-hole temperature (BHT) estimates provided by initial well reports (Dehli Petroleum Ltd, 1966, 1967, 1980, 1983; Santos Ltd, 1989, 1990, 1991, 1993), excluding wells Moomba 1 and Moomba 3, which were not surveyed for geothermal gradient. The thermal gradients for the Moomba 1 and Moomba 3 wells were instead taken from the nearby Moomba 138 (Santos Ltd, 2001) and Moomba 89 (Santos Ltd, 1998) wells, respectively, which showed comparable depths and stratigraphy. Maximum Depth gives the maximum depth of each well below the surface. Date Spudded is the date on which drilling of wells was begun.

Well	GDA94 Latitude	GDA94 Longitude	Thermal Gradient (°C/km)	Maximum Depth (m)	Date Spudded	VR data Available	VR data applied to:
Sample Wells							
Moomba 1	28 09 04.708	140 16 08.669	47.9	2923	10/03/1966	No	-
Moomba 72	28 01 30.445	140 12 19.191	49.9	3099	17/07/1992	No	-
Pinna 1	28 28 47.042	140 15 17.673	42.7	2581	21/12/1979	Yes	Pinna 1
Pogona 1	28 15 41.028	140 03 46.510	50.5	2602	04/02/1990	No	-
Sturt 8	28 08 01.483	139 35 00.602	42.3	2028	13/09/1990	No	-
Additional Wells for VR Data							
Moomba 3	28 08 03.220	140 12 39.671	54.7	2900	18/01/1967	Yes	Moomba 1 & Moomba 72
Cowan 1	28 19 23.377	140 02 52.545	45.5	2209	6/04/1983	Yes	Pogona 1
Taloola 1	28 10 02.069	139 38 21.216	44.5	1923	19/05/1988	Yes	Sturt 8

Table 6: VR data used in thermal history modelling, as obtained from the Petroleum Exploration and Production System – South Australia (PEPS-SA) open source database at Government of South Australia, Department of State Development (2014). No VR analysis was undertaken in this study. Present day temperature was calculated using depth at which sample was taken, and well thermal gradients, as supplied in Table 5.

Formation	Depth (m)	Rv Mean Max Reflectance	Rv Min	Rv Max	Determinations	Present Day Temperature (C)
Moomba 3						
Hutton	2124	1.00	-	-	-	122.8
Pinna 1						
Winton	390.14	0.30	0.18	0.45	30	37.7
Winton	554.74	0.39	0.26	0.46	27	44.7
Winton	691.9	0.47	0.35	0.57	30	50.6
Oodnadatta	847.34	0.42	0.32	0.61	30	57.3
Oodnadatta	1048.51	0.44	0.35	0.54	22	65.8
Bulldog	1203.96	0.44	0.36	0.53	3	72.5
Cadna Owie	1380.74	0.57	0.46	0.67	13	80.0
McKinlay	1441.7	0.54	0.47	0.60	5	82.7
Westbourne	1496.57	0.50	0.42	0.58	18	85.0
Westbourne	1554.48	0.55	0.44	0.63	30	87.4
Adori	1624.58	0.55	0.48	0.60	30	90.4
Hutton	1685.54	0.56	0.44	0.66	19	93.0
Hutton	1752.6	0.57	0.50	0.62	23	95.9
Cowan 1						
Oodnadatta Fm	1180.9994	0.40	0.26	0.49	21	80.7
Bulldog Sh	1285.0002	0.42	0.31	0.60	15	86.0
Bulldog Sh	1372.999	0.48	0.37	0.63	7	90.4
Bulldog Sh	1449.0009	0.49	0.36	0.61	25	94.2
Murta Fm	1527.999	0.55	0.4	0.73	16	98.2
Namur Sst	1599.9988	0.62	0.48	0.68	26	101.9
Westbourne Fm	1680.9994	0.59	0.51	0.72	13	106.0
Birkhead Fm	1807.0007	0.63	0.52	0.73	15	112.3
Hutton Sst	1842.0009	0.64	0.53	0.74	25	114.1
Taloola 1						
Poolowanna Fm	1839.77	0.66	0.57	0.75	26	98.9

[10] APPENDIX B: EXTENDED METHODS

[10.1] Laboratory Processing

Apatite samples were prepared using conventional methods for fission track and U-Pb laser-ablation analysis (e.g. Glorie et al., 2017). Cuttings and core were crushed and panned before being magnetically separated with a Franz system. The non-magnetic fraction was further processed with heavy liquids (lithium heteropolytungstates heavy liquid and methyl iodide) to recover the apatite fraction. Individual apatite grains were picked onto double sided tape in rasters of 100-150 grains (depending on grain availability) and positioned such that the grain c-axis was parallel to the surface of the tape. Grains were mounted in an EpoxyCure resin prepared with 5g epoxy resin and 1.15g epoxy hardener. Resin was poured on the tape to cover the raster of grains, and a glass microscope slide placed over the resin such that the resin would adhere to it. Resin was allowed to set for 24 hours before the tape was removed, leaving grains embedded in the resin mount. To expose apatite grains the top of the resin mount was carefully grinded using #2000 silicon carbide paper. The mounts were subsequently polished on an Autopolisher system using 3µm and 1µm diamond suspension solutions to provide smooth surface for fission track counting. Once sufficiently polished, samples were etched to reveal fission tracks for counting. Each sample was etched in a solution of 5M nitric acid (HNO_3) at 20±0.5^{o}C for 20±0.5 seconds, then immediately washed in distilled water to remove all nitric acid and ensure etching durations were consistent between all samples.

[10.2] Fission Track Counting

After etching, mounts were examined for apatite on a Zeiss AXIO Imager M2m Autoscan System, with apatite identified by the presence of etched features (scratches, fission tracks) on the grain surface. Mounts with no grains displaying these characteristics were judged not to contain any apatite, and were excluded from any further processing. Samples that contained grains with etching features but without fission tracks (so-called zero-age grains) were still processed further. Samples containing apatite were coated in a 3nm layer of gold to enhance the imaging process of the fission tracks. Apatite bearing samples were imaged using the Zeiss AXIO Imager M2m Autoscan System, and surface track densities and confined track lengths measured using FastTracks software. Fission track densities are known to be correlated with the fission track age and ^{238}U concentration (Wagner & Van den haute, 1992). The fission track age reflects the timing of passage through the so-called apatite partial annealing zone (APAZ) at temperatures of ~60-120^{o}C (Wagner & Van den haute, 1992).

[10.3] LA-ICP-MS Analysis

Analysis for U, Pb, Cl and rare earth elements was conducted using laser ablation inductively coupled plasma mass spectrometry (LA-ICP-MS) on a solid state New Wave-213 laser connected to an Agilent 7900x mass spectrometer (analytical details provided in Table 1). A single 30µm spot was ablated for each grain, excluding grains that exhibited clear zonation patterns in fission track densities. Data collection was performed over three analytical sessions, with standard blocks interspaced in the laser session. Standard blocks were comprised of 2x NIST 610 glass, 2x Madagascar apatite, 1x Durango apatite and 1x McClure apatite. Data reduction was performed with

Iolite software (Paton, Hellstrom, Paul, Woodhead, & Hergt, 2011) using Madagascar apatite as the primary standard for AFT and U-Pb analysis, and NIST 610 as the primary standard for REE analysis. Durango and McClure apatite were used as secondary standards to test the accuracy of results.

[10.4] ^{252}Cf Irradiation

Due to the low apatite yield of samples from used in this study, there was insufficient apatite to make two mounts for each sample (one for laser ablation, and one for ^{252}Cf irradiation). Consequently, mounts were repolished after laser ablation using the same protocols as before to remove all previously etched tracks and laser damage, thus allowing both LA-ICP-MS analysis and ^{252}Cf irradiation of grains from a single mount, alleviating the need for duplicate mounts. Samples were irradiated with a ^{252}Cf source at the University of Melbourne to increase the likelihood of exposing confined tracks (e.g. Donelick & Miller, 1991). The irradiated samples were subsequently etched and analysed for confined track lengths using the same protocols as with un-irradiated samples.

[10.5] Apatite Fission Track Thermochronology

Fission track ages were calculated by comparing direct measurements of ^{238}U obtained from LA-ICP-MS for each grain against the number of spontaneous tracks using in-house Excel spreadsheets, following the methodology outlined in Gillespie et al. (2017), Gleadow, Harrison, Kohn, Lugo-Zazueta, & Phillips (2015) and Glorie et al. (2017). A Durango apatite standard was counted and analysed in the same laser sessions as unknown samples to produce a zeta calibration factor (Vermeesch, 2009, 2017), which was applied to calculated AFT ages to correct for analyst counting bias.

Fission track age populations were identified using radial plots, as generated using the Java plugin RadialPlotter (Vermeesch, 2009, 2017). As samples were from detrital apatite, multiple populations were likely to be present, which were identified using the chi-squared test (χ^2) for a single population and dispersion of single grain AFT ages. For $\chi^2>0.05$, single grain age dispersion was regarded as natural, for $\chi^2<0.05$ multiple populations existed in the data set and were distinguished using a finite mixture model. As a second test, samples with high dispersion (>25%) were also considered to contain multiple populations.

Thermal history modelling was performed using QTQt software produced by Gallagher (2012) with modelling inputs of single grain ATF ages and associated uncertainty, confined track lengths, and single grain Cl concentration. Cl content is known to influence fission track annealing rates, thus confined track length and associated Cl content must be considered together to produce meaningful thermal history models. Samples were modelled as a depth profile, constrained to present day depth, to produce internally consistent models. To constrain maximum heating temperatures in the modelled depth profiles, vitrinite reflectance (VR) data obtained from samples at comparable depths to the analysed samples. Each individual sample was constrained to present day temperature (±5^{o}C), and to 22.5±2.5^{o}C at stratigraphic age to represent surface temperatures at the time of deposition.

[10.6] Treatment of Secondary AUPb Populations in Eromanga Basin Samples

As many of the samples used in this study exhibited very high common-Pb and poor distribution of $^{238}U/^{206}Pb$ and $^{207}Pb/^{207}Pb$ ratios across Tera-Wasserburg Concordia plots, a combination of U-Pb and AFT information was required to adequately separate grains in primary and secondary AUPb populations. The following section details

methods and logic used in assigning secondary age populations, and treatments applied to each secondary population.

[10.6.1] UN-ANCHORED REGRESSION

Samples Po1-1, St8-1 and St8-2 yielded multiple grains which exhibited clear deviation from the primary age regression line (Figure 5). These grains also yielded AFT ages greater than those in the primary AUPb age population (>~150Ma), so were interpreted as representative of a second, older population. AFT ages were also used to assist with assigning grains that showed very high common-Pb and plotted close to the upper intercept of Tera-Wasserburg plots assigned to AUPb age populations, where grains that yielded AFT ages above error of the primary AUPb ages of samples Po1-1 (90±14Ma), St8-1 (99.1±7.9Ma) and St8-2 (130±17Ma), and were attributed to the oldest AFT age populations by radial plots (Figure 9), were also included in the older, secondary AUPb population. AUPb age was calculated using a linear regression on Tera-Wasserburg Concordia plots (Figure 5), with no anchored values.

[10.6.2] ANCHORED REGRESION

Samples Pi1-2, Pi1-3, Po1-2 and Po1-3 yielded multiple grains that deviated from the primary AUPb population, and, with the exception of sample Pi1-3, could be satisfied with a single linear regression, producing an AUPb older than the primary age population. Additional grains from this older population were identified from correlating grains that showed very high common-Pb, which yielded AFT ages significantly older than the primary age population, as described above. Unfortunately, secondary AUPb age populations from these samples contained few grains and exhibited a poor spread of $^{238}U/^{206}Pb$ and $^{207}Pb/^{207}Pb$ ratios, usually with very high

common-Pb content, making reliable linear regression problematic. Linear regressions of secondary populations for samples Pi1-2, Pi1-3, Po1-2 and Po1-3 were, therefore, anchored to an upper intercept of 4950±50Ma calculated for a lower intercept of ~250Ma across all samples (Stacey & Kramers, 1975), and consistent with lower intercepts obtained in un-anchored linear regression of samples from secondary AUPb age populations Po1-1 (251±61Ma), St8-1 (269±26Ma) and St8-2 (216±47Ma). Uncertainties for upper and lower intercepts obtained for anchored samples (upper – 50Ma, lower – 50-88Ma) were comparable with those of secondary populations in un-anchored samples (upper – 34-44Ma, lower – 26-61Ma), thus, the process of anchoring and results obtained were considered reasonable. Sample Pi1-3 only produced three grains in the secondary AUPb population, which could not be satisfied by any single linear regression path, but nonetheless produced similar $^{238}U/^{206}Pb$ and $^{207}Pb/^{207}Pb$ ratios and plotted close to one another in Tera-Wassserburg space (Figure 5). When anchored at an upper intercept value as described for other samples, all grains returned AUPb ages within the broad ~300-200Ma observed in other secondary AUPb populations.For consistency with other samples, all grains were attributed to a single population and single linear regression, which fell within this broad range, but produced as larger uncertainty than other samples (228±88Ma).

[10.6.3] AGE POPULATIONS WITHOUT REGRESSION

Samples M1-1, M72-1, M72-2 and Pi1-1 yielded no grains with distinct separation from the primary AUPb age population, as observed on Tera-Wasserburg Concordia plots (Figure 5), as these grains resided in regions of very high common-Pb. Grains attributed to secondary AUPb age population were identified using AFT data for these samples, where grains from AFT populations older than the primary AUPb age

(Figure 9) were assigned to secondary AUPb populations on Tera-Wasserburg Concordia plots. Unfortunately, high common-Pb in secondary AUPb age populations for these samples made linear regression unfeasible, hence no secondary AUPb ages were obtained for these samples.

Sample Pi1-4 exhibited only one AUPb signature that differed significantly from the primary population (Figure 5), however when anchored at an upper intercept of 4950±50Ma, linear regression yielded an AUPb age >1000Ma, notably older than the ~300-200Ma peaks observed in all previous secondary AUPb age populations. Only a single AFT age peak was observed for this sample (Figure 9), so AFT information could not be used to aid in assigning grains from this sample to AUPb age populations. Consequently, this grain was not assigned to a primary nor secondary age population, and no secondary AUPb population was obtained for this sample.

[11] APPENDIX C: INDIVIDUAL THERMAL HISTORY MODELS

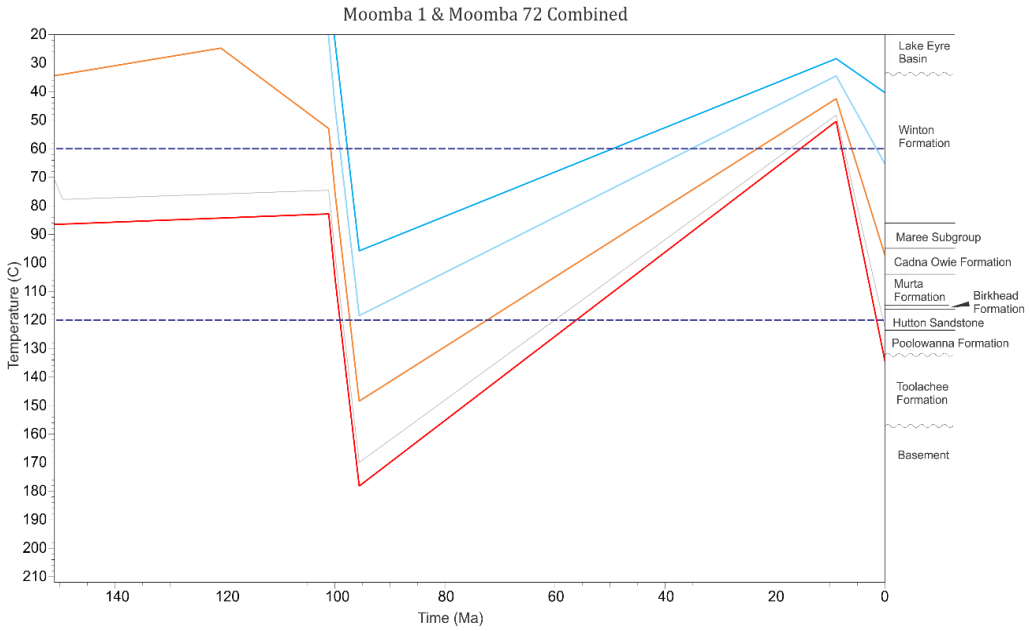

Figure 14: Modelled thermal history of Moomba 1 and Moomba 72 wells, generated by QTQt software. APAZ boundaries shown as dashed lines. Maximum likelihood time-temperature paths of all apatite and VR samples have been shown, where coloured paths represent apatite samples and grey paths denote VR samples. Cooler colours represent thermal history paths of shallower (and thus cooler) apatite samples. This thermal history model suggests a thermal maximum was reached at ~95 Ma, and recent reheating began ~10 Ma. Stratigraphy has been provided on right axis, correlated to present day temperature.

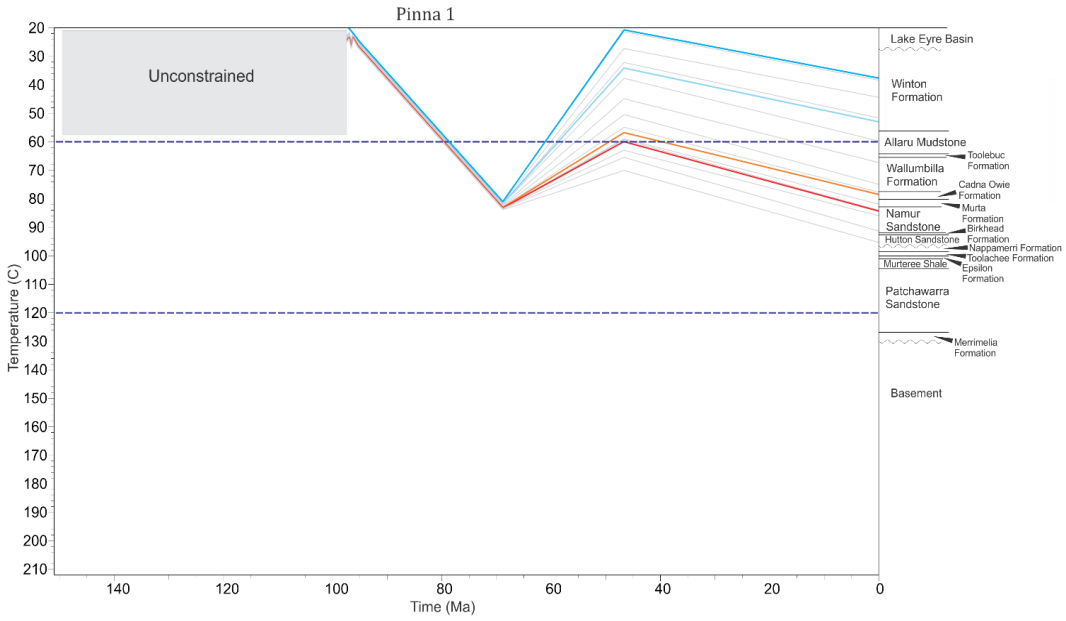

Figure 15: Modelled thermal history of the Pinna 1 well, generated by QTQt software. APAZ boundaries shown as dashed lines. Maximum likelihood time-temperature paths of all apatite and VR samples have been shown, where coloured paths represent apatite samples and grey paths denote VR samples. Cooler colours represent thermal history paths of shallower (and thus cooler) apatite samples. The modelled thermal history predicts a thermal maximum was reached at ~75 Ma, and subsequent reheating began at ~45 Ma. Modelling prior to 105 Ma has not been shown, as no samples before this time yielded confined track number sufficient for use in modelling, thus models are poorly constrained before this point. Stratigraphy has been provided on right axis, correlated to present day temperature.

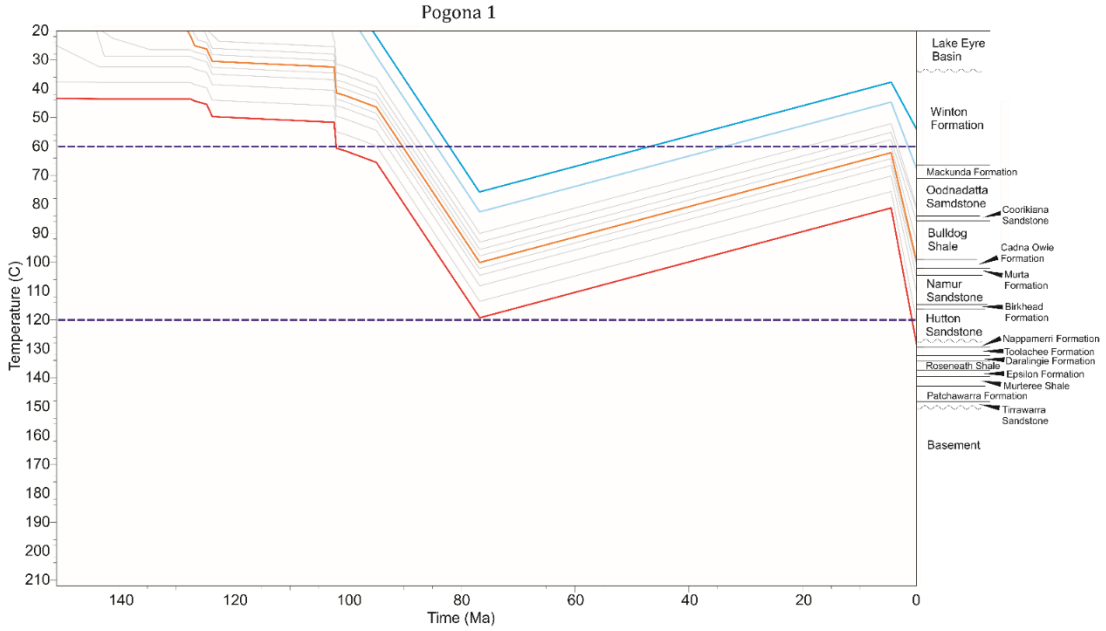

Figure 16: Modelled thermal history of the Pogona 1 well, generated by QTQt software. APAZ boundaries shown as dashed lines. Maximum likelihood time-temperature paths of all apatite and VR samples have been shown, where coloured paths represent apatite samples and grey paths denote VR samples. Cooler colours represent thermal history paths of shallower (and thus cooler) apatite samples. Thermal history modelling for the Pogona 1 well suggests a thermal maximum was reached at ~80 Ma, and recent reheating began at ~10-5 Ma. Stratigraphy has been provided on right axis, correlated to present day temperature.

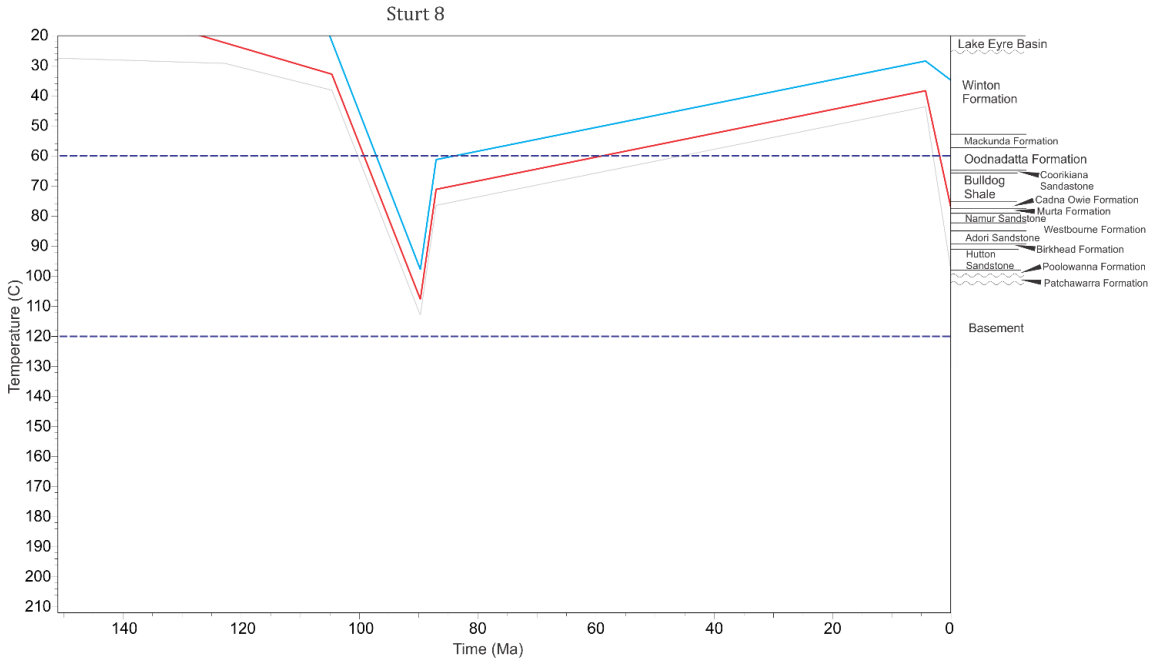

Figure 17: Modelled thermal history of the Sturt 8 well, generated by QTQt software. APAZ boundaries shown as dashed lines. Maximum likelihood time-temperature paths of all apatite and VR samples have been shown, where coloured paths represent apatite samples and grey paths denote VR samples. Cooler colours represent thermal history paths of shallower (and thus cooler) apatite samples. The thermal history model predicts a thermal maximum was reached at ~90 Ma, and recent heating even began ~ 5 Ma. Stratigraphy has been provided on right axis, correlated to present day temperature.

[12] APPENDIX D: DATA TABLES

[12.1] Apatite U-Pb Data

Table 7: Single grain apatite U-Pb data outputs from all samples used in this study, as calculated using Iolite software. Final 207 Age is the common-Pb corrected AUPb age for each grain. Grains unasigned to an AUPb age population, or assigned to a secondary AUPb population for which no regression was performed, have no common-Pb correction, hence no common-Pb corrected age has been reported for these grains.

Sample M1-1						
Grain	Final 238/206	Final 238/206 2SE	Final 207/206	Final 207/206 2SE	Final 207Age (Ma)	Final 207Age 2SE (Ma)
M1-1_1.d	2.666667	0.263111	0.782	0.042	-	-
M1-1_2.d	29.85075	2.940521	0.466	0.023	-	-
M1-1_3.d	11.72333	1.291903	0.632	0.051	-	-
M1-1_4.d	7.92393	0.690675	0.744	0.047	47	87
M1-1_5.d	2.967359	0.255351	0.779	0.036	-	-
M1-1_6.d	18.45018	1.83821	0.63	0.064	85	43
M1-1_12.d	7.440476	0.664328	0.685	0.03	116	56
M1-1_13.d	2.932551	0.378394	0.742	0.029	310	170
M1-1_14.d	3.095975	0.345062	0.799	0.032	32	150
M1-1_15.d	6.544503	0.556797	0.722	0.026	81	73
M1-1_16.d	2.710027	0.257049	0.712	0.03	-	-
M1-1_17.d	1.851852	0.178327	0.806	0.037	-	-
M1-1_18.d	0.8	0.128	0.705	0.081	-	-
M1-1_19.d	4.098361	0.352728	0.799	0.042	-	-
M1-1_21.d	2.710027	0.24236	0.838	0.049	-	-
M1-1_22.d	8.635579	0.969452	0.692	0.038	110	74
M1-1_23.d	1.25	0.359375	0.94	0.19	-	-
M1-1_26.d	1.230012	0.110444	0.83	0.029	110	320
M1-1_27.d	16.15509	1.461527	0.67	0.047	50	50
M1-1_28.d	6.35324	0.565091	0.739	0.033	99	76
M1-1_29.d	4.878049	0.428317	0.725	0.042	121	120
M1-1_30.d	2.923977	0.333436	0.731	0.047	-	-
Sample M72-1						
Grain	Final 238/206	Final 238/206 2SE	Final 207/206	Final 207/206 2SE	Final 207Age (Ma)	Final 207Age 2SE (Ma)
M72-1_1.d	2.506266	0.163316	0.833	0.037	-	-
M72-1_2.d	11.72333	1.058261	0.71	0.062	100	73
M72-1_3.d	5.263158	0.260388	0.79	0.032	107	68
M72-1_4.d	6.756757	0.593499	0.772	0.046	142	89
M72-1_5.d	3.389831	0.218328	0.81	0.039	127	110
M72-1_6.d	2.941176	0.181661	0.779	0.038	170	130
M72-1_7.d	21.14165	2.592422	0.592	0.034	96	18
M72-1_8.d	2.525253	0.165799	0.811	0.036	150	130

M72-1_9.d	5.076142	0.360741	0.821	0.044	80	130
M72-1_10.d	3.205128	0.184911	0.807	0.036	-	-
M72-1_11.d	19.53125	1.411438	0.604	0.053	106	34
M72-1_12.d	5.130836	0.315906	0.803	0.044	81	88
M72-1_13.d	3.448276	0.237812	0.767	0.041	-	-
M72-1_14.d	13.02083	0.864665	0.655	0.031	126	26
M72-1_15.d	2.747253	0.226422	0.883	0.042	-60	160
M72-1_16.d	1.31406	0.093245	0.834	0.041	190	290
M72-1_17.d	1.077586	0.070833	0.842	0.028	120	250
M72-1_18.d	4.219409	0.302658	0.82	0.04	-	-
M72-1_19.d	14.68429	0.862513	0.694	0.038	85	27
M72-1_20.d	3.424658	0.222837	0.805	0.038	144	110
M72-1_21.d	6.968641	0.456482	0.745	0.049	130	69
M72-1_22.d	19.76285	3.476074	0.618	0.036	95	20
M72-1_23.d	3.04878	0.232377	0.883	0.066	-140	220
M72-1_24.d	2.347418	0.15429	0.885	0.041	-140	160
M72-1_25.d	4.768717	0.272888	0.803	0.029	99	87
M72-1_26.d	2.28833	0.151857	0.841	0.03	110	120
M72-1_27.d	6.877579	0.41152	0.742	0.039	127	54

Sample M72-2

Grain	Final 238/206	Final 238/206 2SE	Final 207/206	Final 207/206 2SE	Final 207Age (Ma)	Final 207Age 2SE (Ma)
M72-2_1.d	11.24859	0.784491	0.607	0.038	-	-
M72-2_2.d	5.347594	0.343161	0.768	0.041	73	90
M72-2_3.d	6.697924	0.448622	0.764	0.037	62	62
M72-2_5.d	3.472222	0.373746	0.732	0.057	170	170
M72-2_4.d	2.173913	0.189036	0.795	0.04	140	190
M72-2_6.d	3.04878	0.241672	0.774	0.036	70	130
M72-2_7.d	2.04918	0.142771	0.773	0.037	180	200
M72-2_8.d	4.273504	0.420045	0.769	0.08	80	190
M72-2_10.d	8.53971	0.561535	0.724	0.048	94	65
M72-2_11.d	9.319664	0.590622	0.718	0.041	84	51
M72-2_12.d	3.311258	0.405684	0.813	0.062	20	160
M72-2_13.d	10.15228	0.5978	0.669	0.058	119	72
M72-2_14.d	3.184713	0.202848	0.783	0.039	-	-
M72-2_15.d	2.024291	0.155715	0.794	0.052	50	270

Sample Pi1-1

Grain	Final 238/206	Final 238/206 2SE	Final 207/206	Final 207/206 2SE	Final 207Age (Ma)	Final 207Age 2SE (Ma)
Pi1-1_1.d	1.757469	0.105016	0.837	0.029	10	200
Pi1-1_2.d	1.536098	0.143936	0.81	0.052	240	300
Pi1-1_3.d	5.747126	0.429383	0.839	0.039	10	72
Pi1-1_4.d	3.164557	0.250361	0.693	0.054	-	-
Pi1-1_5.d	4.219409	0.302658	0.808	0.053	60	130
Pi1-1_6.d	5.050505	0.459137	0.754	0.058	-	-

Pi1-1_9.d	2.469136	0.195092	0.835	0.045	-40	160
Pi1-1_10.d	0.142857	0.022449	0.793	0.049	-600	1100
Pi1-1_11.d	1.956947	0.176164	0.792	0.047	-	-
Pi1-1_12.d	6.027728	0.323368	0.769	0.029	84	72
Pi1-1_13.d	1.831502	0.134176	0.79	0.028	190	170
Pi1-1_14.d	17.45201	1.522863	0.657	0.073	73	42
Pi1-1_15.d	6.901311	0.476281	0.794	0.039	47	56
Pi1-1_16.d	1.980198	0.156847	0.839	0.037	50	190
Pi1-1_17.d	1.492537	0.423257	0.93	0.2	-110	360
Pi1-1_18.d	11.87648	0.789885	0.621	0.027	151	29
Pi1-1_19.d	4.273504	0.310468	0.755	0.038	137	92
Pi1-1_21.d	3.558719	0.25329	0.782	0.049	90	170
Pi1-1_22.d	14.55604	0.953453	0.658	0.028	97	23
Pi1-1_24.d	3.717472	0.649521	0.792	0.059	70	140
Pi1-1_25.d	4.347826	0.26465	0.746	0.036	131	100
Pi1-1_26.d	0.833333	0.076389	0.827	0.043	-	-
Pi1-1_28.d	5.681818	0.41968	0.768	0.054	89	110
Pi1-1_29.d	13.15789	1.004155	0.732	0.049	62	40
Pi1-1_31.d	3.663004	0.509869	0.692	0.08	250	180
Pi1-1_32.d	4	0.304	0.753	0.034	151	98
Pi1-1_33.d	1.538462	0.11361	0.817	0.03	-	-
Pi1-1_34.d	3.636364	0.224793	0.766	0.035	174	110
Pi1-1_35.d	3.729952	0.208688	0.81	0.035	68	120
Pi1-1_36.d	5.681818	0.451963	0.788	0.037	61	68
Pi1-1_37.d	2.45098	0.204248	0.792	0.031	130	120
Pi1-1_38.d	2.096436	0.224147	0.783	0.058	210	260
Pi1-1_39.d	6.451613	0.541103	0.784	0.043	40	73
Pi1-1_41.d	2.673797	0.257371	0.716	0.064	320	230
Pi1-1_42.d	3.30033	0.479256	0.76	0.075	180	180
Pi1-1_44.d	3.115265	0.232917	0.779	0.049	160	160
Pi1-1_45.d	7.61035	0.49809	0.771	0.033	74	49
Pi1-1_46.d	1.445087	0.129473	0.828	0.036	-	-
Pi1-1_47.d	4.132231	0.273205	0.789	0.05	100	140
Pi1-1_48.d	1.579779	0.182186	0.799	0.041	-	-
Pi1-1_49.d	5.050505	0.382614	0.763	0.05	125	100
Pi1-1_50.d	1.517451	0.122041	0.837	0.029	-	-
Pi1-1_51.d	2.881844	0.373726	0.803	0.062	-	-
Pi1-1_52.d	1.492537	0.311874	0.724	0.038	130	170
Pi1-1_53.d	1.492537	0.311874	0.724	0.038	-	-
Pi1-1_54.d	2.967359	0.361014	0.791	0.036	110	110
Pi1-1_55.d	4.524887	0.327594	0.738	0.044	181	100
Pi1-1_56.d	2.941176	0.285467	0.812	0.044	-	-
Pi1-1_57.d	5.555556	0.401235	0.768	0.049	82	88
Pi1-1_58.d	1.428571	0.367347	0.84	0.086	230	460

Pi1-1_59.d	3.322259	0.231786	0.842	0.053	40	210
Pi1-1_60.d	4.761905	0.362812	0.784	0.036	-	-
Sample Pi1-2						
Grain	Final 238/206	Final 238/206 2SE	Final 207/206	Final 207/206 2SE	Final 207Age (Ma)	Final 207Age 2SE (Ma)
Pi1-2_1.d	17.27116	1.044025	0.632	0.03	80	21
Pi1-2_2.d	2	0.16	0.821	0.046	-10	260
Pi1-2_3.d	2.5	0.15625	0.801	0.041	10	170
Pi1-2_4.d	2.469136	0.188996	0.839	0.038	120	140
Pi1-2_5.d	7.507508	0.552354	0.75	0.051	63	76
Pi1-2_7.d	4.366812	0.286036	0.695	0.036	199	98
Pi1-2_8.d	3.436426	0.307035	0.738	0.067	170	190
Pi1-2_9.d	1.841621	0.159404	0.775	0.05	80	300
Pi1-2_10.d	2.118644	0.170569	0.806	0.053	80	240
Pi1-2_11.d	12.77139	0.96234	0.639	0.046	115	41
Pi1-2_12.d	3.952569	0.281211	0.747	0.051	260	140
Pi1-2_13.d	5.128205	0.289283	0.739	0.034	97	86
Pi1-2_14.d	3.508772	0.196984	0.762	0.034	111	120
Pi1-2_15.d	2.320186	0.188414	0.796	0.046	10	210
Pi1-2_16.d	1.420455	0.115008	0.808	0.041	40	270
Pi1-2_17.d	16.10306	1.296543	0.624	0.062	93	40
Pi1-2_19.d	2.762431	0.198407	0.773	0.048	70	200
Pi1-2_20.d	14.38849	1.01444	0.595	0.046	126	39
Pi1-2_21.d	4.385965	0.442444	0.765	0.066	160	160
Pi1-2_22.d	1.919386	0.125257	0.796	0.04	50	230
Pi1-2_24.d	7.462687	0.6683	0.769	0.074	56	110
Pi1-2_25.d	20	1.16	0.356	0.014	200.2	13
Pi1-2_26.d	3.311258	0.241218	0.8	0.046	30	150
Pi1-2_27.d	10.85776	0.837026	0.563	0.035	217	40
Pi1-2_28.d	15.36098	1.061819	0.607	0.053	112	37
Pi1-2_29.d	3.484321	0.24281	0.754	0.044	140	140
Pi1-2_30.d	2.688172	0.173431	0.796	0.033	30	140
Pi1-2_32.d	5.952381	0.496032	0.715	0.043	116	69
Pi1-2_33.d	5.988024	0.50199	0.713	0.07	241	110
Pi1-2_34.d	6.045949	0.365535	0.602	0.031	-	-
Pi1-2_35.d	9.21659	0.594619	0.584	0.038	225	52
Pi1-2_36.d	4.926108	0.970662	0.69	0.11	220	230
Pi1-2_37.d	2.923977	0.196642	0.744	0.044	180	170
Pi1-2_38.d	2.824859	0.199496	0.832	0.045	-50	160
Pi1-2_39.d	11.19821	0.890339	0.664	0.054	126	53
Pi1-2_40.d	6.784261	0.36821	0.742	0.031	70	58
Pi1-2_41.d	6.993007	0.733532	0.742	0.067	59	85
Pi1-2_42.d	2.857143	0.187755	0.763	0.033	130	130
Pi1-2_43.d	8.298755	0.488972	0.715	0.04	103	56

Pi1-2_44.d	15.87302	1.713278	0.678	0.073	78	43
Pi1-2_45.d	2.336449	0.245655	0.796	0.048	250	180
Pi1-2_46.d	9.057971	0.713808	0.607	0.038	224	42
Pi1-2_47.d	11.53403	0.758292	0.624	0.052	113	53
Pi1-2_48.d	13.15789	1.592798	0.601	0.061	137	52
Pi1-2_49.d	2.695418	0.181632	0.833	0.04	70	140
Pi1-2_50.d	9.90099	1.274385	0.816	0.093	46	81
Pi1-2_51.d	14.16431	1.16364	0.635	0.056	102	40
Pi1-2_52.d	3.891051	0.227104	0.756	0.031	113	95
Pi1-2_53.d	2.65252	0.182932	0.765	0.043	110	170
Pi1-2_54.d	14.12429	1.097226	0.685	0.061	79	47
Pi1-2_55.d	4.739336	0.561533	0.746	0.061	121	100

Sample Pi1-3

Grain	Final 238/206	Final 238/206 2SE	Final 207/206	Final 207/206 2SE	Final 207Age (Ma)	Final 207Age 2SE (Ma)
Pi1-3_1.d	6.993007	0.45968	0.716	0.041	103	70
Pi1-3_2.d	3.773585	0.355999	0.779	0.035	102	100
Pi1-3_6.d	12.40695	1.431571	0.643	0.042	112	46
Pi1-3_7.d	5.91716	0.420153	0.789	0.046	40	80
Pi1-3_8.d	11.84834	0.884414	0.653	0.049	127	48
Pi1-3_10.d	3.448276	0.356718	0.744	0.066	190	190
Pi1-3_17.d	6.301197	0.365287	0.722	0.039	134	79
Pi1-3_18.d	3.144654	0.593331	0.768	0.031	145	110
Pi1-3_19.d	18.41621	0.983554	0.399	0.021	175	22
Pi1-3_21.d	9.643202	0.613743	0.768	0.049	67	53
Pi1-3_22.d	6.451613	0.665973	0.785	0.07	80	100
Pi1-3_23.d	3.802281	0.260232	0.755	0.046	170	120
Pi1-3_28.d	13.5318	0.970481	0.623	0.048	118	33
Pi1-3_29.d	7.604563	0.404806	0.021	0.019	-	-
Pi1-3_30.d	2.403846	0.161797	0.791	0.034	110	150
Pi1-3_31.d	19.45525	1.362625	0.561	0.058	110	34
Pi1-3_34.d	4.366812	0.40045	0.777	0.045	113	97
Pi1-3_35.d	13.31558	0.74468	0.416	0.024	228	29
Pi1-3_36.d	4.901961	0.288351	0.738	0.038	135	81
Pi1-3_37.d	8.368201	0.511196	0.708	0.039	114	51
Pi1-3_38.d	3.861004	0.313054	0.771	0.046	80	110
Pi1-3_39.d	6.369427	0.486835	0.715	0.052	148	85
Pi1-3_40.d	3.759398	0.211996	0.771	0.042	80	150
Pi1-3_41.d	5.263158	0.415513	0.773	0.05	131	91
Pi1-3_42.d	5.050505	0.357106	0.719	0.041	158	77
Pi1-3_43.d	18.08318	0.915604	0.301	0.016	230	15
Pi1-3_44.d	5.797101	0.36967	0.755	0.045	89	83
Pi1-3_45.d	3.90625	0.244141	0.821	0.039	20	120
Pi1-3_46.d	8.264463	0.635203	0.759	0.062	40	69
Pi1-3_47.d	6.024096	0.725795	0.708	0.07	120	110

Sample Pi1-4						
Grain	Final 238/206	Final 238/206 2SE	Final 207/206	Final 207/206 2SE	Final 207Age (Ma)	Final 207Age 2SE (Ma)
Pi1-4_1.d	4.255319	0.253508	0.786	0.038	127	86
Pi1-4_3.d	6.25	0.859375	0.806	0.042	98	85
Pi1-4_4.d	7.518797	0.452259	0.702	0.041	162	52
Pi1-4_5.d	8.196721	0.671862	0.684	0.043	177	80
Pi1-4_7.d	1.135074	0.097918	0.852	0.031	0	340
Pi1-4_8.d	7.836991	0.595759	0.734	0.056	125	73
Pi1-4_9.d	7.911392	0.588347	0.741	0.052	137	63
Pi1-4_11.d	4.310345	0.260107	0.81	0.037	55	99
Pi1-4_12.d	1.052632	0.808864	0.887	0.069	-110	650
Pi1-4_15.d	2.202643	0.145549	0.546	0.025	-	-
Pi1-4_17.d	5.952381	0.42517	0.778	0.038	112	61
Pi1-4_18.d	6.993007	0.586826	0.718	0.054	177	67
Pi1-4_19.d	3.546099	0.213772	0.828	0.038	81	94
Pi1-4_20.d	25.97403	1.61916	0.481	0.037	119	23
Pi1-4_21.d	7.092199	0.653891	0.727	0.081	180	120
Sample Po1-1						
Grain	Final 238/206	Final 238/206 2SE	Final 207/206	Final 207/206 2SE	Final 207Age (Ma)	Final 207Age 2SE (Ma)
Po1-1_1.d	2.747253	0.211327	0.784	0.034	70	130
Po1-1_2.d	1.388889	0.212191	0.732	0.034	340	250
Po1-1_3.d	6.849315	0.562957	0.582	0.05	254	73
Po1-1_4.d	4.132231	0.478109	0.676	0.061	190	150
Po1-1_5.d	4.484305	0.583161	0.734	0.097	180	190
Po1-1_6.d	13.7741	1.347054	0.655	0.044	98	35
Po1-1_7.d	0.051813	0.009396	0.79	0.025	380	750
Po1-1_8.d	4.672897	0.305704	0.738	0.035	126	84
Po1-1_9.d	4.830918	0.606782	0.77	0.094	130	110
Po1-1_10.d	3.184713	0.233275	0.817	0.051	-40	160
Po1-1_11.d	9.310987	0.823598	0.781	0.079	36	76
Po1-1_12.d	12.10654	0.938037	0.645	0.043	120	40
Po1-1_13.d	12.22494	0.85186	0.663	0.04	103	38
Po1-1_14.d	0.196078	0.073049	0.77	0.031	60	410
Po1-1_15.d	1.858736	0.210749	0.807	0.048	-120	290
Po1-1_16.d	2.610966	0.259052	0.835	0.082	-210	280
Po1-1_17.d	5.952381	0.531463	0.784	0.063	72	100
Po1-1_18.d	0.606061	0.062443	0.805	0.037	-180	530
Po1-1_19.d	15.47988	1.102282	0.637	0.038	92	28
Po1-1_20.d	3.322259	0.386309	0.713	0.056	230	170
Po1-1_21.d	7.142857	0.612245	0.75	0.057	86	74
Po1-1_26.d	6.711409	0.720688	0.699	0.036	114	54
Po1-1_27.d	2.415459	0.326729	0.786	0.056	90	210
Po1-1_28.d	16.44737	1.19027	0.617	0.05	98	33

Po1-1_29.d	9.469697	0.753271	0.764	0.059	39	66
Po1-1_30.d	10.02004	1.004012	0.73	0.054	64	53
Po1-1_37.d	2.12766	0.22182	0.764	0.037	80	140
Sample Po1-2						
Grain	Final 238/206	Final 238/206 2SE	Final 207/206	Final 207/206 2SE	Final 207Age (Ma)	Final 207Age 2SE (Ma)
Po1-2_1.d	1.335113	0.101604	0.797	0.044	230	330
Po1-2_2.d	5.733945	0.394538	0.708	0.056	226	100
Po1-2_3.d	7.680492	0.5899	0.722	0.075	109	100
Po1-2_4.d	10.14199	0.66859	0.688	0.042	114	45
Po1-2_5.d	7.575758	0.522268	0.787	0.051	77	65
Po1-2_6.d	3.597122	0.426997	0.866	0.096	-30	220
Po1-2_9.d	4.950495	0.294089	0.74	0.031	192	73
Po1-2_10.d	10.13171	0.646705	0.716	0.041	95	43
Po1-2_11.d	9.551098	0.757155	0.719	0.045	115	57
Po1-2_12.d	9.140768	0.584876	0.718	0.054	100	69
Po1-2_13.d	10.76426	1.054411	0.717	0.069	98	57
Po1-2_14.d	7.267442	0.528157	0.789	0.035	56	50
Po1-2_15.d	3.484321	0.24281	0.808	0.051	80	150
Po1-2_16.d	6.485084	0.504676	0.74	0.054	120	98
Po1-2_17.d	0.938967	0.087284	0.85	0.043	-20	470
Po1-2_18.d	23.75297	1.974712	0.525	0.037	108	18
Po1-2_19.d	14.26534	1.322749	0.616	0.072	142	50
Po1-2_20.d	6.134969	0.52693	0.729	0.042	131	85
Po1-2_21.d	2.242152	0.170926	0.831	0.038	30	160
Po1-2_22.d	7.122507	0.507301	0.729	0.044	100	69
Po1-2_23.d	11.13586	0.793647	0.652	0.034	139	38
Po1-2_24.d	3.267974	0.427186	0.723	0.061	340	190
Po1-2_25.d	10.94092	0.622459	0.525	0.025	244	33
Po1-2_26.d	2.770083	0.230201	0.823	0.062	170	220
Po1-2_27.d	9.765625	0.648499	0.711	0.039	94	46
Po1-2_28.d	16.44737	1.514889	0.612	0.043	116	24
Po1-2_29.d	10.17294	0.817561	0.725	0.063	78	57
Sample Po1-3						
Grain	Final 238/206	Final 238/206 2SE	Final 207/206	Final 207/206 2SE	Final 207Age (Ma)	Final 207Age 2SE (Ma)
Po1-3_3.d	3.802281	0.260232	0.781	0.037	107	110
Po1-3_4.d	6.993007	0.635728	0.788	0.072	35	100
Po1-3_5.d	4.56621	0.479556	0.756	0.08	160	170
Po1-3_6.d	4.329004	0.299845	0.696	0.046	334	120
Po1-3_7.d	3.311258	0.274111	0.746	0.05	170	150
Po1-3_9.d	4.950495	0.441133	0.811	0.081	30	170
Po1-3_10.d	2.083333	0.177951	0.811	0.042	60	170
Po1-3_11.d	4.906771	0.312993	0.685	0.03	318	73
Po1-3_12.d	4.56621	0.437856	0.686	0.064	320	140

Po1-3_13.d	3.012048	0.254028	0.809	0.041	30	140
Po1-3_15.d	1.577287	0.11444	0.824	0.045	30	330
Po1-3_21.d	3.496503	0.293413	0.747	0.055	170	170
Po1-3_22.d	1.338688	0.177417	0.809	0.045	70	220
Po1-3_25.d	2.610966	0.197697	0.814	0.048	220	170
Po1-3_26.d	3.472222	0.831887	0.85	0.14	190	300
Po1-3_27.d	6.369427	0.567974	0.753	0.054	67	70
Sample Po1-6						
Grain	Final 238/206	Final 238/206 2SE	Final 207/206	Final 207/206 2SE	Final 207Age (Ma)	Final 207Age 2SE (Ma)
Po1-6_2.d	13.51351	1.205259	0.541	0.035	169	49
Po1-6_3.d	14.66276	1.397477	0.79	0.044	-	-
Po1-6_7.d	8.826125	0.732265	0.754	0.047	87	90
Po1-6_8.d	9.165903	0.840138	0.765	0.04	49	63
Po1-6_9.d	8.4246	0.681349	0.73	0.045	97	83
Po1-6_11.d	6.802721	0.694155	0.801	0.052	58	95
Po1-6_13.d	5.102041	0.546647	0.709	0.054	349	98
Po1-6_14.d	10.68376	0.958799	0.509	0.028	286	43
Po1-6_15.d	3.134796	0.324289	0.818	0.046	300	180
Po1-6_16.d	16.92047	4.580839	0.606	0.046	-	-
Po1-6_19.d	16	1.7152	0.617	0.032	-	-
Po1-6_23.d	3.508772	0.320099	0.782	0.13	70	120
Po1-6_24.d	5.154639	0.425125	0.771	0.027	248	80
Sample St8-1						
Grain	Final 238/206	Final 238/206 2SE	Final 207/206	Final 207/206 2SE	Final 207Age (Ma)	Final 207Age 2SE (Ma)
St8-1_3.d	5.32198	0.339882	0.739	0.033	88	63
St8-1_4.d	4.739336	0.404304	0.747	0.039	102	83
St8-1_5.d	4.504505	0.36523	0.753	0.066	130	160
St8-1_6.d	4.716981	0.333749	0.733	0.043	116	110
St8-1_7.d	2.463054	0.139533	0.806	0.033	10	160
St8-1_8.d	2.906977	0.245065	0.688	0.043	360	130
St8-1_9.d	2.932551	0.309595	0.813	0.047	-100	160
St8-1_10.d	5.589715	0.343694	0.764	0.035	67	75
St8-1_11.d	3.717472	0.290212	0.762	0.039	95	100
St8-1_12.d	3.533569	0.249722	0.755	0.039	109	96
St8-1_13.d	8.319468	0.567551	0.696	0.032	116	43
St8-1_16.d	5.624297	0.306837	0.722	0.032	124	77
St8-1_19.d	19.76285	1.874736	0.541	0.061	104	24
St8-1_20.d	3.731343	0.459456	0.682	0.064	280	170
St8-1_21.d	4.672897	0.32754	0.714	0.047	128	110
St8-1_22.d	4.926108	0.315465	0.774	0.045	58	99
St8-1_23.d	1.011122	0.098147	0.811	0.042	-90	390
St8-1_24.d	52.63158	4.155125	0.197	0.032	100	12
St8-1_25.d	3.610108	0.247625	0.796	0.084	140	130

St8-1_26.d	3.030303	0.20202	0.792	0.04	40	150
St8-1_27.d	3.968254	0.456664	0.662	0.051	310	130
St8-1_28.d	1.631321	0.180962	0.733	0.028	340	170
St8-1_29.d	5.681818	0.484246	0.697	0.056	162	99
St8-1_30.d	7.29927	0.959028	0.697	0.078	122	89
St8-1_32.d	3.571429	0.57398	0.705	0.061	220	150
St8-1_33.d	0.671141	0.044593	0.797	0.032	20	590
St8-1_35.d	11.53403	0.678472	0.431	0.023	272	35
St8-1_37.d	5.208333	0.352648	0.754	0.056	91	110
St8-1_38.d	3.278689	0.214996	0.804	0.035	-	-
St8-1_39.d	3.690037	0.217862	0.754	0.033	119	110
St8-1_40.d	2.114165	0.196667	0.769	0.04	130	180
St8-1_41.d	0.414938	0.041322	0.776	0.028	-	-
St8-1_42.d	19.72387	1.205996	0.584	0.033	99	23
St8-1_43.d	4.484305	0.382071	0.76	0.06	50	140

Sample St8-2

Grain	Final 238/206	Final 238/206 2SE	Final 207/206	Final 207/206 2SE	Final 207Age (Ma)	Final 207Age 2SE (Ma)
St8-2_1.d	2.777778	0.277778	0.747	0.027	356	100
St8-2_2.d	15.5521	1.088405	0.615	0.045	116	32
St8-2_3.d	3.597122	0.232907	0.818	0.033	133	99
St8-2_4.d	4.149378	0.292695	0.77	0.046	119	120
St8-2_5.d	7.423905	0.485006	0.734	0.032	109	50
St8-2_6.d	4.716981	0.689747	0.782	0.083	30	270
St8-2_7.d	6.69344	0.492824	0.743	0.041	114	71
St8-2_8.d	20.4499	1.045496	0.1999	0.0087	251	16
St8-2_9.d	6.329114	0.52075	0.763	0.057	96	96
St8-2_10.d	4.854369	0.518428	0.7	0.04	200	81
St8-2_11.d	4.739336	0.426765	0.821	0.074	50	140
St8-2_12.d	11.14827	0.69599	0.474	0.027	264	30
St8-2_13.d	1.908397	0.134753	0.814	0.032	80	170
St8-2_14.d	4.385965	0.461681	0.791	0.065	120	140
St8-2_15.d	7.29927	2.131174	0.729	0.052	112	50
St8-2_16.d	33.33333	2	0.34	0.02	118.5	11
St8-2_17.d	1.428571	0.112245	0.843	0.034	120	230
St8-2_18.d	2.80112	0.219696	0.788	0.037	90	140
St8-2_19.d	4.132231	0.648863	0.743	0.096	190	190
St8-2_20.d	3.571429	0.395408	0.794	0.068	100	170
St8-2_21.d	18.55288	1.927572	0.486	0.043	149	36
St8-2_23.d	5.208333	0.352648	0.694	0.054	219	110

[12.2] Apatite Fission Track Data

Table 8: Single grain apatite fission track data from all samples used in this study. ρs represents the surface density of spontaneous fission tracks. Ns gives the total number of spontaneous fission tracks counted per grain. t is the single grain AFT age (Donelick, O'Sullivan, & Ketcham, 2005), as calculated by in house Excel spreadsheets (e.g. Glorie et al., 2017), and t SD represents associated uncertain for single grain AFT age. Single grain AFT ages and uncertainties were used to identify AFT age populations using RadialPlotter. ^{238}U (µg/g) represents concentration of ^{238}U in each grain, and 1σ uncertainty has been represented by ^{238}U 1σ.

Sample M1-1						
Grain	ρs (x10^5)	Ns	^{238}U (µg/g)	^{238}U 1σ (µg/g)	t (Ma)	t SD (Ma)
M1-1_1.d	3.587	5	1.626	0.087	141.3624	71.08477
M1-1_2.d	1.833	29	35.9	3.2	91.19312	18.78403
M1-1_3.d	1.433	3	3.37	0.16	128.179	74.25396
M1-1_4.d	1.773	1	3.9	0.36	30.06837	30.1962
M1-1_5.d	6.175	18	2.35	0.15	253.4537	61.89139
M1-1_6.d	6.463	6	4.13	0.25	46.67564	19.26358
M1-1_12.d	1.908	10	8.24	0.58	105.18	37.91654
M1-1_15.d	4.019	1	7.26	0.34	7.138408	7.146232
M1-1_16.d	4.438	13	1.96	0.24	281.2712	88.19863
M1-1_17.d	1.623	5	1.79	0.12	141.8948	100.7847
M1-1_19.d	5.792	12	2.71	0.14	157.3865	46.15536
M1-1_21.d	9.971	17	2.45	0.13	143.417	35.60644
M1-1_22.d	1.901	8	5.08	0.25	170.3684	60.81506
M1-1_23.d	1.228	2	1.47	0.22	226.8542	163.9636
M1-1_27.d	10.56	23	7.24	0.35	62.3905	13.35438
M1-1_28.d	4.34	14	9.38	0.57	71.27363	19.53486
M1-1_30.d	3.434	9	3.95	0.38	136.8122	47.46537
Sample M1-5						
Grain	ρs (x10^5)	Ns	^{238}U (µg/g)	^{238}U 1σ (µg/g)	t (Ma)	t SD (Ma)
M1-5_3	0	0	44.7	3	0	-
M1-5_4	0	0	39.1	2.4	0	-
M1-5_9	0	0	95.1	9.5	0	-
Sample M72-1						
Grain	ρs (x10^5)	Ns	^{238}U (µg/g)	^{238}U 1σ (µg/g)	t (Ma)	t SD (Ma)
M72-1_1.d	1.699	13	2.55	0.15	508.5262	156.2171
M72-1_2.d	2.266	5	2.38	0.16	190.3712	86.09313
M72-1_3.d	5.924	29	7.68	0.35	158.3591	27.72339
M72-1_4.d	1.641	5	3.33	0.15	150.77	75.69032

M72-1_5.d	2.488	6	3.73	0.18	133.3487	54.81841
M72-1_6.d	11.95	13	2.82	0.21	79.89667	22.9442
M72-1_7.d	3.154	29	18.6	1.7	102.2051	21.15332
M72-1_9.d	3.002	15	4.85	0.3	155.5558	47.87866
M72-1_10.d	2.947	17	2.84	0.16	315.8341	89.38555
M72-1_11.d	3.326	27	14.98	0.68	111.9565	22.1373
M72-1_12.d	5.183	11	5.01	0.29	87.68257	26.92007
M72-1_13.d	1.726	6	2.87	0.18	166.1215	83.71166
M72-1_15.d	3.319	12	2.38	0.17	78.6649	45.76346
M72-1_17.d	2.257	7	3.1	0.17	118.0539	59.38093
M72-1_18.d	3.058	24	4.28	0.27	371.2454	79.31653
M72-1_19.d	6.078	50	22.5	2.2	75.74765	13.02342
M72-1_20.d	2.775	8	2.99	0.15	173.4619	66.13744
M72-1_21.d	1.582	3	3.75	0.24	104.5331	60.72191
M72-1_23.d	0.7648	3	1.57	0.11	171.2644	171.6843
M72-1_24.d	10.42	7	1.69	0.11	82.31224	31.56905
M72-1_25.d	4.937	26	6.62	0.46	163.6904	34.05779
M72-1_26.d	8.121	19	3.06	0.15	157.4006	36.92528
M72-1_27.d	4.836	21	8.07	0.49	100.6688	23.8902

Sample M72-2

Grain	ρs (x10^5)	Ns	^{238}U (µg/g)	^{238}U 1σ (µg/g)	t (Ma)	t SD (Ma)
M72-2_1.d	5.274	66	8.06	0.51	306.3659	42.92271
M72-2_2.d	4.365	25	4.41	0.28	160.3804	42.64367
M72-2_3.d	15.93	60	7.59	0.49	102.5958	14.80884
M72-2_4.d	12.41	19	2.07	0.16	120.5531	32.4915
M72-2_5.d	1.6	8	3.27	0.24	157.3897	79.53814
M72-2_6.d	7.727	24	3.56	0.24	171.9329	37.67769
M72-2_7.d	2.92	5	2.19	0.18	155.3495	70.63802
M72-2_10.d	4.084	12	5.57	0.34	109.0083	32.16381
M72-2_11.d	10.07	37	7.17	0.55	105.9197	19.21537
M72-2_12.d	7.725	28	3.06	0.25	133.1131	41.58244
M72-2_13.d	13.07	41	6.94	0.42	88.98669	15.23299
M72-2_14.d	4.936	33	4.19	0.24	324.2304	59.41821
M72-2_15.d	12.58	32	2.1	0.13	171.2528	38.01919

Sample Pi1-1

Grain	ρs (x10^5)	Ns	^{238}U (µg/g)	^{238}U 1σ (µg/g)	t (Ma)	t SD (Ma)
Pi1-1_1.d	4.567	5	3.64	0.25	62.37796	28.22333
Pi1-1_2.d	4.193	4	2.31	0.14	85.49418	43.05997
Pi1-1_3.d	12.31	37	4.85	0.27	127.8745	22.19504
Pi1-1_4.d	3.203	11	4.69	0.2	150.8235	45.92757
Pi1-1_5.d	5.257	18	4.56	0.19	154.6136	37.0078
Pi1-1_6.d	8.638	41	4.32	0.35	224.9998	39.58606

Pi1-1_9.d	4.666	6	3.57	0.22	74.63085	30.81308
Pi1-1_10.d	2.789	4	2.92	0.21	101.5546	51.29988
Pi1-1_11.d	15.33	33	2.69	0.19	164.6486	30.93111
Pi1-1_12.d	3.184	25	12.81	0.51	126.4872	25.79379
Pi1-1_13.d	3.199	5	3.38	0.38	95.65538	44.10943
Pi1-1_15.d	1.741	3	5.76	0.37	62.04472	36.04257
Pi1-1_16.d	2.551	7	5.73	0.47	99.0351	38.30305
Pi1-1_17.d	1.497	5	6.49	0.48	106.3683	48.21546
Pi1-1_19.d	3.802	10	6.38	0.46	85.34648	27.68154
Pi1-1_20.d	2.939	7	2.05	0.16	237.6894	91.73358
Pi1-1_21.d	11.29	21	4.72	0.32	81.60711	18.64779
Pi1-1_24.d	8.591	12	4.46	0.25	64.93963	19.0966
Pi1-1_25.d	3.264	5	4.53	0.21	70.08983	31.51308
Pi1-1_26.d	8.007	8	1.285	0.094	160.0338	57.77888
Pi1-1_28.d	6.043	12	4.91	0.23	83.73748	24.48911
Pi1-1_31.d	4.511	3	1.184	0.08	116.0058	67.43307
Pi1-1_32.d	1.566	4	5.61	0.28	94.19439	47.33126
Pi1-1_33.d	6.595	13	2.24	0.14	180.8304	51.41099
Pi1-1_34.d	3.21	8	4.9	0.27	105.133	37.61885
Pi1-1_36.d	2.834	13	6.15	0.34	153.5963	43.43801
Pi1-1_37.d	3.705	12	6.77	0.33	98.93816	28.96529
Pi1-1_38.d	3.054	4	1.81	0.18	149.0658	75.99281
Pi1-1_39.d	4.288	10	6.31	0.55	76.56507	25.11491
Pi1-1_41.d	2.342	3	2.39	0.15	110.7382	64.31137
Pi1-1_42.d	12.76	26	3.9	0.26	107.9723	22.36513
Pi1-1_44.d	4.144	4	3.12	0.17	64.15335	32.26657
Pi1-1_45.d	4.655	17	12.08	0.84	62.69676	15.81883
Pi1-1_46.d	4.596	8	1.98	0.15	180.6516	65.31978
Pi1-1_48.d	5.833	13	2.36	0.15	193.8605	55.16101
Pi1-1_49.d	9.902	28	5.37	0.31	108.8145	21.50203
Pi1-1_50.d	5.639	18	2.22	0.18	292.894	73.00625
Pi1-1_51.d	5.208	19	4.37	0.29	171.673	40.99911
Pi1-1_53.d	2.306	18	8.15	0.52	196.5685	47.99913
Pi1-1_54.d	3.496	7	6.68	0.5	62.16571	23.95274
Pi1-1_56.d	2.74	11	3.72	0.3	221.0689	68.99784
Pi1-1_57.d	5.2	10	3.8	0.25	104.6119	33.78951
Pi1-1_58.d	7.327	8	2.08	0.15	108.477	39.14211
Pi1-1_59.d	4.83	4	2.86	0.19	60.06458	30.29622
Pi1-1_60.d	7.54	23	3.45	0.48	181.6769	45.54098
Sample Pi1-2						
Grain	ρs (x10^5)	Ns	^{238}U (µg/g)	^{238}U 1σ (µg/g)	t (Ma)	t SD (Ma)
Pi1-2_1.d	3.437	59	24	1.2	132.5286	19.37273
Pi1-2_3.d	1.662	8	3.76	0.26	66.35452	47.14355

Pi1-2_4.d	2.153	2	4.07	0.24	47.39043	33.62642
Pi1-2_5.d	2.518	20	6.28	0.38	143.3625	44.0873
Pi1-2_7.d	3.407	7	4.76	0.35	89.33113	34.39698
Pi1-2_8.d	6.423	30	7.89	0.57	106.042	22.16269
Pi1-2_9.d	3.827	14	5.43	0.27	138.8926	37.7576
Pi1-2_10.d	3.255	18	2.1	0.12	209.9581	80.2585
Pi1-2_11.d	3.253	10	6.33	0.41	100.4203	32.41497
Pi1-2_12.d	2.535	14	2.82	0.23	229.097	83.12531
Pi1-2_13.d	2.112	8	8.5	0.4	69.2786	28.47015
Pi1-2_14.d	3.577	25	4.81	0.27	179.1737	47.3431
Pi1-2_17.d	1.967	10	5.24	0.22	120.1869	49.3249
Pi1-2_19.d	2.088	7	5.93	0.34	83.61069	37.69789
Pi1-2_20.d	2.135	12	6.94	0.36	69.94407	31.48966
Pi1-2_21.d	3.205	21	3.5	0.21	272.8157	72.31762
Pi1-2_22.d	4.503	6	3.38	0.34	81.63498	34.32412
Pi1-2_24.d	3.117	17	3.53	0.22	296.1361	76.29984
Pi1-2_25.d	2.374	35	43	2.1	71.05907	12.50246
Pi1-2_26.d	2.954	3	3.32	0.23	63.43524	36.88707
Pi1-2_27.d	3.232	28	9.03	0.52	196.9001	38.89981
Pi1-2_28.d	2.831	27	12.04	0.65	103.1101	25.61992
Pi1-2_29.d	2.072	3	3.12	0.18	95.99218	55.69712
Pi1-2_30.d	9.844	33	6.85	0.6	101.1894	19.71903
Pi1-2_31.d	7.4	9	1.98	0.12	126.7551	42.94438
Pi1-2_32.d	4.439	6	5.45	0.4	51.47909	21.35318
Pi1-2_33.d	4.194	11	2.5	0.27	176.4466	61.82563
Pi1-2_34.d	2.753	14	5.17	0.32	116.0843	41.66619
Pi1-2_35.d	3.303	22	5.41	0.35	251.6	56.05656
Pi1-2_36.d	2.204	1	0.627	0.074	149.0686	150.1033
Pi1-2_37.d	6.361	9	4.93	0.49	59.53327	20.70781
Pi1-2_38.d	1.733	2	3.01	0.17	79.41155	56.33128
Pi1-2_39.d	4.019	6	3.59	0.19	86.08594	35.43853
Pi1-2_40.d	2.569	30	22.6	1.3	106.793	20.44246
Pi1-2_41.d	2.915	12	8.32	0.89	102.2976	31.49306
Pi1-2_42.d	2.943	9	4.65	0.29	120.69	43.32915
Pi1-2_43.d	2.801	16	14.35	0.65	82.42746	20.94237
Pi1-2_44.d	2.81	15	5.89	0.57	186.1574	51.33083
Pi1-2_45.d	4.188	17	2.23	0.18	359.7362	117.406
Pi1-2_46.d	4.582	51	14.36	0.8	150.2646	23.2483
Pi1-2_47.d	7.466	17	6.37	0.34	74.0663	18.39358
Pi1-2_48.d	2.678	19	10.87	0.47	113.5393	28.80623
Pi1-2_49.d	1.902	6	4.87	0.36	133.5981	55.42809
Pi1-2_50.d	1.318	2	1.48	0.17	210.208	150.5879
Pi1-2_51.d	2.852	17	6.07	0.34	178.0889	47.05192
Pi1-2_52.d	1.588	5	6.62	0.45	98.36494	44.4954

Pi1-2_53.d	1.678	2	3.06	0.17	80.66646	57.21558
Pi1-2_54.d	4.873	18	4	0.24	189.6309	46.12188
Pi1-2_55.d	4.153	4	2.62	0.17	76.15971	38.39916
Pi1-2_56.d	1.807	11	14.6	0.96	86.31127	26.63547
Pi1-2_57.d	5.662	6	1.8	0.12	101.4385	45.86594
Sample Pi1-3						
Grain	ρs (x10^5)	Ns	^{238}U (µg/g)	^{238}U 1σ (µg/g)	t (Ma)	t SD (Ma)
Pi1-3_1.d	2.999	7	5.09	0.32	94.86387	36.34779
Pi1-3_2.d	1.492	7	5.86	0.51	164.728	63.89057
Pi1-3_6.d	1.209	14	7.12	0.37	171.0469	77.0092
Pi1-3_7.d	1.354	2	3.3	0.19	92.61268	65.70378
Pi1-3_8.d	3.549	5	3.71	0.24	78.65645	35.54234
Pi1-3_10.d	3.01	4	4.81	0.4	57.32085	29.05413
Pi1-3_17.d	8.648	24	4.88	0.33	117.4384	25.25323
Pi1-3_18.d	2.686	15	6.25	0.44	171.494	47.39714
Pi1-3_19.d	3.131	75	40.7	2.4	121.5013	15.75332
Pi1-3_21.d	3.363	12	5.65	0.3	130.2885	38.242
Pi1-3_22.d	3.613	1	1.49	0.12	38.59593	38.72089
Pi1-3_23.d	3.35	1	2.82	0.17	22.02219	22.06217
Pi1-3_24.d	1.301	2	1.92	0.18	164.7354	117.5049
Pi1-3_28.d	1.703	6	7.99	0.53	91.245	37.73913
Pi1-3_29.d	2.879	8	13.34	0.74	43.26441	15.48341
Pi1-3_30.d	1.445	2	2.86	0.22	100.0731	71.17983
Pi1-3_31.d	4.69	8	5.46	0.28	64.77942	23.14265
Pi1-3_34.d	2.636	2	4.86	0.25	32.45272	23.00818
Pi1-3_35.d	2.502	24	20.74	0.98	95.67202	20.04537
Pi1-3_36.d	1.717	6	5.01	0.4	143.7437	59.79479
Pi1-3_37.d	2.037	11	10.2	0.95	89.64469	31.02609
Pi1-3_38.d	2.469	7	2.15	0.18	193.3647	87.97757
Pi1-3_39.d	1.682	4	3.56	0.22	103.5734	60.1397
Pi1-3_40.d	3.443	22	6.58	0.43	161.1643	44.3419
Pi1-3_41.d	2.773	3	3.13	0.2	71.63221	41.60939
Pi1-3_42.d	1.704	4	4.76	0.33	101.9626	51.46902
Pi1-3_43.d	1.822	34	59.9	3.8	64.59849	11.81221
Pi1-3_44.d	2.577	4	4.44	0.25	72.44634	36.45213
Pi1-3_45.d	2.163	5	4.68	0.26	102.1221	46.02142
Pi1-3_46.d	2.308	7	3.39	0.21	183.8031	70.39793
Pi1-3_47.d	4.25	5	2.07	0.19	107.0695	54.42931
Sample Pi1-4						
Grain	ρs (x10^5)	Ns	^{238}U (µg/g)	^{238}U 1σ (µg/g)	t (Ma)	t SD (Ma)
Pi1-4_3.d	1.623	2	2.58	0.14	98.77719	70.05138
Pi1-4_4.d	0.9892	2	4.47	0.29	93.57909	66.44834

Pi1-4_8.d	3.422	3	2.86	0.18	63.56656	36.91758
Pi1-4_9.d	1.651	1	3.71	0.26	33.93375	34.01698
Pi1-4_11.d	0.8826	3	5.23	0.3	134.0384	77.7681
Pi1-4_12.d	3.236	5	1.7	0.16	186.6833	85.31613
Pi1-4_15.d	0.6938	3	6.33	0.7	94.21304	67.42843
Pi1-4_17.d	1.03	3	6.1	1	98.74614	59.26479
Pi1-4_18.d	0.8278	1	4.53	0.29	55.33597	55.44924
Pi1-4_19.d	2.75	5	5.16	0.31	73.0167	32.94739
Pi1-4_20.d	1.616	16	13.54	0.74	150.6167	38.54343
Pi1-4_21.d	2.538	4	1.78	0.1	181.9291	91.53694
Pi1-4_22.d	4.557	10	5.57	0.31	81.58515	26.19602
Sample Po1-1						
Grain	ρs (x10^5)	Ns	^{238}U (µg/g)	^{238}U 1σ (µg/g)	t (Ma)	t SD (Ma)
Po1-1_1.d	11.98	55	7.06	0.4	134.1134	19.61537
Po1-1_2.d	2.443	6	2.42	0.18	208.1038	86.35658
Po1-1_3.d	2.828	19	6.52	0.29	200.2984	48.04402
Po1-1_5.d	5.022	37	2.1	0.24	156.1777	58.0303
Po1-1_6.d	3.398	17	9.99	0.67	103.5296	26.05194
Po1-1_7.d	1.673	8	5.83	0.93	126.9405	55.63894
Po1-1_8.d	6.156	12	4.46	0.32	97.92723	28.05423
Po1-1_9.d	7.388	20	5.13	0.29	98.2227	23.80786
Po1-1_10.d	16.23	27	3.78	0.21	91.07068	18.24222
Po1-1_11.d	5.674	17	4.63	0.34	102.3101	29.35349
Po1-1_12.d	3.96	7	6.12	0.4	59.91397	22.98144
Po1-1_13.d	7.526	52	11.21	0.65	115.0649	18.06142
Po1-1_14.d	2.99	4	3.35	0.2	103.1976	46.5608
Po1-1_15.d	3.659	6	1.69	0.14	199.1015	82.93939
Po1-1_17.d	9.518	29	8.5	0.47	74.27208	14.39043
Po1-1_18.d	3.963	8	2.57	0.18	161.6489	58.26214
Po1-1_19.d	4.48	39	24.8	1.2	72.74092	12.16804
Po1-1_20.d	4.503	18	6.64	0.49	117.4125	29.76569
Po1-1_21.d	7.296	22	5.71	0.29	109.1232	23.91616
Po1-1_22.d	8.223	13	2.2	0.12	159.2923	43.45024
Po1-1_23.d	4.941	17	3.98	0.29	156.8332	39.71714
Po1-1_24.d	4.925	18	8.4	0.44	90.04235	21.74095
Po1-1_25.d	2.877	16	3.71	0.19	267.7083	72.84978
Po1-1_26.d	1.81	18	17.43	0.95	111.3304	27.675
Po1-1_27.d	12.36	33	4.61	0.26	112.3951	21.15863
Po1-1_28.d	3.526	19	13.12	0.85	85.0289	20.26988
Po1-1_29.d	7.018	24	7.24	0.42	97.69242	20.73105
Po1-1_30.d	6.063	41	5.16	0.27	222.5965	39.91233
Po1-1_31.d	2.603	5	1.99	0.17	198.0841	90.18764
Po1-1_32.d	8.277	11	3.4	0.17	80.94829	24.74015

Po1-1_33.d	6.5	25	4.27	0.37	163.1068	37.53688
Po1-1_34.d	3.633	20	9.79	0.47	104.6146	25.16417
Po1-1_36.d	3.311	14	8.04	0.5	108.6784	29.82149
Sample Po1-2						
Grain	ρs (x10^5)	Ns	^{238}U (µg/g)	^{238}U 1σ (µg/g)	t (Ma)	t SD (Ma)
Po1-2_1.d	2.801	1	1.78	0.13	83.0601	59.0448
Po1-2_2.d	1.088	2	4.62	0.33	82.39053	58.55539
Po1-2_3.d	4.196	5	2.88	0.18	102.6496	42.39479
Po1-2_4.d	3.598	20	6.28	0.35	100.6637	30.86541
Po1-2_5.d	10.63	62	6.71	0.39	141.5984	21.83847
Po1-2_6.d	1.253	1	1.392	0.094	118.3892	118.6588
Po1-2_7.d	0.678	4	3.45	0.41	230.799	136.0455
Po1-2_8.d	0.7898	3	5.16	0.35	151.6121	88.1353
Po1-2_9.d	0.5563	9	9.53	0.52	344.4163	116.3334
Po1-2_10.d	3.212	56	20.9	1.5	168.5188	25.74138
Po1-2_11.d	3.008	27	14.4	1.1	119.1724	25.51382
Po1-2_12.d	7.69	31	6.77	0.37	107.1839	21.44321
Po1-2_13.d	1.913	3	2.84	0.17	114.0608	66.20605
Po1-2_14.d	4.969	33	6.61	0.41	138.0984	30.66341
Po1-2_15.d	7.682	15	4.5	0.24	89.79921	23.67553
Po1-2_16.d	2.103	3	2.36	0.17	124.7548	72.58567
Po1-2_17.d	3.955	1	0.822	0.072	63.78635	64.03057
Po1-2_18.d	0.8618	6	12.3	1.2	116.8941	49.06557
Po1-2_19.d	1.455	3	4.48	0.32	95.20631	55.38646
Po1-2_20.d	1.686	7	4.64	0.25	131.8385	59.38634
Po1-2_21.d	9.747	13	2.44	0.14	56.60303	16.03127
Po1-2_22.d	20.93	121	5.16	0.45	227.4956	28.72108
Po1-2_23.d	3.137	12	11.55	0.84	68.65411	20.43802
Po1-2_24.d	2.615	1	1.19	0.1	66.62414	66.85897
Po1-2_25.d	2.635	35	16.61	0.8	141.2861	26.67768
Po1-2_26.d	5.725	23	1.85	0.16	437.3817	98.73418
Po1-2_27.d	20.11	110	6.19	0.37	168.5405	19.4931
Po1-2_28.d	3.473	9	11.12	0.8	43.02558	15.52357
Po1-2_29.d	5.045	39	4.88	0.28	216.4107	44.22073
Sample Po1-3						
Grain	ρs (x10^5)	Ns	^{238}U (µg/g)	^{238}U 1σ (µg/g)	t (Ma)	t SD (Ma)
Po1-3_4.d	3.628	5	2.42	0.12	94.25297	47.35767
Po1-3_5.d	2.676	3	2.28	0.15	101.6641	59.07565
Po1-3_6.d	4.44	10	3.04	0.15	107.1822	40.8548
Po1-3_7.d	2.495	2	2.25	0.23	37.01655	37.20944
Po1-3_9.d	1.911	1	1.65	0.13	65.75593	65.95971
Po1-3_10.d	7.639	17	1.96	0.15	178.4523	51.34344

Po1-3_11.d	5.036	44	7.35	0.33	210.4737	35.42693
Po1-3_12.d	1.611	3	2.04	0.13	125.5924	89.16714
Po1-3_13.d	1.668	2	2.51	0.15	98.79264	70.10599
Po1-3_15.d	12.5	17	1.46	0.11	148.5276	42.68705
Po1-3_21.d	3.089	7	3.06	0.17	27.16267	27.20455
Po1-3_22.d	1.112	4	1.9	0.14	194.3149	138.1454
Po1-3_25.d	13.06	32	2.26	0.14	194.7274	38.72662
Po1-3_26.d	2.835	9	6.45	0.4	68.02078	28.08794
Po1-3_27.d	7.436	17	4.38	0.19	95.27108	24.94363
Sample Po1-6						
Grain	ρs ($x10^5$)	Ns	^{238}U (µg/g)	^{238}U 1σ (µg/g)	t (Ma)	t SD
Po1-6_1.d	1.117	0	1.63	0.15	0	-
Po1-6_2.d	2.784	6	8.05	0.45	55.55331	22.89117
Po1-6_3.d	2.14	1	8.75	0.95	11.11988	11.18522
Po1-6_4.d	0.9387	0	3.94	0.31	0	-
Po1-6_7.d	3.994	11	7.32	0.42	77.93671	23.9205
Po1-6_8.d	2.79	11	6.15	0.29	132.2354	40.35514
Po1-6_9.d	2.263	5	7.82	0.47	58.61372	26.44851
Po1-6_11.d	2.149	6	2.86	0.031	133.6275	55.19766
Po1-6_13.d	3.238	9	2.32	0.18	125.1561	42.71481
Po1-6_14.d	6.45	8	14.2	0.17	76.93402	27.73462
Po1-6_15.d	1.517	6	3.05	1	135.7195	56.04859
Po1-6_16.d	2.989	14	20.6	0.19	95.89349	26.23032
Po1-6_19.d	1.466	9	11.4	1.2	58.51385	20.96921
Po1-6_23.d	2.799	6	7.97	1.5	79.67315	32.87846
Po1-6_24.d	1.957	2	10.74	0.48	37.31521	26.49769
Sample St8-1						
Grain	ρs ($x10^5$)	Ns	^{238}U (µg/g)	^{238}U 1σ (µg/g)	t (Ma)	t SD (Ma)
St8-1_1.d	2.456	11	1.97	0.51	376.4455	158.8813
St8-1_2.d	2.885	7	3.34	0.27	128.4756	53.4683
St8-1_3.d	1.46	6	7.43	0.44	95.34744	43.01289
St8-1_4.d	1.406	2	5.24	0.39	56.32629	40.04872
St8-1_5.d	5.144	8	2.4	0.13	133.6486	47.80326
St8-1_6.d	2.567	8	5.83	0.39	96.7469	37.1352
St8-1_7.d	6.76	19	4.64	0.25	111.9705	27.81886
St8-1_8.d	1.688	2	2.25	0.13	108.818	77.2024
St8-1_9.d	6.592	11	2.19	0.18	114.4626	41.54781
St8-1_10.d	4.724	38	5.89	0.38	220.8673	42.76829
St8-1_11.d	4.143	14	5.34	0.32	102.7935	31.59962
St8-1_12.d	2.339	11	7.75	0.45	113.9516	36.63708
St8-1_13.d	3.075	14	5	0.34	187.0227	51.57642
St8-1_15.d	1.471	18	13.07	0.96	181.6865	46.04185

St8-1_16.d	3.942	14	7.45	0.36	98.58854	26.77611
St8-1_20.d	1.701	6	1.99	0.23	359.1985	152.4056
St8-1_21.d	5.132	10	4.7	0.45	85.82577	28.35721
St8-1_22.d	7.188	21	4.95	0.34	116.0905	27.15573
St8-1_23.d	1.887	3	2.14	0.13	132.219	76.75805
St8-1_24.d	7.683	120	31.2	1.5	103.4907	10.67748
St8-1_25.d	2.994	2	4.25	0.26	16.35704	16.38762
St8-1_26.d	4.921	12	4.35	0.27	96.6262	31.13892
St8-1_27.d	3.394	4	3.68	0.25	66.3985	33.50428
St8-1_28.d	0.7774	7	3.69	0.24	105.7383	53.31459
St8-1_29.d	3.769	16	2.48	0.14	132.4043	54.56817
St8-1_30.d	2.294	9	4.24	0.46	146.71	51.42837
St8-1_32.d	2.327	17	5.12	0.51	104.1046	43.74731
St8-1_33.d	4.234	3	1.236	0.088	79.15676	56.25529
St8-1_34.d	2.382	18	15.3	1.3	102.1155	25.58497
St8-1_35.d	3.377	84	18.69	0.84	153.348	23.40582
St8-1_36.d	2.965	27	4.88	0.28	336.7219	71.39679
St8-1_37.d	4.117	12	6.25	0.28	96.46358	28.17998
St8-1_38.d	2.375	3	4.4	0.31	59.55166	34.63722
St8-1_39.d	2.092	7	4.55	0.22	130.0429	53.46086
St8-1_40.d	1.797	10	3.96	0.21	173.3611	71.36898
St8-1_41.d	2.506	7	4.98	0.36	82.95807	37.58153
St8-1_42.d	3.332	61	32	1.5	118.137	16.10771
St8-1_43.d	4.88	9	3.08	0.25	96.33297	37.24058
Sample St8-2						
Grain	ρs (x10^5)	Ns	^{238}U (µg/g)	^{238}U 1σ (µg/g)	t (Ma)	t SD (Ma)
St8-2_1.d	1.294	6	13.69	0.76	70.20097	28.92319
St8-2_2.d	2.053	9	5.3	0.35	113.9044	47.10571
St8-2_3.d	2.573	12	3.93	0.2	182.8657	61.66153
St8-2_4.d	2.78	11	3.73	0.21	99.71252	44.94477
St8-2_5.d	1.287	7	9.22	0.5	104.5232	43.04624
St8-2_6.d	1.032	6	12.4	1.1	96.97851	40.51521
St8-2_7.d	4.288	9	4.74	0.27	91.62538	30.98453
St8-2_8.d	0.4701	30	191	17	69.25627	14.06691
St8-2_9.d	1.413	3	2.81	0.24	104.1276	74.16447
St8-2_10.d	1.85	5	3.06	0.2	73.20907	51.9873
St8-2_11.d	1.5	4	2.62	0.21	105.1927	74.85882
St8-2_12.d	1.847	10	18.1	1.3	62.03825	20.11787
St8-2_13.d	1.842	10	3.29	0.18	335.0247	107.518
St8-2_14.d	3.377	6	1.45	0.13	132.4916	77.41087
St8-2_15.d	1.249	3	5.63	0.45	88.3017	51.46724
St8-2_16.d	1.484	35	51	2.9	95.66082	17.06006
St8-2_18.d	1.904	2	1.78	0.14	121.823	86.67314

St8-2_19.d	4.14	3	0.546	0.05	181.8005	129.6259
St8-2_20.d	1.769	3	1.85	0.16	188.2613	109.9055
St8-2_21.d	0.7181	8	14.75	0.98	97.63299	44.14203
St8-2_22.d	3.776	5	3.45	0.19	79.4941	35.81939
St8-2_23.d	0.3897	1	3.65	0.26	144.8719	145.2389

[12.3] Rare Earth Element Data

Table 9: Un-adjusted Rare Earth Elemental (REE) concentrations for each grain used in this study. REE data used to produce chondrite normalised spider diagrams was normalised to chondrite values contained within Sun & McDonough (1989).

Sample M1-1																	
Grain	La (ppm)	Ce (ppm)	Pr (ppm)	Nd (ppm)	Sm (ppm)	Eu (ppm)	Gd (ppm)	Tb (ppm)	Dy (ppm)	Y (ppm)	Ho (ppm)	Er (ppm)	Tm (ppm)	Yb (ppm)	Lu (ppm)	Sr (ppm)	Mn (ppm)
M1-1_1.d	268	742	104.8	466	77.9	16.04	50.4	5.9	27.8	132.9	4.65	12.18	1.51	8.46	1.205	978	1712
M1-1_2.d	1530	3600	361	1520	231	19.4	155	16.3	87	411	15.6	37.5	4.16	23.7	3.38	575	1020
M1-1_3.d	335	855	119.8	634	141.8	30.1	144.2	17.63	92	425	17.85	40.4	4.57	23.9	3.26	883	887
M1-1_4.d	531	1470	222	1176	272	41.8	271	33.4	188.8	872	34.2	83.5	9.42	54.2	6.64	1110	1125
M1-1_5.d	730	1539	179	664	101.3	18.5	72	7.83	42.8	205.1	8.15	18.4	2.27	12.64	1.98	1061	1404
M1-1_6.d	220	608	87.1	452	106.5	24.1	109.9	12.12	60.9	272.1	11.39	26.2	2.9	14.5	2.05	1010	555
M1-1_12.d	1760	3620	370	1343	209	12.3	160	17.6	89.2	480	17	43	5.75	36.9	5.64	265	1140
M1-1_13.d	1076	2190	216	781	110.8	23.4	70.3	7.53	35.9	182	6.28	14.3	1.8	9.97	1.53	1479	1350
M1-1_14.d	1287	2670	287	1122	157.4	29.9	98.8	10.11	49.7	204.6	7.7	17.4	1.96	12.79	1.64	1920	1125
M1-1_15.d	412	950	110.6	438	73.1	15.84	59.6	6.76	33.3	198.1	6.72	16	2.13	13.55	1.98	705	1110
M1-1_16.d	841	2040	260	1200	195	28.4	126	12.2	56.7	253	8.78	21.8	2.81	17.7	2.33	1220	832
M1-1_17.d	1108	2450	321	1325	191.1	30.7	107	10.13	45.1	202.7	7.81	18.4	2.03	12.62	1.74	2410	1263
M1-1_18.d	84.3	263	53.7	351	130	33.7	172	25.3	145	704	28.5	68.8	8.25	43.5	5.79	320	1435
M1-1_19.d	1005	2380	305	1289	204	36.2	114.2	12.66	55	272	9.7	22.7	2.7	14.96	2.21	1876	1261
M1-1_21.d	404	923	119.1	509	89.1	16.62	66.9	7.75	35	159.1	5.99	11.88	1.38	7.89	1.01	587	1034
M1-1_22.d	420	1211	172.2	942	225	37.9	221	30.2	159.8	762	28.5	69.5	7.94	44.1	6	804	1072
M1-1_23.d	227	560	82	414	85.8	25.5	82.1	9.2	46.7	205	7.89	18.2	2.12	12.3	1.42	1830	1050
M1-1_26.d	1040	2470	310	1281	205	36.5	112.3	10.92	45.5	189.9	7.28	16.8	1.81	10.66	1.36	3270	888
M1-1_27.d	460	1141	165.8	850	199	34.8	171	21.2	107.7	498	19.2	44.2	4.79	25.4	3.63	922	664

M1-1_28.d	1348	2980	359	1440	209	30.6	132.2	15.5	78.8	374	13.83	34.4	4.33	24	3.45	1158	1611
M1-1_29.d	1370	2950	365	1412	211	31.3	135.9	15.38	75.8	355	13.57	32.5	3.71	24.5	2.96	1382	1437
M1-1_30.d	1430	3440	431	1930	363	69.6	300	39.8	192	936	35.7	85.9	10.5	58.3	7.53	1022	2120
Sample M72-1																	
Grain	La (ppm)	Ce (ppm)	Pr (ppm)	Nd (ppm)	Sm (ppm)	Eu (ppm)	Gd (ppm)	Tb (ppm)	Dy (ppm)	Y (ppm)	Ho (ppm)	Er (ppm)	Tm (ppm)	Yb (ppm)	Lu (ppm)	Sr (ppm)	Mn (ppm)
M72-1_1.d	262	606	84.9	412	83.7	20.5	76.6	9.75	51.4	263.3	9.89	24.1	2.89	17.4	2.33	2088	923
M72-1_2.d	426	960	138.4	625	138.6	34.6	130.1	16.54	82.7	391	16.04	34.3	4.24	23.1	2.98	1237	595
M72-1_3.d	1001	2087	228.3	928	132.3	24.8	86.3	9.72	45.3	219.1	8.6	19	2.32	14.61	2.03	1158	2160
M72-1_4.d	605	1412	199.8	971	205.7	43.6	189.6	23.4	123.6	569	23.08	54.4	6.4	36.4	4.62	1130	1268
M72-1_5.d	604	1531	207.3	960	157.1	31.2	102.9	11.17	53.6	246.6	9.27	22.4	2.53	15.1	2.19	1690	978
M72-1_6.d	766	1812	236	1001	145.9	26.4	93.4	10.11	43.7	209	7.46	18	1.93	11.8	1.57	1585	2190
M72-1_7.d	536	1210	150	646	109	23.6	88.6	10.25	58.6	305	10.41	27	3.51	20.2	2.87	2020	1200
M72-1_8.d	1329	2880	347	1389	191.9	36.1	102.4	9.85	43.8	192.9	7.27	16.6	2.05	12.9	1.86	2530	858
M72-1_9.d	738	1683	202.6	797	126.5	20.1	92.1	10.51	51.4	262	9.21	21.2	2.85	16.8	2.3	955	1370
M72-1_10.d	1211	2710	347	1413	210	34.5	128.2	12.75	60.5	301	10.8	27	3.18	18.1	2.38	2100	1388
M72-1_11.d	1182	2460	275	1149	192	17.9	159.7	18.2	96.1	467	18.83	46.6	5.62	36	5.43	299	622
M72-1_12.d	1226	2860	336	1445	205	31.4	125.7	12.69	60.6	273	10.59	24.5	2.91	15.7	2.35	1430	1234
M72-1_13.d	290	798	120.7	571	110.7	21.8	96.4	11.5	53.3	244	8.65	18.8	2.06	11.8	1.84	519	1550
M72-1_14.d	897	1439	137.7	504	70.1	16.5	57.4	6.01	31.6	181.6	6.18	15.85	1.97	12.9	2.16	1103	1748
M72-1_15.d	354	971	137.6	692	139.2	25.7	103.2	10.94	47.7	210	7.81	17.2	1.89	11.1	1.46	1072	997
M72-1_16.d	923	2400	313	1340	209	45.8	119.3	10.96	47.7	204.8	7.56	15.86	1.75	10.35	1.36	3360	689
M72-1_17.d	1547	3600	446	1808	265	36.9	150.3	14.35	65.2	297	10.64	26.1	3.03	17.6	2.31	1990	1740
M72-1_18.d	1812	3890	458	1871	260	40.7	139	13.04	54.8	254.9	9.52	20.1	2.3	14.6	1.96	1328	910
M72-1_19.d	960	2490	215	1050	204	27.6	160	18.6	104	580	21.4	57.1	6.6	41.9	6.07	389	1240
M72-1_20.d	1266	2930	348	1501	222	36.8	134.2	14.17	67.3	340	12.69	29.4	3.72	22.8	3.01	2640	1271
M72-1_21.d	453	1094	141.3	689	145.2	28.4	123.3	14.21	72.6	339	12.19	28.8	3.16	17.5	2.39	1464	603

M72-1_22.d	1590	3760	484	2070	301	41.8	181	16.7	80.4	378	14	35.7	4.12	21.3	2.73	1780	1370
M72-1_23.d	316	742	101.7	482	93.4	25.3	82.9	10.25	51.2	252	9.71	23.2	2.87	16.2	2.06	1821	1063
M72-1_24.d	406	1075	150	702	128	23.7	89.4	8.6	35	154.2	5.87	11.94	1.15	7.05	0.91	1134	823
M72-1_25.d	1448	2730	293	1123	158.5	26.8	101.6	10.47	48.1	210	7.7	17.6	1.93	11.5	1.5	1000	1325
M72-1_26.d	1749	4060	479	1960	286	39.8	157.5	15.6	66.4	292	10.99	21.9	2.68	14.9	1.98	2130	1435
M72-1_27.d	759	2030	275	1260	263	18.8	223	27.2	135.8	669	23.7	53.4	6.23	33.7	4.02	716	477
Sample M72-2																	
Grain	La (ppm)	Ce (ppm)	Pr (ppm)	Nd (ppm)	Sm (ppm)	Eu (ppm)	Gd (ppm)	Tb (ppm)	Dy (ppm)	Y (ppm)	Ho (ppm)	Er (ppm)	Tm (ppm)	Yb (ppm)	Lu (ppm)	Sr (ppm)	Mn (ppm)
M72-2_1.d	1780	3960	497	2260	413	67	319	38.7	204	999	37.9	85.6	10.62	56.9	7.35	1900	1800
M72-2_2.d	1113	2450	304	1313	246	45.7	197	25	138.8	745	26.5	65.4	8.14	46.9	6.39	1248	1628
M72-2_3.d	1783	3570	381	1412	191	41.5	118.1	11.73	55	255	8.52	20	2.5	14.2	1.94	2270	1013
M72-2_4.d	1086	2550	349	1485	221	49.4	126	11.99	50.9	230.1	8.4	19.6	2.14	10.81	1.42	3340	872
M72-2_5.d	576	1116	127.9	482	73.4	15.8	51.8	5.53	27.1	136.2	5.22	11.7	1.19	8.44	1.24	991	1329
M72-2_6.d	936	2170	282	1305	202	43.4	132.9	13.97	65.9	300	11.37	26.4	3.32	19.3	2.42	3570	1313
M72-2_7.d	870	2200	300	1428	235	29.7	145.2	15.42	64.8	298	10.95	25.5	2.82	14.2	1.75	1074	1023
M72-2_8.d	641	1355	162.6	681	114	21	84.8	10.8	56	289	10.84	27.3	3.46	19.8	3.15	1275	1830
M72-2_10.d	812	1842	225	942	156.2	28.6	114.6	13.07	67.9	358	12.49	30.1	3.67	21.9	3.17	933	1620
M72-2_11.d	1438	3050	370	1638	300	44.4	258	32.6	165	826	31	79.9	9.51	54.6	6.95	1490	1730
M72-2_12.d	527	1128	130	467	67	13.95	48.4	5.35	24.6	123.3	4.56	10.43	1.34	7.48	1.02	949	1105
M72-2_13.d	1822	2890	295	1266	225	27.8	200	25	127	626	24.8	60.5	7.86	44.4	6.43	1066	2080
M72-2_14.d	1501	3350	418	1707	234	44.8	134.8	12.47	57.1	251	9.55	21.3	2.59	14.8	2.01	3200	1243
M72-2_15.d	1082	2740	340	1449	234	47.5	126.2	12.28	51.3	232	8.36	17.9	2.07	11.9	1.41	3660	800
Sample Pi1-1																	
Grain	La (ppm)	Ce (ppm)	Pr (ppm)	Nd (ppm)	Sm (ppm)	Eu (ppm)	Gd (ppm)	Tb (ppm)	Dy (ppm)	Y (ppm)	Ho (ppm)	Er (ppm)	Tm (ppm)	Yb (ppm)	Lu (ppm)	Sr (ppm)	Mn (ppm)
Pi1-1_1.d	1394	3040	343	1418	202	28.2	119.5	12.53	58.9	277	10.19	23	2.91	16.1	2.17	1361	1101

Pi1-1_2.d	884	2390	304	1376	233	31.7	153.9	15.63	70.5	307	11.7	26.1	2.65	15.07	1.83	1100	1084
Pi1-1_3.d	359	808	99.1	422	69.1	14.5	54.8	5.86	29.5	153.5	5.44	12.84	1.45	8.34	1.3	706	1223
Pi1-1_4.d	630	1690	235	1195	271	39.9	247	32.9	177	876	33.9	80.5	9.32	51.9	6.39	598	1350
Pi1-1_5.d	598	1062	103.6	385	53.8	11.17	42.9	4.85	24.2	143.1	4.51	11.97	1.42	10.14	1.59	830	1042
Pi1-1_6.d	764	1700	201	865	141.1	26.2	92	10.32	47.9	231	8.56	19.5	2.64	15.4	2.13	1351	1089
Pi1-1_9.d	956	1980	234	940	141.3	26.6	93.6	10.38	49.5	239	8.6	20.9	2.36	15.6	2	1481	1226
Pi1-1_10.d	915	2010	236	914	138	25.9	86.3	8.7	42.1	203.2	7.47	16.5	2.21	10.9	1.66	1759	1226
Pi1-1_11.d	1029	2450	306	1307	201	28.5	120.4	11.91	55.9	254	9.46	21.3	2.33	14.1	1.73	1385	1333
Pi1-1_12.d	1619	3440	390	1463	216.5	33.7	142.1	16.6	80.5	400	14.66	35	4.42	26	3.61	1335	1220
Pi1-1_13.d	1074	2650	279	1182	172	23.8	102.8	11.3	52.5	243	9.86	19.9	2.28	15.1	1.88	1330	1390
Pi1-1_14.d	941	2085	273	1210	231.3	56.8	194.6	22.5	110.1	504	20.04	47.7	5.29	28.3	3.66	1765	958
Pi1-1_15.d	466	951	99.2	402	57.4	13.88	43.1	5.09	24.2	121.9	4.4	9.93	1.28	8.65	1.11	870	1619
Pi1-1_16.d	1169	2620	320	1215	195	27.1	132	13.9	68.4	339	13	27.4	3.61	21.2	2.7	808	1490
Pi1-1_17.d	894	2080	265	1142	222	48.2	185	22.5	121	549	21.9	49.5	6.01	37.1	4.3	2150	1172
Pi1-1_18.d	1196	2740	330	1354	215.6	37	145.3	16.12	74.2	374	14.12	31.2	3.83	22.9	3.37	1230	1116
Pi1-1_19.d	919	2070	245	1004	154	24.3	114.5	13.14	68.9	336	13.52	32.2	4.11	25.3	3.48	1132	1288
Pi1-1_21.d	550	1267	162.9	734	118.6	23.5	88.7	9.27	42.9	205.5	7.33	16	1.81	10.5	1.46	1130	1071
Pi1-1_22.d	972	2270	308	1260	207	28.7	136	14.3	61.1	279	11.13	23.2	2.89	16.4	2.2	1390	1160
Pi1-1_24.d	701	1591	188.4	814	125	24.7	87.6	10.08	51	251.1	9.17	22.1	2.6	15.7	2.24	1212	1203
Pi1-1_25.d	1008	2261	269	1124	166.8	24.2	112.9	11.95	60.8	301	10.83	25.2	3.06	18.5	2.44	1117	1264
Pi1-1_26.d	704	1840	250	1104	181.3	23.3	114	11.71	54.9	244	9.15	18.9	2.23	10.99	1.55	1212	1131
Pi1-1_28.d	412	1109	150.1	630	122.1	23.6	91.2	10.21	44.6	187.1	7.02	14.9	1.7	8.92	0.928	581	1169
Pi1-1_29.d	275	578	65.3	264	44.1	11.84	37.1	4.84	26	164.6	5.29	15.1	2	13.3	2.36	837	1768
Pi1-1_31.d	160.2	468	70.9	381	94	25.5	97.5	13.03	70.9	327	12.7	30.5	3.5	18.9	2.55	909	850
Pi1-1_32.d	905	1931	212.2	858	142.8	28.5	103.3	12.07	63.4	366	12.92	30.1	4.01	25.4	3.32	1351	1092
Pi1-1_33.d	894	2310	336	1424	238	31.3	150.6	16.15	71	310	12.12	26.6	2.83	16.6	1.93	1069	1024

Pi1-1_34.d	1057	2500	302	1215	194	25.8	122.8	13.9	67.9	322	12.25	27.6	3.49	20.7	2.57	1167	1348
Pi1-1_35.d	1132	2550	320	1323	198	27.6	128	14.91	66.8	340	13.22	28.2	3.55	21.2	2.97	1198	1512
Pi1-1_36.d	1707	4020	487	2097	372	64.3	280	33.2	169	818	31.6	71.1	8.56	49	6.28	1339	2340
Pi1-1_37.d	1092	2500	312	1222	171.7	26.1	118.1	13.66	69.4	338	12.54	31.1	3.97	24.9	3.34	1154	1749
Pi1-1_38.d	272	833	122	545	108.6	24.1	81.1	10.4	50.8	245	8.8	21.9	2.74	16.4	2.18	1370	1260
Pi1-1_39.d	753	1970	252	1027	184	25.7	147	17.7	89.7	455	17.4	45	5.54	32	4.46	1036	1135
Pi1-1_41.d	246	720	109.5	548	113.4	23.4	89.3	10.55	52.7	253.2	8.97	21.3	2.61	16.4	2.08	1166	966
Pi1-1_42.d	646	1252	137.5	546	80.3	17.6	62.8	6.48	33.7	162.6	5.83	13	1.78	11.2	1.53	1246	930
Pi1-1_44.d	336	899	126.3	571	104.1	21.5	70.7	8.02	37.5	187.8	6.82	16.24	2.02	10.43	1.59	1416	992
Pi1-1_45.d	1620	3900	451	1850	287	42.9	189	20.3	107	492	18.6	44.3	5.36	30.6	4.53	1220	1300
Pi1-1_46.d	871	2250	293	1262	201	26.5	118.8	12.29	56.6	260	9.51	20.8	2.48	13.7	1.72	1330	1057
Pi1-1_47.d	1108	2580	318	1330	216	28.3	135.5	15.32	74.6	357	13.42	30.8	3.72	20.8	3.06	1082	1222
Pi1-1_48.d	822	2140	300	1271	218	27.8	134.1	14.41	65.2	274.2	10.56	24.5	2.3	13.5	1.85	1204	1039
Pi1-1_49.d	880	1724	190	776	109.7	20	85.5	9.34	48.3	256	8.98	21.4	2.8	17.3	2.51	780	1027
Pi1-1_50.d	876	2200	296	1249	202	27.3	125.9	12.63	58.8	255	9.3	21.4	2.29	12.7	1.56	1350	1109
Pi1-1_51.d	294	816	120.5	555	109.6	23	83.4	8.56	39	175	5.98	13.21	1.61	8.81	1.24	815	928
Pi1-1_52.d	539	1220	136.4	550	91	20.3	67	7.33	33.9	190.1	6.56	15.38	2.08	11.21	1.67	839	1795
Pi1-1_53.d	680	1653	223	1092	232	43	220	27.3	142.7	703	26.4	64	7.38	42.8	5.89	1004	1136
Pi1-1_54.d	212.5	575	86.4	419	85.7	21.2	74.5	8.51	48.2	225	8.17	18.8	2.3	15.6	2.08	1066	974
Pi1-1_55.d	1063	2310	289	1192	187.5	23.4	126	13.73	68.8	326	12.56	29.6	3.17	19.8	2.81	1013	1222
Pi1-1_56.d	465	995	96.5	354	52.1	10.48	42.3	4.4	22.7	119	4.43	9.96	1.44	7.9	1.36	809	1090
Pi1-1_57.d	469	955	116	484	83	18	70	8.8	45.8	228	8.83	19.4	2.67	15.3	2.17	787	1467
Pi1-1_58.d	851	2150	294	1305	228	28.6	137.7	14.34	66.9	296	10.48	24.2	2.74	14.5	1.64	1082	1062
Pi1-1_59.d	847	2170	272	1193	211	33.1	138.8	14.03	63.4	277	10.37	23.5	2.72	13.7	1.61	1537	821
Pi1-1_60.d	1050	2090	222	914	159	26.9	116	16	87.7	492	16.9	43.1	5.98	32.6	5.12	940	2010

Sample Pi1-2																	
Grain	La (ppm)	Ce (ppm)	Pr (ppm)	Nd (ppm)	Sm (ppm)	Eu (ppm)	Gd (ppm)	Tb (ppm)	Dy (ppm)	Y (ppm)	Ho (ppm)	Er (ppm)	Tm (ppm)	Yb (ppm)	Lu (ppm)	Sr (ppm)	Mn (ppm)
Pi1-2_1.d	1096	2060	243	1162	234.1	14.8	206	25.8	135.9	650	25.4	60.9	7.18	40	6	452	766
Pi1-2_2.d	915	2280	288	1315	239	30.6	173.2	20.1	100.1	453	18.09	39.7	4.5	24.4	3.72	1210	757
Pi1-2_3.d	1233	2600	311	1264	180.4	26	113.7	11.99	54	244.7	8.98	20.2	2.5	14	1.69	1378	1376
Pi1-2_4.d	1126	2230	251	968	141.7	21.1	92	9.82	45	216	8.26	17	2.33	12.3	1.51	1366	1005
Pi1-2_5.d	564	1250	130.3	544	78.9	17.5	57	6.4	34.8	172	6.3	15	1.8	12.4	1.76	1329	1202
Pi1-2_7.d	2110	4960	560	2180	359	27.8	281	37.6	199	1001	37.5	91.6	12.37	69.3	9.27	403	3390
Pi1-2_8.d	1274	2790	325	1284	204	30.9	132.5	13.99	67.7	329	12.26	28.4	3.5	21	2.93	956	2240
Pi1-2_9.d	1199	2880	362	1546	293	30.7	216	25.5	122.6	566	21.5	48.1	5.35	29.2	3.79	1088	709
Pi1-2_10.d	809	2030	240	1049	176	33.7	121.7	12.88	65.3	328	12.3	28.6	3.26	19.4	2.72	893	1591
Pi1-2_11.d	626	1332	155.7	630	104.6	26.1	93.1	11.7	62.2	371	12.78	33.5	4.41	27.4	4.24	1090	1630
Pi1-2_12.d	638	1324	147	562	93.6	21.8	68.5	8.78	45.6	264	9.68	24.4	2.94	19.3	2.45	708	2010
Pi1-2_13.d	1403	3190	408	1753	319	22.9	252	31.8	167	767	30.9	71	7.86	41.4	5.18	786	663
Pi1-2_14.d	1034	2260	268	1058	146.1	31.7	96.4	10.05	48.7	235	8.66	19.2	2.06	12.41	1.7	1994	2030
Pi1-2_15.d	894	2080	256	1021	148.3	26	90.5	8.41	38.9	178.2	7.25	14.8	1.66	9.92	1.33	1558	1237
Pi1-2_16.d	912	2200	289	1178	196.7	26.7	120.8	12.27	55.4	255.9	9.62	21	2.47	13.3	1.69	1578	1210
Pi1-2_17.d	103.2	297	40.1	194.7	46.7	12.6	47	6.25	36.2	239	7.5	20.5	2.97	18.9	2.97	626	1834
Pi1-2_19.d	680	1549	201	952	197.3	35.7	176.1	22.5	116.9	582	22.6	50.7	6.53	33	4.63	1182	1080
Pi1-2_20.d	1129	2270	272	1136	197	44.5	159.8	19.8	101.7	512	20.2	46.5	5.97	33.6	4.69	1169	1678
Pi1-2_21.d	536	1222	139.5	570	88.6	17.21	63.3	6.69	34.1	168.9	6.38	13.9	1.94	11.03	1.65	968	1501
Pi1-2_22.d	805	1840	218	851	124.6	22.4	79.6	9.7	44.4	233	8.8	22.4	2.51	14.3	2.29	1310	1640
Pi1-2_24.d	300	717	86.6	368	59.9	16.2	56.5	7.58	41.6	287	9.1	25.7	3.55	26	3.99	961	1733
Pi1-2_25.d	329	1132	182	845	151.5	34	126.7	14.48	71.6	360	13.95	33.6	4.08	26.2	3.86	412	1370
Pi1-2_26.d	670	1689	230.8	1026	154	27.8	93.1	9.54	42.9	190.8	7.06	16.8	1.74	10.9	1.3	1600	842

Pi1-2_27.d	1429	3600	478	2250	407	18.6	331	41.1	220	1075	40.8	97	11.92	64.4	8.09	541	615
Pi1-2_28.d	1739	2790	252	858	120	17.8	81	8.71	43	232	7.79	19.9	2.81	18.1	2.74	1066	1860
Pi1-2_29.d	511	1139	139.3	574	92.3	19.2	63.9	6.64	34.2	151.3	5.46	12.49	1.5	10.15	1.32	1297	1673
Pi1-2_30.d	260	618	78.4	348	72.9	19	66.1	7.34	43	233	7.62	18.9	2.45	14	1.94	693	2550
Pi1-2_32.d	711	1642	189	787	123.5	22.5	91.4	11.24	56	273	10.61	24.5	2.93	18.6	2.66	836	1646
Pi1-2_33.d	290	810	104	431	85	18.3	60.7	7.9	41.8	213	7.8	19.3	2.49	14.2	2.03	687	2080
Pi1-2_34.d	976	3050	348	1520	333	21.3	308	38.5	233	1020	39.5	92.4	12	66	7.34	416	1110
Pi1-2_35.d	396	1126	161.4	861	207	43.3	198	25.8	139.2	666	27	59.9	7.17	40.5	5.12	675	944
Pi1-2_37.d	1503	3190	352	1460	189	31.4	125	13.5	63.7	295	11.1	24.4	2.64	15.8	2.55	1118	1540
Pi1-2_38.d	797	2010	259	1161	186	28.1	126	12.39	54.1	255	9.65	22.8	2.69	15.4	2.04	1294	1111
Pi1-2_39.d	502	1170	163	785	166.6	38.6	150.9	18.4	96.2	447	17.66	41.5	4.75	26.2	3.4	1697	929
Pi1-2_40.d	1465	3910	499	2267	440	18.2	364	46.6	246	1233	47.9	117.4	14.92	79.3	11.18	518	1156
Pi1-2_41.d	1410	3310	427	2020	373	54.8	293	34.5	181	901	34.7	73.4	8.07	51.6	6.18	967	1590
Pi1-2_42.d	838	1906	226	918	142	22.6	94.3	10.59	46.6	230.9	8.95	19.4	2.46	12.8	1.84	1116	1226
Pi1-2_43.d	833	1879	222	913	147.4	21.5	108.3	11.45	53.8	262	9.61	22.6	2.79	15.9	2.35	753	993
Pi1-2_44.d	347	929	127	630	123	33.3	111	13.1	69.9	285	12.9	29.9	3.1	19.1	2.45	1510	960
Pi1-2_45.d	676	1600	206	914	131	26.3	84.8	8.61	39.4	189	7.19	15.8	1.79	9.5	1.3	2130	865
Pi1-2_46.d	207	955	182	1098	387	28.1	456	77.1	445	2424	88.7	213	25.1	151	19.4	310	4170
Pi1-2_47.d	770	1428	157.6	653	115.4	25.2	90.1	11.52	64.5	354	13.09	32.3	4.12	25.7	3.65	874	1786
Pi1-2_48.d	702	1330	118.8	439	68.1	18.2	52.3	6.2	35.1	241	7.54	21.9	3.06	20.5	3.57	823	1940
Pi1-2_49.d	1139	2430	265	924	133.4	18.1	87.4	8.85	48	270	9.46	23.3	2.99	18.8	2.56	797	1546
Pi1-2_50.d	201	518	75.5	360	83.6	20.8	79	9.25	49.3	217	9.55	18.7	2.3	12.4	1.34	1550	575
Pi1-2_51.d	548	1317	161.3	666	107.4	22.6	81.6	9.43	46.8	250	8.68	22.3	3.05	17	2.22	702	2230
Pi1-2_52.d	1054	2350	274	1092	173	26.2	110.4	11.31	56.5	264	9.52	22	2.51	14.5	1.95	847	1687
Pi1-2_53.d	653	1596	191.8	780	113.1	21.1	78.9	8.47	42.4	203.3	7.53	18	2.14	12.6	1.95	1146	1240
Pi1-2_54.d	367	916	115.5	514	80.3	16.1	59.3	6.83	35.4	169.4	6.56	16.7	1.9	11.41	1.64	679	1750

Pi1-2_55.d	458	1041	150.2	740	166.3	33.6	149.4	18.9	98.6	465	18.7	43.6	4.96	28.2	3.52	1337	1010
Sample Pi1-3																	
Grain	La (ppm)	Ce (ppm)	Pr (ppm)	Nd (ppm)	Sm (ppm)	Eu (ppm)	Gd (ppm)	Tb (ppm)	Dy (ppm)	Y (ppm)	Ho (ppm)	Er (ppm)	Tm (ppm)	Yb (ppm)	Lu (ppm)	Sr (ppm)	Mn (ppm)
Pi1-3_1.d	1822	1980	121.9	366	43.9	7.42	36.4	4.22	20	131.4	4.29	12.4	1.78	12.7	2.74	231	1151
Pi1-3_2.d	2100	5230	663	2760	487	43.2	396	50.5	250	1190	48.7	114.4	12.6	75	9.7	514	4160
Pi1-3_22.d	234	632	82.5	390	83	21.2	71.4	7.68	40.9	178.9	6.83	14.8	1.88	9.25	1.14	1867	699
Pi1-3_6.d	1156	2920	367	1622	334	18.4	292	37.4	201.4	1081	38.2	91.6	11.09	59.5	7.48	185.2	606
Pi1-3_7.d	592	1083	112.2	417	66.3	16.1	52.2	6.24	36.8	208.2	7.04	18.9	2.63	16	2.56	950	1965
Pi1-3_8.d	396	1003	142	737	175	33.7	168.1	19.4	106.1	511	19.4	45.2	5.34	27.2	3.89	995	1086
Pi1-3_10.d	523	1345	191.6	858	136	23.1	96	11.03	53.4	242	8.43	20	2.02	13.6	1.6	1021	1305
Pi1-3_17.d	695	1772	252	1312	264	50	247	30.7	157.3	753	29.1	68.4	7.71	44	5.49	1086	1305
Pi1-3_18.d	1832	4840	613	2550	505	10.37	421	55.3	292	1438	51.6	125.4	14.14	74.6	8.78	265	805
Pi1-3_19.d	193	693	119.9	587	257	44.9	341	71.1	416	2088	78.6	190	25.6	158	20.1	162.5	9610
Pi1-3_21.d	533	1313	184.3	872	173.2	43.2	134.9	16.14	85.3	403	15.1	35.4	4.22	22.7	3.12	1595	2033
Pi1-3_23.d	500	1312	165.5	719	108.3	18.9	65.5	6.95	32	154.8	5.35	13.6	1.61	9.69	1.2	1089	1301
Pi1-3_28.d	505	1280	168.5	750	146	29.1	113.4	13.91	70.3	365	13.08	33.9	4.32	26.2	3.89	1056	1810
Pi1-3_29.d	1550	4060	507	2420	445	48.5	337	40.6	201	846	33.8	71	7.96	46.9	5.34	622	226
Pi1-3_30.d	2130	5210	672	3270	615	102.7	517	62.9	329	1449	57.8	131.3	14.8	78.3	10.01	746	4320
Pi1-3_31.d	379	892	125.4	621	133.2	30.7	118.9	14.02	72.7	333	13.78	31.7	3.58	20.6	2.76	1703	649
Pi1-3_34.d	1433	3260	431	1866	382	14.53	326	42.5	223	1129	40.9	97.6	10.93	60.5	7.82	392	425
Pi1-3_35.d	1048	2520	308	1390	295	20.4	279	43.3	230	1206	45.6	113.9	13.3	76	8.55	234	481
Pi1-3_36.d	1417	3340	428	1870	378	36.7	332	43.8	235	1148	43.7	110	13.2	72.8	9.53	587	1009
Pi1-3_37.d	3010	7630	807	3170	537	43.3	407	54	288	1488	55.6	151	17.4	103.2	14.3	310	3350
Pi1-3_38.d	396	1097	158.9	840	205	46.1	194	22.7	114.7	560	21.6	51.3	5.73	31.5	4.18	1570	1960
Pi1-3_39.d	796	2220	329	1636	378	84.6	390	52.7	299	1427	56.9	137.3	15.5	82.1	10.9	736	1417
Pi1-3_40.d	1288	3100	376	1569	271	15.2	234	27.4	150.8	727	27.3	67.3	8.51	47.7	6.79	418	1098

Pi1-3_41.d	443	1248	187	963	234	43.3	228	27.7	150.4	745	28.6	64.8	7.74	41.8	5.54	1020	1286
Pi1-3_42.d	1499	3780	472	2370	483	76.4	411	51.5	269	1300	51.1	113.9	12.83	68.9	9.61	1003	2140
Pi1-3_43.d	1726	3540	396	1625	303	32.3	272	34.9	168	801	32.6	80.2	9.35	56.1	7.75	480	641
Pi1-3_44.d	788	2028	286	1280	238	34.4	193	23.8	118.9	584	22	51	6.46	38.4	5.38	989	2640
Pi1-3_45.d	1804	4280	532	2460	445	68.2	360	45.9	232	1107	41.2	100	11.67	69.6	9.17	806	3620
Pi1-3_46.d	498	1133	140.3	583	95.2	18.3	76.8	8.03	39.6	173.8	6.63	15	1.74	10.22	1.29	958	764
Pi1-3_47.d	358	960	148	812	213	37.2	215	27.9	153	813	29.4	67.5	7.52	39.8	5.14	795	591
Sample Pi1-4																	
Grain	La (ppm)	Ce (ppm)	Pr (ppm)	Nd (ppm)	Sm (ppm)	Eu (ppm)	Gd (ppm)	Tb (ppm)	Dy (ppm)	Y (ppm)	Ho (ppm)	Er (ppm)	Tm (ppm)	Yb (ppm)	Lu (ppm)	Sr (ppm)	Mn (ppm)
Pi1-4_1.d	1476	3230	368	1425	237	13.36	184.2	21.9	117.5	639	23.4	58.4	7.45	46.8	6.41	304	1045
Pi1-4_4.d	928	2170	309	1493	315	57.5	280	35.9	191	891	34.9	85.9	9.19	54	7.07	1301	1561
Pi1-4_3.d	957	2270	290	1266	243	45.2	199.4	24.6	123.8	601	22.9	52.9	6.6	37.2	5.09	1316	1592
Pi1-4_5.d	1400	2330	227	878	121	10.3	94.3	10.8	49.7	279	9.5	24.6	2.77	18.5	2.9	347	1014
Pi1-4_7.d	774	1532	175.8	679	109.3	23.5	89	9.85	52.1	276.8	9.64	24.4	2.84	19.4	2.87	1256	1950
Pi1-4_8.d	464	1247	184.4	974	215	49.9	191.2	22.7	120.1	536	21	50.8	5.28	27	3.69	1747	675
Pi1-4_9.d	355	931	140	743	172.4	34.2	177.4	22.8	120.1	593	23.1	52.7	6.27	33.5	4.48	997	939
Pi1-4_11.d	799	1910	244	1022	149.6	25	95.6	10.6	46.8	225.1	8.35	19.2	2.3	13.1	1.9	1207	1357
Pi1-4_12.d	339	887	113	502	81.5	16.8	56.2	6.15	26.7	139.6	5.19	11.22	1.44	8.11	1.22	991	1480
Pi1-4_15.d	1770	2730	208	721	100	17.2	95	12.3	69.6	449	14.1	41.9	5.44	37.4	6.52	165	1261
Pi1-4_17.d	723	2110	249	990	176	29.3	144	17.8	94	483	17.9	47	5.67	31.8	4.05	1170	990
Pi1-4_18.d	330	950	139.1	720	187	24.8	202	27.6	156	751	28.6	70.4	8	45.7	5.94	595	987
Pi1-4_19.d	826	1904	222	900	131.6	20.7	83.1	8.42	39.2	177.2	6.7	15.5	1.7	11.3	1.52	1144	1364
Pi1-4_20.d	906	2021	227	986	173	7.4	157.1	18.79	97.6	472	18.6	43.7	5.28	29.8	4.01	262.5	987
Pi1-4_21.d	227.2	579	85.1	438	105	27	99.7	12.69	66.1	294	11.54	26.7	2.82	16.8	2.11	1161	859

Sample Po1-1																	
Grain	La (ppm)	Ce (ppm)	Pr (ppm)	Nd (ppm)	Sm (ppm)	Eu (ppm)	Gd (ppm)	Tb (ppm)	Dy (ppm)	Y (ppm)	Ho (ppm)	Er (ppm)	Tm (ppm)	Yb (ppm)	Lu (ppm)	Sr (ppm)	Mn (ppm)
Po1-1_1.d	216	614	89.7	459	126.5	33.8	130.8	17.8	102.1	567	20.3	50.2	6.19	39.5	5.22	1151	1655
Po1-1_2.d	266	700	99.2	508	122.1	22.2	134.2	19	104.8	532	19.5	47.9	5.79	31.3	4.44	462	944
Po1-1_3.d	564	1318	182.6	892	184.6	38	156.1	19.4	98	468	17.5	39.5	4.78	26.7	3.72	1680	1022
Po1-1_4.d	285	548	63	272	68.9	15.8	74.6	9.7	54.4	284	10.46	27.4	3.47	22.2	4.08	1043	1590
Po1-1_5.d	279	595	74.5	328	56.3	15.8	53.7	6.25	36.3	199	6.87	17.4	2.46	15.5	2.04	1005	1260
Po1-1_6.d	770	1620	192	880	152	32.7	129.5	14.4	67.7	328	11.94	28.2	3.19	17.4	2.18	2350	623
Po1-1_7.d	921	1775	202	800	115	21.7	68.8	8.3	39.1	185	6.1	15.6	1.59	11.4	1.7	1420	1360
Po1-1_8.d	889	1700	193	750	103.8	22.3	69.1	8.09	39.9	197.6	6.86	16.9	2.27	12.4	1.93	1662	1277
Po1-1_9.d	670	1619	232	1134	245	41.1	225	28.8	145.3	720	28	63.7	7.6	40.2	5.21	948	1100
Po1-1_10.d	711	1414	170	671	95.5	19.6	64.1	7	34.8	172.4	6.82	16.2	1.96	11.14	1.76	1310	1216
Po1-1_11.d	188	486	63.4	300	55.8	14.3	51.1	6.33	33.8	254	7.93	21.1	3.16	19.8	3.51	948	2440
Po1-1_12.d	586	1378	184.6	843	165.6	36.2	150.1	16.4	89.8	412	14.95	37.1	4.42	24.1	3.26	1975	677
Po1-1_13.d	863	1619	193	788	132.4	20.4	104.1	13.11	66.3	372	12.9	32.6	4.43	25.2	4.11	542	1131
Po1-1_14.d	343	939	134.4	646	123.1	25.5	109.6	12.18	66.1	311	12.07	24.4	2.99	16.4	2.05	1251	591
Po1-1_15.d	170.1	547	87.1	487	116.9	24.2	94.2	9.28	40.4	178.2	6.43	13.47	1.48	8.02	0.9	1145	938
Po1-1_16.d	184.7	439	58.5	258	53.8	12.78	42.4	4.33	20.4	77.6	3.28	6.8	0.68	3.89	0.515	1553	916
Po1-1_17.d	914	2200	282	1321	241	38.4	201	23.6	118.8	578	21.2	48.6	5.77	32.1	4.21	1346	793
Po1-1_18.d	19.8	57.6	9.72	54.1	18	6.74	24.7	3.53	20.6	135.4	4.33	11.4	1.44	7.1	1.09	1043	1536
Po1-1_19.d	933	2010	254	1087	201	10.36	170.6	21	109.5	537	20.3	47.2	5.24	27.1	3.41	488	801
Po1-1_20.d	1530	2560	289	1056	148	30.6	90.5	9.57	45.4	198.1	7.4	17.1	2.22	12.9	2.03	2180	921
Po1-1_21.d	584	1497	202.3	1003	198.7	34.9	174.9	22.2	114.9	520	20.01	45.3	5.23	30.8	3.92	1087	660
Po1-1_26.d	1212	2260	204.9	709	103.6	9.9	75	7.6	39.2	261.1	7.69	21.9	3.02	24	4.57	144	1143
Po1-1_27.d	696	1706	208.2	897	132.3	25.7	92.9	10.29	47.5	229.5	9.06	20.3	2.47	12.7	1.7	1353	979

Po1-1_28.d	1082	2200	262	1093	186	45.8	146.8	16.6	88.8	448	16.2	41.8	5.5	27.8	3.9	2730	711
Po1-1_29.d	619	1550	213	968	200	28.6	178	22.3	116.1	536	21.5	48.3	5.61	30.4	3.78	958	582
Po1-1_30.d	668	1627	216	1048	211	56.2	172.1	19.3	97.5	404	16.8	35.6	4.12	21.7	2.67	2880	757
Po1-1_37.d	1013	2360	280	1185	174.8	26.1	105.6	11.08	53.2	243	9.23	20.7	2.3	13.8	2.07	1038	1194
Sample Po1-2																	
Grain	La (ppm)	Ce (ppm)	Pr (ppm)	Nd (ppm)	Sm (ppm)	Eu (ppm)	Gd (ppm)	Tb (ppm)	Dy (ppm)	Y (ppm)	Ho (ppm)	Er (ppm)	Tm (ppm)	Yb (ppm)	Lu (ppm)	Sr (ppm)	Mn (ppm)
Po1-2_1.d	635	1768	257	1173	198	25.9	115.5	11.45	51.3	228	8.6	17.4	1.94	11.74	1.28	1453	921
Po1-2_2.d	325	803	125	582	124	23.6	118.9	13.3	71.8	344	13.51	29.9	3.5	18.6	2.61	1084	618
Po1-2_3.d	371	892	110.4	503	89.8	18.8	68.8	8.08	42.3	199.9	7.19	17	2.14	11.92	1.63	825	1690
Po1-2_4.d	1054	2500	318	1465	277	58.1	224	27.1	149.2	741	27.1	64.2	8.04	46.1	5.55	1333	1709
Po1-2_5.d	829	1930	232	961	148.3	29.6	103.6	11.24	51.5	247	9.18	20.6	2.59	14.4	2.03	1273	1551
Po1-2_6.d	179.4	554	74.9	346	62.6	14.6	45.9	5.02	28.2	133.4	5.24	12.65	1.55	9.55	1.47	2040	866
Po1-2_9.d	1268	2680	302	1174	179.5	29.2	123.1	14.12	63.3	322	11.54	26.7	3.29	19.3	2.62	1582	1584
Po1-2_10.d	1310	3280	400	1630	260	15.2	194	23.4	114	620	22.4	59.8	7.7	47.6	6.64	493	828
Po1-2_11.d	1491	2750	256	873	115.5	28.5	69.9	7.65	40.6	217.6	7.72	19.9	2.54	17.5	2.41	626	606
Po1-2_12.d	515	1356	190	930	187	34.2	168	21.9	109.7	533	20.4	47.9	5.63	30	3.94	1105	787
Po1-2_13.d	378	945	124.1	598	124.9	30.4	114.4	14.21	72.9	339	13.76	29.5	3.54	18.9	2.51	1694	816
Po1-2_14.d	776	1830	230	909	143.9	28.4	92	10.1	48.5	228	8.79	19.2	2.25	13.8	1.93	1373	1657
Po1-2_15.d	947	2000	235	1018	158.1	31.6	112.5	12.43	57.3	256	9.26	21.1	2.44	14	1.82	1459	844
Po1-2_16.d	448	967	118	489	82	18.4	68.9	8.15	41.6	198.5	7.81	19	2.35	14.6	1.98	888	1619
Po1-2_17.d	212	538	76.9	350	61.8	15.2	42.2	4.57	20.6	93.9	3.52	7.72	0.89	4.92	0.72	1790	922
Po1-2_18.d	780	1058	85.1	287	37.7	9.03	29.6	2.88	15.2	85.4	3.14	9.02	1.11	7.27	1.41	597	1047
Po1-2_19.d	440	992	136.6	634	133.8	30.3	123.8	14.45	73	347	13.18	31.8	3.38	18.9	2.51	1582	719
Po1-2_20.d	787	1830	236	929	135.2	27.4	94	10.52	53.6	270	9.69	25.5	2.81	17.7	2.2	1490	1591
Po1-2_21.d	905	2770	367	1722	283	37.3	165	16.7	74.7	332	12.86	28.4	3.02	16.7	2.13	1433	994
Po1-2_22.d	294	625	74.4	303	51.1	14.4	43.8	5.38	30.5	179	6.04	16.6	2.22	13.9	2.11	679	2100

Po1-2_23.d	742	1625	198	882	234	33.6	312	45.2	275	1164	53.7	121.5	14.34	77	9.37	397	2050
Po1-2_24.d	388	1002	131	615	119.5	30.3	102.7	11.51	55.1	240	9.74	21.2	2.38	12.6	1.61	2020	958
Po1-2_25.d	2130	4470	458	1646	232	32.8	154.1	16.95	83.3	408	14.98	36.7	4.53	25.5	3.55	666	2306
Po1-2_26.d	181	567	88.6	466	101.3	22.4	76.7	8.92	37.6	166	6.18	13.7	1.62	8.5	1.08	930	1067
Po1-2_27.d	685	1471	168	637	95.2	19.3	71.5	8.21	40.3	227.2	8.03	19	2.64	16.3	2.39	1021	2196
Po1-2_28.d	986	2060	238	970	151	35.8	122.2	13.8	77.1	430	14.95	37.5	5.03	31.7	4.46	1670	1235
Po1-2_29.d	641	1468	197	893	180	40.5	150.6	18	96.3	458	17.8	41.1	4.86	26.6	3.72	1403	1374
Sample Po1-3																	
Grain	La (ppm)	Ce (ppm)	Pr (ppm)	Nd (ppm)	Sm (ppm)	Eu (ppm)	Gd (ppm)	Tb (ppm)	Dy (ppm)	Y (ppm)	Ho (ppm)	Er (ppm)	Tm (ppm)	Yb (ppm)	Lu (ppm)	Sr (ppm)	Mn (ppm)
Po1-3_4.d	358	930	140.6	732	183.6	36.2	192.5	26.5	142.4	663	26.7	64.2	7.41	40.2	5.61	742	1170
Po1-3_5.d	351	876	130.9	668	143.4	35.9	153.7	18.8	96.5	453	18.52	40.6	4.71	24.9	3.46	1279	995
Po1-3_6.d	387	1057	160.6	848	203.8	39.7	205.8	26.5	140.9	677	26.4	62.4	6.98	41.2	5.15	908	973
Po1-3_7.d	452	1091	154.3	772	157.3	34.9	145.5	18.2	99.9	497	19.7	46	5.27	30.3	4.29	1153	1420
Po1-3_9.d	162.9	456	68.7	370	86.3	20.9	89.5	10.83	59.8	257.9	10.28	23.1	2.6	15.3	2.07	1248	758
Po1-3_10.d	203.8	603	84.8	454	94	19.3	74.5	8.34	41.5	192.2	7.03	15.6	1.81	10.03	1.31	1333	832
Po1-3_11.d	911	2030	249	945	146.2	25.5	109.1	12.45	64.8	318	11.43	27.2	3.65	20.8	3.07	939	1702
Po1-3_12.d	175.3	525	86	465	128.5	27.2	143.6	19.27	107.9	534	21.5	51.5	5.85	33.4	4.23	551	967
Po1-3_13.d	336	922	120.8	537	79.4	17.56	54.3	6.21	30	162.1	5.48	13.43	1.78	10	1.47	1483	993
Po1-3_15.d	534	918	98.2	399	57.2	10.9	35.9	3.44	15.18	74.7	2.47	6.37	0.676	4.02	0.519	1073	834
Po1-3_21.d	594	1352	165.6	670	100.1	19.92	65	7.13	31.9	153.8	5.75	13.26	1.68	9.03	1.31	1312	1125
Po1-3_22.d	297	842	123.2	575	99	18.6	64.7	7.18	34.5	178.2	6.22	14.7	2.03	11.9	1.99	817	2300
Po1-3_25.d	289	775	108.4	462	73.8	17.7	52.7	6.51	29.2	152.8	5.25	13.71	1.64	10.83	1.52	1173	1194
Po1-3_26.d	638	1609	218	1050	226	41.8	224.9	28.1	147.3	687	27.8	63.9	7.36	41.8	5.16	992	880
Po1-3_27.d	607	1374	157.5	674	96.7	20.1	65.5	7.06	37.9	185	6.73	16.15	1.95	13.7	2	1142	1774

Sample Po1-6																	
Grain	La (ppm)	Ce (ppm)	Pr (ppm)	Nd (ppm)	Sm (ppm)	Eu (ppm)	Gd (ppm)	Tb (ppm)	Dy (ppm)	Y (ppm)	Ho (ppm)	Er (ppm)	Tm (ppm)	Yb (ppm)	Lu (ppm)	Sr (ppm)	Mn (ppm)
Po1-6_2.d	695	1616	237	1190	254	39.2	205	24.8	124.5	540	23	54.3	6.18	33.4	4.12	1350	1077
Po1-6_3.d	1.09	6.7	1.1	9.4	15.3	12	135	24.8	98	502	14.8	27.4	3.32	20	2.57	870	17
Po1-6_7.d	610	1530	213	974	198	23.6	163	20.9	98.8	495	18.6	42.9	4.91	26.8	3.07	858	616
Po1-6_8.d	112.2	279	42	206	56.9	16.08	64.1	8.95	54.2	343	11.35	31.7	4.13	25.9	4.15	1041	1674
Po1-6_9.d	1205	2410	236	879	117.3	22.3	77.3	9.7	45.3	215	7.91	18.7	2.42	15.1	1.86	1283	1506
Po1-6_11.d	689	1478	201.7	941	200	44.3	163.6	19.6	99.2	513	18.57	42.6	4.83	28.1	3.66	1570	1082
Po1-6_13.d	395	1026	158	817	196	37.6	193	25.7	141.1	699	27.1	62.4	7.32	39.1	5.44	892	1206
Po1-6_14.d	1001	2240	318	1436	281	38	227	28.5	139	668	24.3	58.6	7.22	37.1	4.97	1430	1017
Po1-6_15.d	687	1587	196.7	812	123.4	23.3	78.7	8.8	40.1	196.6	7.25	17	2.1	12.6	1.66	1299	1159
Po1-6_16.d	1867	2115	152.5	495	62.9	9	44.6	5.24	24.7	163.4	5.3	13.9	1.84	13.2	2.43	240	722
Po1-6_19.d	1380	2320	188	690	92	19.3	54.3	5.77	27.9	143	4.85	13.5	1.39	10.5	1.39	1980	472
Po1-6_23.d	1626	3740	471	2140	399	36.1	317	40.1	201.6	1006	37.2	85.3	10.58	55	7.09	695	2039
Po1-6_24.d	1125	2500	310	1222	188	26.1	127.7	13.85	75.3	339	12.8	30.8	3.63	21.8	3.46	970	1860
Sample St8-1																	
Grain	La (ppm)	Ce (ppm)	Pr (ppm)	Nd (ppm)	Sm (ppm)	Eu (ppm)	Gd (ppm)	Tb (ppm)	Dy (ppm)	Y (ppm)	Ho (ppm)	Er (ppm)	Tm (ppm)	Yb (ppm)	Lu (ppm)	Sr (ppm)	Mn (ppm)
St8-1_3.d	863	2230	296	1426	310	34.4	275	35.9	201	1012	36.4	87.3	10.47	55.6	7.25	706	874
St8-1_4.d	439	1130	153	682	119.1	23.3	87.1	9.32	46	221	8.48	18.3	2.05	11.8	1.64	954	956
St8-1_5.d	283	715	104	460	89.1	19.6	70.3	7.74	35.8	160.8	5.9	13.66	1.48	8.97	1.23	869	1164
St8-1_6.d	671	1570	194	858	145.6	25.3	105.2	11.5	52	233.3	8.7	20.1	2.07	12.4	1.63	842	1303
St8-1_7.d	872	2150	258	1154	188	31.8	123.7	14.51	68.6	304	11.25	25.2	2.7	15.5	1.82	1333	1019
St8-1_8.d	382	1123	169.6	894	233	65.1	271	36.2	204	960	39.3	87.2	10.01	55.3	6.88	690	795
St8-1_9.d	341	826	101.3	421	76.9	14.7	48.6	5.62	24.8	121.1	4.45	9.2	0.98	5.67	0.91	900	1126

St8-1_10.d	788	1770	221	910	147	22.9	104.2	12.39	65.2	324	12.39	28.8	3.74	22.5	3.2	955	1360
St8-1_11.d	851	1890	210	837	126.7	26	92.5	9.85	46.5	213	7.99	17.3	1.92	12	1.55	964	1266
St8-1_12.d	1542	3310	369	1435	207	33.2	142.8	17.1	85.9	422	15.9	35.9	4.75	29	3.73	1163	1566
St8-1_13.d	856	1880	223	981	164.6	36.5	120.2	13.82	65.2	311	11.94	27.6	3.28	19.7	2.9	1539	1670
St8-1_16.d	347	1153	201.1	1160	347	82.7	390	55.6	326	1566	65.2	161.7	21.1	113.6	14.83	873	1506
St8-1_19.d	935	2170	244	978	149.6	6.7	104.6	11.07	50.9	266.9	10.38	25.3	2.95	18.5	2.66	273	792
St8-1_20.d	240	572	78	364	67.9	14.7	59.8	7.25	39.1	181	7.13	16.2	1.9	12.3	1.64	647	1310
St8-1_21.d	1040	2590	307	1380	258	23.2	201	29.2	133	695	27.8	62.4	7.76	43.8	5.53	635	1240
St8-1_22.d	499	1264	172.7	759	126.1	21.5	94.5	10.16	55.9	271	9.79	24.4	3.19	18.1	2.42	1050	1219
St8-1_23.d	335	953	138.2	666	130.1	22.2	88.8	9.6	48	217.4	8.44	19.9	2.41	12.8	1.63	1422	1238
St8-1_24.d	1639	1774	142.9	530	74	11.8	76.9	8.73	50	277	10.35	27.4	3.3	21.8	3.71	425	928
St8-1_25.d	733	1648	193.1	812	122.7	23.6	81.7	9.46	46.9	227.5	8.67	19.7	2.57	15.1	2.03	1148	1464
St8-1_26.d	731	1680	205	855	129.6	25.1	89	10.94	55.1	263	10.17	23.8	3.01	18.3	2.56	1234	1235
St8-1_27.d	1181	2590	355	1560	337	20.7	314	43.1	239	1190	44.3	109.5	12.31	66.9	9.48	268	894
St8-1_28.d	977	2050	242	943	137.9	26.3	85.8	10.24	44.3	208	7.82	19.6	2.12	12	1.74	2252	885
St8-1_29.d	344	1000	161	897	244	40.2	258	37.5	204	1018	41.4	97.8	11.15	58.8	7.95	604	1329
St8-1_30.d	146.6	484	66.1	353	74.3	18.8	50.2	5.68	26.4	112.4	4.66	10	1.16	5.69	0.68	1430	427
St8-1_32.d	414	1076	140	649	128	22.9	95	12.1	58.9	317	12.2	28.5	3.63	21.5	3.13	399	704
St8-1_33.d	202	521	71.1	345	64.9	16.8	40.9	4.53	20.8	89.4	3.69	7.12	0.72	4.85	0.556	1729	1596
St8-1_35.d	1138	1818	193.1	832	161.9	5.73	149	18.3	100.2	534	20	52.8	6.44	36.4	5.46	371	1418
St8-1_36.d	228	553	67.7	334	62.7	13.45	51.5	5.76	33.9	181	6.26	14.7	1.85	11.1	1.67	894	830
St8-1_37.d	669	1411	169.9	759	132.6	20.94	106.3	12.02	61.5	272.8	10.71	25.1	2.9	16.7	2.6	785	995
St8-1_38.d	1010	2390	330	1320	202	32.6	121	11.8	52.3	239	8.96	19.8	2.45	12.7	1.65	1450	1140
St8-1_39.d	823	1977	221.2	895	135.7	21.9	103	12	63.8	322	11.96	29.4	3.47	21.2	3.03	1109	1387
St8-1_40.d	557	1490	191.9	843	152	27.8	102.7	11.62	55.6	254.4	9.49	21.6	2.63	13.89	1.92	977	1122
St8-1_41.d	1230	2550	323	1230	173.1	23.9	100	12.6	65.3	313	11.49	28.7	3.02	21.1	2.93	1170	1780

St8-1_42.d	1101	2420	244	957	162.6	13.82	135.1	16.55	88.8	478	18.1	44.9	5.89	39.9	5.57	254	926
St8-1_43.d	488	1345	175	842	169	35.1	156.7	20	107.1	513	20.9	50.9	6.56	38	5.2	973	1740
Sample St8-2																	
Grain	La (ppm)	Ce (ppm)	Pr (ppm)	Nd (ppm)	Sm (ppm)	Eu (ppm)	Gd (ppm)	Tb (ppm)	Dy (ppm)	Y (ppm)	Ho (ppm)	Er (ppm)	Tm (ppm)	Yb (ppm)	Lu (ppm)	Sr (ppm)	Mn (ppm)
St8-2_1.d	855	2360	347	1712	432	50.5	421	54.8	292	1379	55	130	15.28	83.2	10.89	716	1079
St8-2_2.d	815	1910	250	1162	239	45.4	204	22.7	117.4	538	19.7	43.7	5.17	28	3.63	1604	668
St8-2_3.d	1297	2760	303	1167	186.6	29.1	139.6	15.47	84.1	444	16.58	41.7	5.21	32.3	4.3	916	3030
St8-2_4.d	1101	2520	299	1271	210	40.9	164.9	18.8	99.9	477	18.2	46.2	5.49	32.5	4.41	1502	1931
St8-2_5.d	753	1418	154.8	627	95.9	15.5	65.5	7	29.9	150.9	5.35	12.38	1.47	8.52	1.42	959	984
St8-2_6.d	1250	3330	496	2230	483	64.5	464	57.2	306	1420	57.3	126	16	82.8	11.1	824	1480
St8-2_7.d	424	1141	168.3	820	187.7	28.2	193.8	25.6	139.2	685	26.4	62.6	7.19	41.7	5.02	707	988
St8-2_8.d	295	1030	162	875	445	4.22	611	126	729	2960	113.1	258	37.1	242	30.2	50.7	8690
St8-2_9.d	105.8	298	46.7	237	51.4	15.1	48.6	6.75	38.5	245	7.86	22.2	3.19	19.4	3.12	959	2120
St8-2_10.d	736	1890	272	1323	278	56.3	268	35.5	176	867	34.3	77.1	9.33	51.2	6.56	1079	1930
St8-2_11.d	253	625	77.5	327	55.3	13.8	48	5.84	32.3	179.9	6.43	17.2	2.36	14.8	2.1	839	2150
St8-2_12.d	833	1920	253	1111	234	32.8	223	28.9	151	761	29.2	74.5	9.23	54.5	7.75	308	809
St8-2_13.d	743	1680	198.1	834	142	25.5	106	11.81	59.8	305	11.24	27.8	3.46	20.8	2.69	1105	1725
St8-2_14.d	217	663	115.5	659	179	33.8	208	27.4	158.3	753	31.9	71.8	7.97	46.4	6.21	773	1110
St8-2_15.d	452	1109	138.8	705	140.3	35.9	124.6	15.1	76.8	335	14.03	34.6	4.29	22.7	2.96	2310	1025
St8-2_16.d	1620	3360	348	1344	228	34.7	168	24.6	135.2	685	25.7	66.3	9.04	57.2	7.99	1040	1643
St8-2_17.d	562	1423	190	862	163	32	128.5	15.4	87.9	443	15.61	38.9	4.91	26.7	4.06	1346	1096
St8-2_18.d	365	966	118.8	527	85.8	17.4	54.8	5.73	24.6	105.4	3.96	8.8	1.08	7.39	1.05	1062	1307
St8-2_19.d	96.6	297	48.9	277	76.6	22.4	86	11.17	55	254	10.25	22.9	2.48	13.53	1.78	788	694
St8-2_20.d	366	872	125.5	659	137	35.6	132	15.5	84.3	349	14.3	33.6	3.46	20.8	2.59	1490	957
St8-2_21.d	843	2080	249	975	159	9.72	119.5	13.2	71.8	393	14.1	32.9	4.32	27.9	4.18	267	487
St8-2_23.d	576	1392	192	892	188	35.6	164.6	20.8	107.1	550	20.5	48.7	5.75	34.1	4.44	1139	1065